MOLECULAR-LEVEL ORGANIZATION OF COASSEMBLED B-SHEET PEPTIDE NANOFIBERS

A Dissertation
Presented to
The Academic Faculty

by

Kong Ming Wong

In Partial Fulfillment
of the Requirements for the Degree
Doctor of Philosophy in the
School of Chemical and Biomolecular Engineering

Georgia Institute of Technology
May 2020

MOLECULAR-LEVEL ORGANIZATION OF COASSEMBLED B-SHEET PEPTIDE NANOFIBERS

Approved by:

Dr. Anant K. Paravastu, Advisor
School of Chemical & Biomolecular Engineering
Georgia Institute of Technology

Dr. Andreas Bommarius
School of Chemical & Biomolecular Engineering
Georgia Institute of Technology

Dr. Martha Grover
School of Chemical & Biomolecular Engineering
Georgia Institute of Technology

Dr. Nicholas Hud
School of Chemistry and Biochemistry
Georgia Institute of Technology

Dr. Julie Champion
School of Chemical & Biomolecular Engineering
Georgia Institute of Technology

Date Approved: March 4, 2020

This thesis is dedicated to my po po (grandmother) living in Hong Kong, Tam Oi-Lin, a strong and caring woman that helped raise me into the person I am today.

ACKNOWLEDGEMENTS

First and foremost, I would like to thank my adviser, Dr. Anant Paravastu, whom I was fortunate to meet during a tough period in my PhD career and who graciously welcomed me into his unconventional research group. He has served as a valuable mentor, sounding board, supporter, and friend who has taught me about the joys and oddities of solid-state NMR. His patience and enthusiasm for science are qualities that inspire me as a scientist and a mentor. While I'll miss discussing research and hearing his thoughts on how the government should be run, I look forward to his mentorship and continued interest in my development.

I would also like to thank my thesis committee, Dr. Martha Grover, Dr. Julie Champion, Dr. Andreas Bommarius, and Dr. Nicholas Hud. They have provided thoughtful and helpful feedback on my presentations and research throughout the past 4 years. Amongst my committee, I would like to especially thank Martha and Julie. Martha provided me a home in Chemical Engineering at the start of my PhD and supported me through my uncertain transition between research group. Julie has also been a great supporter that entertained my future research ideas and provided invaluable advice on my future career path.

Research has become increasingly collaborative, and I have been the lucky enough to benefit from the advice and support of two wonderfully talented PIs, Dr. Carol Hall and Dr. Greg Hudalla. Carol and Greg have provided endless advice that has only strengthened me as a writer and scientist. Along with Anant, they have serve as great role models of

passionate and highly intelligent researchers. I am indebted to them for their support in my growth.

As an NMR spectroscopist, access to well-maintained magnets is critical. Luckily, I have Dr. Anil Mehta, Dr. Johannes Leisen, and Dr. Les Gelbaum as resources in this arena. They have also provided great training on these magnets. Hanno taught me how to tune my first probe. Anil willingly shared his secrets to getting impeccable REDOR NMR results. Les introduced me to the more automated world of solution NMR.

Dr. Hong Yi, Dr. David Botwick, Dr. Mick Robbins, and Dr. Bettina Bommarius have supported my research efforts through instrument training and measurements that have significantly contributed to my ability to conduct research.

Professors are busy people. So, I must thank Dr. Koros, Dr. Reichmanis, and Dr. Platt for responding to my emails asking for advice. Without their encouragement at the time, I may not have continued on my path towards a PhD.

My research career would not have started if it were not for the opportunity provided by Dr. Paul Sides. He taught me about surface chemistry, electric double layers, and designing experiments. I still follow the advice he gave me early on.

The influence of educators early on is important. This is was the case for my high school chemistry teacher, Dr. Sandra Strubinger. Had it not been for her passion for developing the next generation of scientists, I would not have known about chemical engineering. I also would like to thank all the other teachers and educators that taught me over the years and helped put me on this career path.

During my time at Georgia Tech, I have been fortunate to meet a wide range of people from different universities, departments, and backgrounds.

First and foremost, I would like to thank past and present Paravastu Lab members, Serena Huang, Ben Hudson, Yuan Gao, Evan Roberts, Dipam Patel, Annabelle Lint, and Grant, and Alicia Robang. They helped me run my first few NMR experiments and provided fruitful discussions on solid-state NMR experiments and data analysis.

Much of the insights from my thesis would not be possible without the contributions from a wonderful group of collaborators. Dr. Qing Shao, Dr. Yiming Wang, and Dr. XingQing Xiao are masters of computer simulations that helped demystify the world of peptide aggregation. When I need a peptide synthesized and purified, Dillon Seroski is the man I call. He is also adept at running the many assays that characterize peptides every which way. Dr. Renjie (Jackie) Liu's skills at TEM are inspiring.

My first few years at Georgia Tech would have been dreadfully more painful without my former Payne lab members, Dr. Scott Thourson and Emily Warren. Their late-night discussions, scrabble games, and general support were invaluable.

When I first joined the Paravastu Lab, the probability of seeing two people in the lab was almost zero. Eventually in 2019, the Blazeck lab moved in. Thank you to Andrew Cazier, Andrew Kristof, John Cox, and Maria Jennings for allowing me to share my "wisdom" from over the years and for keeping me in the loop with the latest memes.

As a solid-state NMR spectroscopist, I sometimes wonder what it is like on solution side of things. Thanks to David Fialho, I was able to mask as a solution NMR spectroscopist for a few weeks using his 3mm NMR tubes.

Experiments can be fickle, and when met with an fast-approaching deadline, the pressure can be intense. Thankfully for Alex Tsoras and me, Christmas miracles do happen. I hope the next Christmas miracle is a platter of chicken wellingtons for Alex and me to share.

When I am not in lab, I am sometimes at home wondeing where my former roommate, Ben Musci, or my current roommate, Dan Fries, are given our non-overlapping schedules. Hopefully, our schedules will overlap more after this thesis is done.

Taking breaks from research to recaffeinate is sometimes necessary. I will miss coffee chats with two outstanding leaders, Adrian Ildefongo and Kris Stopka, whenever Adrian can pencil us in.

Even when properly caffeinated, research work can give the feeling of being lost at sea. Thankfully, I can always depend on Cesia Cortes, Alex Tsoras, Andrew Tadros, Weipeng Zhuo, and Jason Lee to be my anchors.

Graduate school has its challenging moments, but with a crew of friends like Nils Persson, Christine He, Andrew Tadros, Weipeng Zhuo, Kevin Ling, and Jeff Camp, there is always a shoulder to lean on. This crew has made graduate school an unforgettable experience, TBH.

Sylvia has accompanied me to fancy nights out at the symphony to omelettes at Majestic Diner that provided routine escapes from the graduate school life. Hopefully, we can continue our adventures in Europe.

To the best Bob Ross impersonator that I know, Alex Brittain, thank you for joining me on explorations of the happy trees along the beltline with obligatory pitstop at Jake's Ice Cream.

Thinking takes a lot of energy requiring constant refueling. Thankfully, Christa Lee and Mark Conley are always ready to consume massive amounts of KBBQ, Sushi, and Boba Tea.

Writing also takes a lot of energy and an inspiring environment. Without Kara, Brandon's home in San Leandro, my thesis writing would have been much less productive. Being in the same house as them reminds me of our days enjoying tea on the balcony of our penthouse apartment together.

Having worked in industry prior to graduate school, Abhinav Malholtra and I decided to gamble with a portion of our savings learning about investing in the stock market as we went. Not only did he teach me about being a savvy investor, Abhinav introduced me to the Indian box lunches and biryani in Sandy Springs where I seemed to sweat buckets.

Nathan Ellecbracht has been there for my highest of highs and lowest of lows and everything in between. Without him, my graduate school experience would not have been the same.

Venturing into a higher degree can be daunting as a first-generation student. Fortunately, my sister, Sue Mei Rivera, and my brother, Sonny Wong, have always been there to understand and support me in my ambitious career goals.

Finally, I would like to thank my parents who worked tirelessly to provide for three children in a foreign country where they barely had a grasp of the language. I would not have been able to participate in the countless educational opportunities afforded to me without their support.

TABLE OF CONTENTS

LIST OF TABLES

LIST OF FIGURES

LIST OF SYMBOLS AND ABBREVIATIONS

NMR	Nuclear magnetic resonance
FTIR	Fourier-transform infrared
CD	Circular dichroism
ThT	Thioflavin T
Cryo-EM	Cryogenic Electron Microscopy
TFA	Trifluoroacetic acid
DIW	Distilled Water
FWHM	Full width half maximum
MAS	Magic Angle Spinning
CPMAS	Cross-polarized Magic Angle Spinning
QCPMAS	Quantitative CPMAS
fpRFDR	frequency-pulse R
DARR	Dipolar-assisted Rotational Resonance
kHz	kilohertz
nm	Nanometer
μs	Microsecond
TEDOR	Transfer Echo Double Resonance
REDOR	Rotational Echo Double Resonance
NAMD	Nanoscale Molecular Dynamics
VMD	Visual Molecular Dynamics
PDB	Protein databank
DMD	Discontinuous Molecular Dynamics

kJ	kilaJoule
mM	Millimolar
PBS	Phosphate-buffered saline

SUMMARY

Functional biomaterials that recapitulate the complexity and sophistication of biological systems can be difficult to access given current techniques. Coassembling β-sheet peptides offer a new supramolecular approach towards designing these functional biomaterials. One of the predominant design motifs used in these coassembling peptides is the concept of charge complementarity in which the sequences of two peptides are modified with charged amino acids giving rise to an overall positive or overall negative charge. Electrostatic repulsion prevents self-assembly while attraction between oppositely charged peptides promotes β-sheet assembly. While studies have assessed the secondary structure of peptide nanofibers fabricated from charge-complementary molecules, there is no detailed molecular-level description of how these peptides strands arrange within the nanostructure. Consequently, we lack an understanding of how these peptides coassemble and how to design the sequences to form a specific coassembled nanofiber structure.

In this thesis, we investigate the molecular-level organization within coassembling β-sheet peptide nanofibers by a combination of experimental and computational techniques. A detailed characterization of existing charge complementary β-sheet peptides indicates that patterning electrostatic interaction between peptide molecules can successfully promote selective coassembly at the molecular level. However, significant deviation from the expected structural arrangement occurs within the peptide nanofibers showcasing the difficulty in producing finely controlled nanostructures. With this in mind, we begin to explore new coassembling peptides based on this concept of charge complementarity to gain further insight into sequence design rules to encode peptide

coassembly. In the first approach, we evaluate the structural composition of a family of peptides systematically designed such that the overall charge is iteratively increased. In the second approach, coassembling peptide pairs are generated through a computational search algorithm that are further screened through a combined computational and experimental pipeline to identify new pairs. Peptides designed by both methods are characterized and evaluated to shed light on the design rules for selectively coassembling peptide sequences. These results begin to piece together the sequence to structure relationships governing the coassembly of charge-complementary β-sheet peptides and the sequence design rules for imparting selective coassembly behavior.

CHAPTER 1. INTRODUCTION

1.1 Coassembling Peptides as Functional Biomaterials

Building multifunctional biomaterials that mimic the complexity and sophistication of native biological systems represents one of the grand challenges in biotechnology. Two ways in which nature creates a level of sophistication important in regulating biological processes are co-stimulatory and multivalent signaling. One such process is in determining the fate of T cells in the immune system. The binding co-stimulatory and co-inhibitory receptors in addition to T cell receptors plays an important role in dictating how a T cell is activated.[1] Multivalent presentation and clustering of proteins provide sharp transition points for regulating the interactions in extracellular and intracellular signaling.[2, 3] Thus, it is desirable to engineer synthetic systems with these functionalities to manipulate cellular processes for applications such as drug delivery, immunoengineering and regenerative medicine. Not only would control of bioactive molecules be important in designing therapeutics, but the development of these types of sophisticated systems may unveil insights on the biological processes that rely on these multiplexed interactions.

While significant progress has led to the development of immobilization chemistries that impart function onto biocompatible polymer scaffolds, the ability to controllably and reproducibly organize biomolecules at the nanoscale giving rise to functionality remains an active field of research. An attractive alternative towards creating these materials is through supramolecular assembly of a self-recognizing molecule. The self-templating of this “monomer” molecule can lead to long polymer-like fibers that physically entangle to form a hydrogel. One well-known class of molecule that exhibits this behavior is self-

assembling peptides. By attaching a bioactive ligand to this self-assembling peptide, materials can be engineered with a specific function. Rudra et al. have demonstrated that self-assembled Q11 peptide nanofibers functionalized with OVA antigens can elicit an immune response.[4-6] Assembly of a mixture of Q11 peptide and glycosylated Q11 peptides organize into nanofibers that exhibit hierarchical order similar to collagen fibers.[7] These examples demonstrate the utility of peptide self-assembly, wherein molecule A associates with other A molecules to form fibrillar β-sheet structures, as an alternative route to fabricating synthetic biomaterials.

Biomaterials developed through this supramolecular approach may improve upon some of the drawbacks observed in conventional polymeric systems. Characterizing the efficiency of a reaction used in conventional immobilization techniques can be challenging making it difficult to control this density. In contrast, the density of the biomolecule covalently attached to a peptide can be manipulated in a controlled manner by simply changing the relative amounts of the unmodified and modified peptides. Immobilization chemistries also often use reactive sites that are present on multiple locations on a biomolecule such as a protein. Through solid-phase peptide synthesis methods or recombinant protein expression, the site of attachment can be specified with a higher degree of control for the peptide-based method. A "bottom-up" approach also facilitates the colocalization of multiple distinct ligands in a functional biomaterial as has been demonstrated by Ardoña et al.[8] Co-immobilization of multiple ligands onto a conventional polymer scaffold often requires orthogonal chemistries.

The next generation in hierarchical peptide assembly is in the design of peptide pairs that selectively coassemble expanding the forms and functions accessible in biomaterials.

Peptides are considered to selectively coassemble when each peptide component remains in a random coil configuration in single-peptide solutions but when combined, organize into two-component fibers as illustrated in Figure 1.1. Biomaterials developed with selectively coassembling peptides as the physical scaffold could enable more complex, multifunctional materials with finer control over nanoscale organization shown in Figure 1.2. Compared to self-assembling peptides, selectively coassembling peptides benefit from a lack of external stimuli such as heat, salts, and pH which can be harmful to cells or biological molecules. Instead, peptides that exhibit selective coassembly are triggered by complementary interactions within peptide mixtures. Researchers have already made progress in creating functional biomaterials from selectively coassembling β-sheet peptides. Seroski et al. demonstrated the ability to create coassembled β-sheet nanofibers with superfolding green fluorescent protein immobilized onto the peptide nanofiber surface.[9] Another coassembling peptide pair, p1 and p2, has shown potential as a cell culture scaffold displaying favorable adhesion and growth of human 3T3 fibroblast cells when functionalized with the RDG sequence.[10] While several peptides that exhibit this behavior of selective coassembly have been reported, there has been no study evaluating the molecular-level organization and composition of these coassembled peptide nanofibers. More importantly, we do not understand how to design two peptides sequences with selective coassembly behavior. As such, this work aims to provide **molecular-level insights on the sequence to structure relationships dictating organization within coassembled peptide nanofibers** and thus, their inherent ability to organize functional biomolecular ligands.

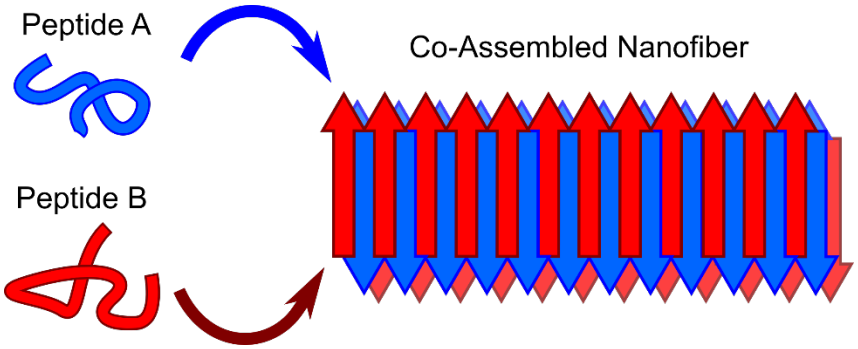

Figure 1.1. Cartoon illustrating peptide coassembly into a two-component nanofiber

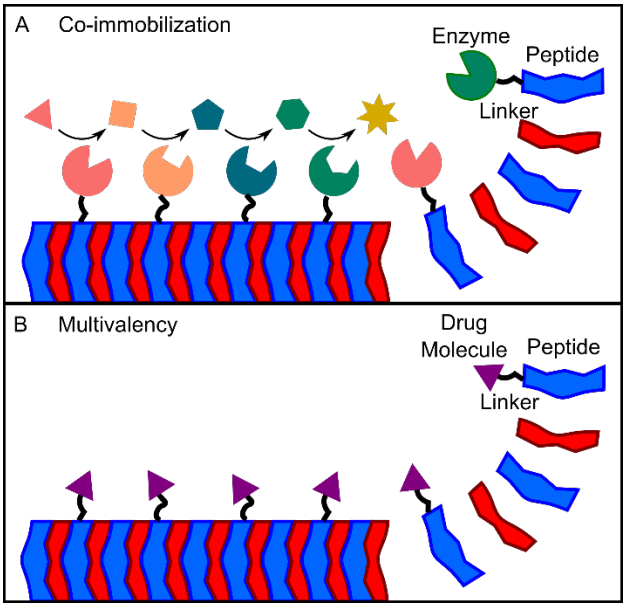

Figure 1.2 Cartoon illustrating the possibility for (A) enzyme co-immobilization and (B) multivalent drug presentation in coassembled nanofibers

1.2 From Disease to De Novo: A Brief History in Peptide Coassembly

One of the hallmarks of neurodegenerative conditions Alzheimer's disease is the formation and accumulation of amyloid plaques composed of insoluble amyloid fibrils.

Since their discovery, research has been conducted to understand the structures that the amyloidβ peptide can form and its role in loss of cognitive function. Interest in the misfolding and aggregation of amyloidβ, α-synuclein, and prion proteins has led to the expansion of study into short subsequences of larger proteins. In 1993, Zhang et al. discovered a 16-residue peptide sequence derived from the protein zuotin that spontaneously assembled into stable β-sheet tapes in aqueous solutions.[11] These fibrillar structures showed morphological similarities to the amyloid fibrils found in neurogenerative diseases.[11] This spurred the study and design of self-assembling peptide sequences as a biomaterial. Through this process of isolating β-sheet segments of larger proteins, self-assembling peptide sequences such as 24-residue peptide K24 and lysozyme-derived peptide Lysβ-21.[12] These initial peptides formed gels only in the presence of lipid bilayers and formamide, respectively.

As technology made it possible to synthesize de novo peptide sequences, deconstructing the interplay of intermolecular forces governing protein folding could be studied in greater detail. Xiong et al demonstrated that the pattern of hydrophobic and hydrophilic amino acids dictated the secondary structure, either α-helix or β-strand, adopted in self-assembling oligomeric peptides.[13] Despite individual amino acids prevalence in certain secondary structures in proteins, the pattern of (HP)n resulted in β-sheets (Figure 1.3) while a heptad sequence of HPPHHPP resulted in α-helical coiled coils.[13] Two years later, Aggeli et al. reported the first peptide de novo self-assembling peptide adequately named DN1 which built off their previous work on K24 and Lysβ-21.[12] From these initial studies, hundreds of self-assembling peptides have been discovered. Most notably, the design of RADA16-II was based off these early amphipathic de novo

peptide sequences.[14] Another well-known self-assembling peptide Q11 was similarly designed by Collier and Messersmith based on the alternating QFQFQ pattern found in microfibril-associated glycoprotein-1 and other designer peptides.[15] Early insights from these self-assembling peptides have since spurred the discovery of hundreds more.[16]

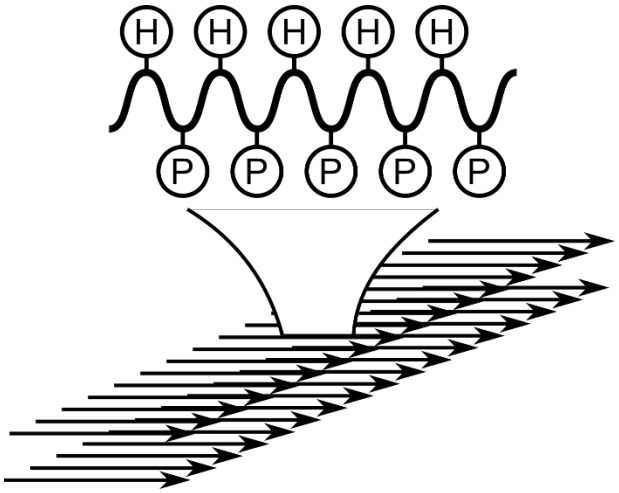

Figure 1.3 Cartoon illustrating the patterning of hydrophobic (H) and polar (P) residues that promotes β-sheet formation

Peptide coassembly has emerged as a new frontier in peptide design that expand the functionality of supramolecular biomaterials. Within peptide coassembly, significant progress has been made on α-helical coiled-coil peptides, while coassembled β-sheets have received far less attention. Pandya et al. developed the SAF p1 and p2a peptides with oppositely charged "sticky-ends" that coassembled into highly-organized peptide nanofibers.[17] Analysis by cryo-EM has shown that the SAF p1 and p2a peptide nanofibers do organize into the 3D arrangement it was designed to form.[18] These results highlight the success achieved in α-helical peptide assemblies. The significant strides in understanding sequence to structure relationships in α-helical systems may be in part due to the nature of

intermolecular forces in coiled-coil systems. α-helices have intramolecular hydrogen bonds and thus, mainly interact with other molecules through sidechain-sidechain interactions. This behavior results in efficient packing through a knobs-into-holes principle.[19, 20] In contrast, coassembled β-sheets are a relatively unexplored concept with only a handful of known coassembling β-sheet forming peptide systems. No naturally occurring β-sheet forming peptide pairs are known. Programming peptide coassembly has been achieved through two distinct design motifs. First, peptide enantiomers have been shown to coassemble into rippled β-sheets.[21, 22] Second, charge complementarity peptides, where a well-known self-assembling peptide is modified to produce a positively charged and a negatively charged variant, are observed to form gels as a result of complementary interactions.[9, 10, 23-25] Due to charge repulsion, each peptide does not self-assemble, but oppositely charged peptides are attracted to one another triggering β-sheet formation.

β-sheet-forming peptides that exhibit selectively coassemble commonly rely on this principle of charge complementarity with several peptide pairs designed along this principle. P_{11}-4 and P_{11}-5, one of the first coassembling β-sheet-forming pairs, were designed based off the self-assembling peptide DN1 created by Aggeli and coworkers to have opposing isoelectric points that prevented their self-association at neutral pH.[12, 25] Mixtures of the P_{11}-4 and P_{11}-5 peptides readily formed β-sheet rich nanofibers as observed by FTIR and CD spectroscopy.[25] Other iterations utilizing this design principle of charge complementarity led to the P_{11}-14 and P_{11}-13 peptides by Kyle et al. and the p1 and p2 peptides by King, Webb, and coworkers.[10, 24] Seroski et al. also developed charged variants of the self-assembling Q11 peptide that exhibit selective coassembly behavior as assessed by CD and ThT fluorescence measurements.[9, 15] A complete list of coassembling β-sheet

peptides is shown in Table 1.1. To date, there have been no structural studies on these coassembling β-sheet peptides. Therefore, it is not known whether these peptides truly coassemble at the molecular level. The coassembled peptides are also assumed to behave ideally and form coassembled antiparallel β-sheets with perfect alternation of the two peptide components. To further our understanding of complementary β-sheet-forming peptide and their design, we investigate charge-complementary coassembling pairs through a series of studies on the 3D arrangement within coassembled nanofibers.

Table 1.1 Existing Coassembling β-sheet Peptide Designs

Peptide Names	Sequences	Self-Assembly	Coassembly
L-Ac-$(FKFE)_2$-NH_2	L-Ac-FKFEFKFE-NH_2	Yes	Yes
D-Ac-$(FKFE)_2$-NH_2	D-Ac-FKFEFKFE-NH_2		
p1 (KW-)	EEFKWKFKEE	No	Yes
p2 (KW+)	KKEFEWEFKK	No	
KF_4K	KFFFFK	Yes	Yes
EF_4E	EFFFFE	Yes	
P_{11}-4	Ac-QQRFEWEFEQQ-Am	No	Yes
P_{11}-5	Ac-QQOFOWOFQQQ-Am	No	

Table 1.1 continued

P_{11}-13	Ac-QQOFOWOFOQQ-Am	No	Yes
P_{11}-14	Ac-EQEFEWEFEQE-Am	No	
CATCH+	Ac-QQKFKFKFKQQ-Am	No	Yes
CATCH-	Ac-EQEFEFEFEQE-Am	No	
CATCH(2+)	Ac-QQKFQFQFKQQ-Am	Yes	Yes
CATCH(2-)	Ac-QQEFQFQFEQQ-Am	No	
CATCH(4+)	Ac-QQKFKFKFKQQ-Am	No	Yes
CATCH(4-)	Ac-QQEFEFEFEQQ-Am	No	
CATCH(6+)	Ac-KQKFKFKFKQK-Am	No	Yes
CATCH(6-)	Ac-EQEFEFEFEQE-Am	No	

1.3 Overview of Work Presented

In this work, solid-state NMR studies on the molecular-level organization of coassembling β-sheet peptide designs are presented assessing our understanding of the sequence to structure relationships governing peptide interactions. First, we examine two known coassembling peptide designs, KingWebb and CATCH peptides. These charge-complementary peptides are hypothesized to arrange into antiparallel β-sheets that alternate

along the β-sheet nanofiber axis. In Chapters 3 and 4, we present experimental and computational results that while the proposed organization predominates, several types of structural defects are also observed. Then, we systematically assess the role of electrostatic forces in the imparting selective coassembly behavior within a series of peptides derived from the CATCH peptides. Solid-state NMR analysis of the nanofiber composition in Chapter 5 reveals an imbalance in the relative abundance of the complementary peptides. Finally, we combine computational tools with experimental characterization to identify new coassembling β-sheet peptide pairs in Chapter 6. This design framework successfully discovers 4 new pairs that appear to improve upon previous pairs informing the sequence patterning of new coassembling β-sheet peptides.

1.4 References

1. L. Chen and D. B. Flies, *Nature reviews. Immunology*, 2013, **13**, 227-242.

2. T. Pawson and P. Nash, *Science*, 2003, **300**, 445-452.

3. S. Tsunoda, J. Sierralta, Y. Sun, R. Bodner, E. Suzuki, A. Becker, M. Socolich and C. S. Zuker, *Nature*, 1997, **388**, 243-249.

4. J. S. Rudra, T. Sun, K. C. Bird, M. D. Daniels, J. Z. Gasiorowski, A. S. Chong and J. H. Collier, *ACS Nano*, 2012, **6**, 1557-1564.

5. J. S. Rudra, S. Mishra, A. S. Chong, R. A. Mitchell, E. H. Nardin, V. Nussenzweig and J. H. Collier, *Biomaterials*, 2012, **33**, 6476-6484.

6. J. S. Rudra, Y. F. Tian, J. P. Jung and J. H. Collier, *Proceedings of the National Academy of Sciences*, 2010, **107**, 622-627.

7. A. Restuccia and G. A. Hudalla, *Biomaterials Science*, 2018, **6**, 2327-2335.

8. H. A. M. Ardoña, E. R. Draper, F. Citossi, M. Wallace, L. C. Serpell, D. J. Adams and J. D. Tovar, *J. Am. Chem. Soc.*, 2017, **139**, 8685-8692.

9. D. T. Seroski, A. Restuccia, A. D. Sorrentino, K. R. Knox, S. J. Hagen and G. A. Hudalla, *Cell. Mol. Bioeng.*, 2016, **9**, 335-350.

10. P. J. King, M. Giovanna Lizio, A. Booth, R. F. Collins, J. E. Gough, A. F. Miller and S. J. Webb, *Soft Matter*, 2016, **12**, 1915-1923.

11. S. Zhang, T. Holmes, C. Lockshin and A. Rich, *Proc. Natl. Acad. Sci. U. S. A.*, 1993, **90**, 3334-3338.

12. A. Aggeli, M. Bell, N. Boden, J. N. Keen, P. F. Knowles, T. C. B. McLeish, M. Pitkeathly and S. E. Radford, *Nature*, 1997, **386**, 259-262.

13. H. Xiong, B. L. Buckwalter, H. M. Shieh and M. H. Hecht, *Proceedings of the National Academy of Sciences*, 1995, **92**, 6349-6353.

14. H. Yokoi, T. Kinoshita and S. Zhang, *Proc. Natl. Acad. Sci. U.S.A.*, 2005, **102**, 8414-8419.

15. J. H. Collier and P. B. Messersmith, *Bioconj. Chem.*, 2003, **14**, 748-755.

16. C. J. Wilson, A. S. Bommarius, J. A. Champion, Y. O. Chernoff,, D. G. Lynn, A. K. Paravastu, C. Liang, M-C. Hsieh. *Chemical Reivews*, 2018, **118**, 11519-11574.

17. M. J. Pandya, G. M. Spooner, M. Sunde, J. R. Thorpe, A. Rodger and D. N. Woolfson, *Biochemistry*, 2000, **39**, 8728-8734.

18. D. Papapostolou, A. M. Smith, E. D. T. Atkins, S. J. Oliver, M. G. Ryadnov, L. C. Serpell and D. N. Woolfson, *Proceedings of the National Academy of Sciences*, 2007, **104**, 10853-10858.

19. C. Aronsson, S. Dånmark, F. Zhou, P. Öberg, K. Enander, H. Su and D. Aili, *Sci. Rep.*, 2015, **5**, 14063.

20. A. Lomander, W. Hwang and S. Zhang, *Nano Lett.*, 2005, **5**, 1255-1260.

21. K. Nagy-Smith, P. J. Beltramo, E. Moore, R. Tycko, E. M. Furst and J. P. Schneider, *ACS Cent Sci*, 2017, **3**, 586-597.

22. R. J. Swanekamp, J. T. M. DiMaio, C. J. Bowerman and B. L. Nilsson, *J. Am. Chem. Soc.*, 2012, **134**, 5556-5559.

23. J. K. Sahoo, M. A. VandenBerg, E. E. Ruiz Bello, C. D. Nazareth and M. J. Webber, *Nanoscale*, 2019, **11**, 16534-16543.

24. S. Kyle, S. H. Felton, M. J. McPherson, A. Aggeli and E. Ingham, *Advanced Healthcare Materials*, 2012, **1**, 640-645.

25. A. Aggeli, M. Bell, L. M. Carrick, C. W. G. Fishwick, R. Harding, P. J. Mawer, S. E. Radford, A. E. Strong and N. Boden, *J. Am. Chem. Soc.*, 2003, **125**, 9619-9628.

CHAPTER 2. METHODOLOGY FOR CHARACTERIZING COASSEMBLED PEPTIDE NANOFIBERS

2.1 Solid-State NMR for Structural Information

Techniques commonly employed to structurally characterize peptide nanofibers range from optical spectroscopy to microscopy, but these techniques do not provide the high-resolution structural information necessary to describe the peptide nanofiber in atomistic detail. Thioflavin T fluorescence and circular dichroism measurements can report on the β-sheet content within a sample as a function of time, but these methods cannot inform on the exact β-sheet structure formed. Similarly, FTIR can provide insight into the secondary structure formed in the sample and some evidence suggest it can differentiate between parallel and antiparallel oriented β-strands.[1, 2] However, these measurements are insufficient in building a high-resolution model of the peptide nanofiber structure necessary in uncovering the sequence to structure relationships within protein folding and protein-protein interactions.

To this end, X-ray crystallography, cryo-electron microscopy, and solid-state nuclear magnetic resonance (NMR) have become the primary tools for developing atomistic models of folded protein structures and amyloid fibers. X-ray crystallography for protein structure determination dates back to 1934 with the study of myoglobin and has since led to the tens of thousands of protein structures in the Protein Data Bank (PDB).[3] One of the limiting factors in the use of X-ray crystallography is the need for diffraction-quality crystals reach the resolution necessary for structure determination. Obtaining protein

crystals in itself can be challenging requiring considerable labor to determine suitable sample preparation conditions. X-ray crystallography of self-assembling peptides often only provides measurements of the unit cell along bundled peptide nanofibers and requires computational models for comparison.[3-5] Due to recent technological advancements, cryo-EM has garnered interest as a tool for characterizing the structure of proteins and peptide assemblies not amenable to crystallography. This technique has led to new insights into the polymorphic nature of amyloidogenic peptides, such as α-synuclein and amyloid β.[6, 7] In spite of these advances, cryo-EM requires careful sample preparation in order to prevent preferential orientation of particles and robust computational analysis to correctly and reproducibly reconstruct electron density maps at atomic-level resolution.[8]

The last of the aforementioned specialist techniques, solid-state NMR, is the method utilized in the Paravastu Lab and subsequently, is the method used throughout this research to provide high-resolution structural data of coassembled β-sheet peptide nanofibers. One of the features of solid-state NMR is its' insensitivity. While the low sensitivity of solid-state NMR requires a large volume of sample and long signal averaging periods, only local order is needed for measurements. In contrast, x-ray crystallography requires highly crystalline samples that may neglect disorder and heterogeneity within a system.[4] Similarly, cryo-EM also may not efficiently sample regions of disorder and heterogeneity within samples neglecting some of the complexity found in peptide assemblies.[8] Another feature of solid-state NMR is the site-specific isotopic enrichment of samples often needed to enhance detection of these local interactions. However, isotopically enriched samples can be quite costly.

Solid-state NMR measurements can provide two pieces of information from NMR active nuclei such as ^{13}C and ^{15}N isotopes. First, the chemical environment surrounding a ^{13}C or ^{15}N site is reflected in the value of the chemical shift. Chemical shift values allow us to identify nuclei and to detect slight changes in their chemical environments that result from changes in the peptide structure.[9-11] Second, dipolar coupling measurements report on the distance-dependent interactions between ^{13}C and/or ^{15}N sites.[12-14] By labeling peptides with isotopically enriched amino acids in a site-specific manner, different structural models such as antiparallel and parallel β-sheets can be distinguished by comparing predicted and measured distances as illustrated in Figure 2.1. An atomistic model of the coassembled peptide nanofibers can be built from structural constraints identified in this manner.

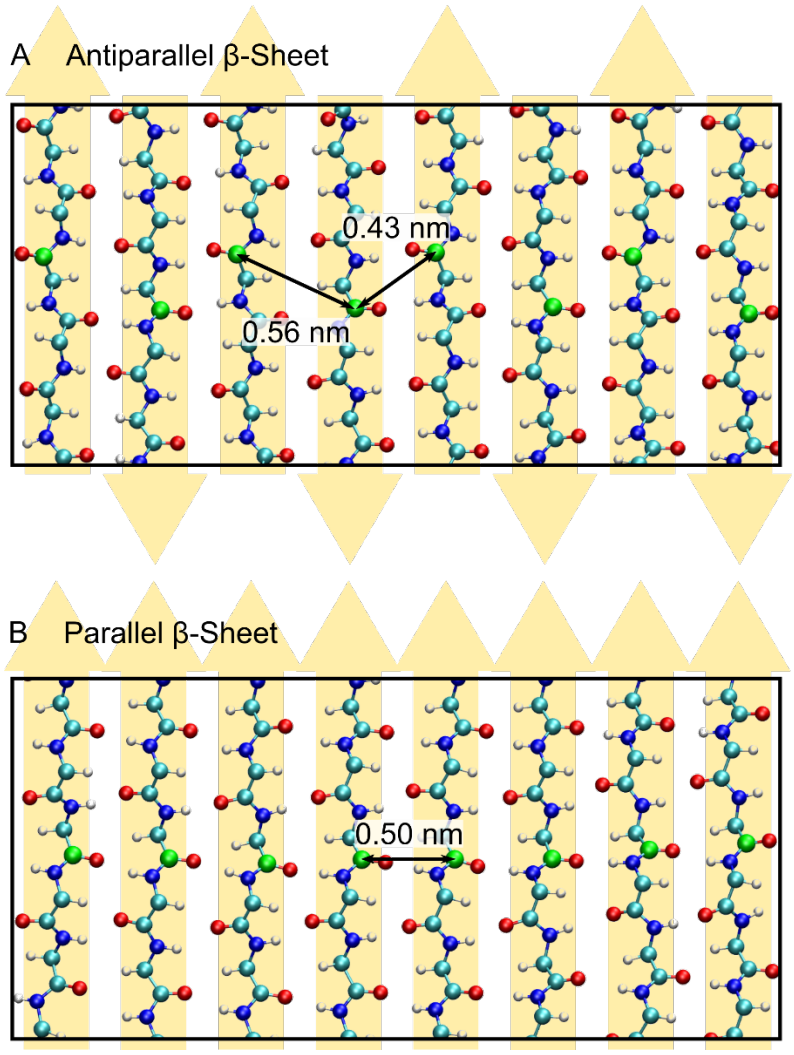

Figure 2.1 Comparison of inter-strand distances for carbonyl carbons (green) along the center of the peptide. (A) Model of antiparallel β-sheets and (B) parallel β-sheets.

2.1.1 Synthesis of Isotopically Labelled Samples

The process of synthesizing isotopically labeled peptide samples relies on Fmoc-protected amino acids isotopically enriched at targeted ^{13}C and ^{15}N sites and conventional solid-phase synthesis methods for peptide synthesis. Through solid-phase synthesis, peptides are grown through the sequential addition of amino acids though a cycle of

reaction steps shown in Figure 2.2. This piecewise addition of amino acid blocks allows us to incorporate readily available amino acids isotopically enriched with ^{13}C and ^{15}N at targeted locations within the peptide molecule. Two categories of isotopically enriched amino acids are commonly employed: uniformly labelled and partially labelled amino acids. In the uniformly labelled amino acid, all carbon atoms and all nitrogen atoms are isotopically enriched with ^{13}C and ^{15}N. Partially labelled amino acids mostly have one carbon or nitrogen site ^{13}C or ^{15}N enriched most commonly at the backbone carbonyl carbon or backbone nitrogen. Selective labeling of a single carbon or nitrogen is necessary for more quantitative analysis of solid-state NMR measurements.

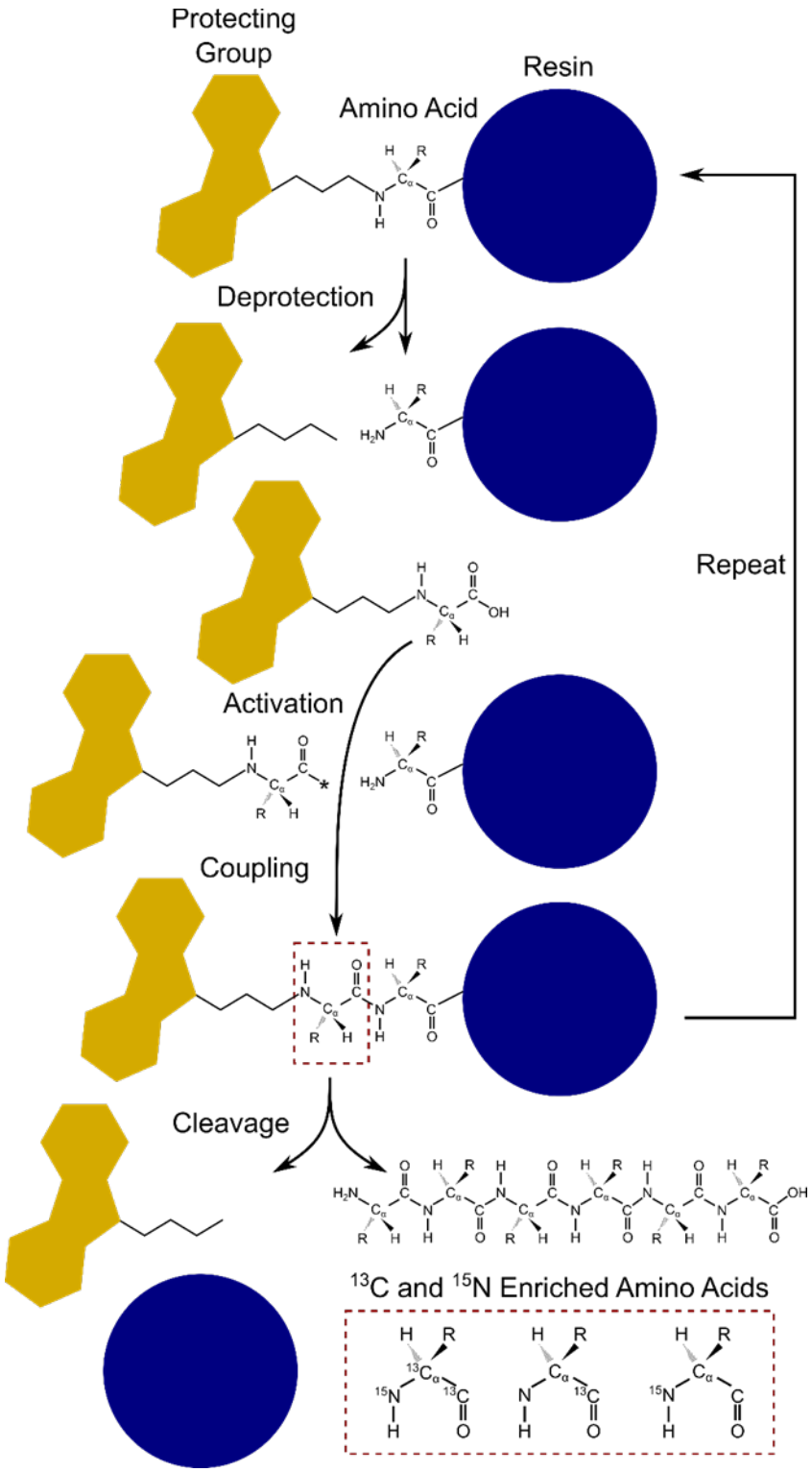

Figure 2.2 Illustration of solid-phase peptide synthesis. Examples of isotopically enriched amino acids that can be incorporated are highlighted by a red box.

2.1.1.1 Standard Peptide Synthesis and Purification Details

Peptides were synthesized using standard Fmoc solid-phase peptide synthesis on a CS336X automated peptide synthesizer (CS Bio), according to established methods.[15] Peptides were acetylated at their N-termini with an acetylation cocktail (10% acetic anhydride (Sigma), 80% dimethylformamide (Fisher), and 10% N,N-Diisopropylethylamine (Fisher)). Synthesis resin was collected and washed with acetone (Fisher) and placed in a desiccator overnight. Peptides were cleaved from resin and deprotected using a cocktail containing 95% trifluoroacetic acid (TFA) (Fisher), 2.5% triisopropylsilane (sigma), and 2.5% ultrapure water. Soluble peptide is then separated from the solid-resin support and then precipitated using diethyl ether (Fisher) on ice for 5 minutes. To remove residual TFA, precipitated peptide was then pelleted via centrifugation and resuspended with cold diethyl ether three times and then dried by vacuum overnight. Peptides were dissolved in water, frozen, and freeze-dried with a FreeZone 1 lyophilizer (Labconco).

Peptides were purified to greater than 90% purity by reverse phase high-performance liquid chromatography (RP-HPLC) using a DionexTM Ultimate 3000TM System (Thermo Scientific) equipped with a C18 column (Thermo Scientific) or a PFP column (Thermo Scientific). The mobile phase consisted of (A) water and (B) acetonitrile, both containing 0.1% TFA. Peptides were detected by absorbance at 215 nm.

For MALDI-TOF MS analysis, RP-HPLC purified peptide was mixed 1:1 (v/v) with α-cyano-4-hydroxycinnamic acid (Sigma) (10 mg/mL) in 70% acetonitrile and 30% water both containing 0.1% TFA. 2 µl of the solution was spotted and dried onto a MSP 96-target

polished steel BC MALDI plate. Samples were analyzed using reflectron, positive mode on an AB SCIEX TOF/TOFTM 5800 (Bruker) equipped with a 1 kHz N2 Opti-BeamTM on axis-laser.

2.1.2 Standard Solid-State NMR Sample Prep of Peptide Nanofiber

Peptide nanofiber samples are prepared in salt solutions according to published protocols for the given peptide pair and allowed to incubate for 1-3 days to ensure samples reach equilibrium. Nanofiber samples are then centrifuged, and the pellet is resuspended in distilled water (DIW) to remove unassembled peptide and salts that reduce signal to noise in our solid-state NMR measurements. This wash procedure is done up to 2 times to remove as much unassembled peptides and salts without significant loss of assembled material. Once sufficiently washed, the resuspended peptide nanofiber sample is lyophilized. Lyophilized peptide nanofiber samples are then packed into Bruker 3.2 mm NMR rotors and are minimally hydrated within the NMR rotor by adding 1μL of DIW per 1 mg of nanofiber sample unless otherwise specified. Rehydration of the assembled peptide sample improves NMR linewidths and signal to noise without changing the nanofiber structure.[16] In cases where the peptide nanofibers do not easily pellet by tabletop centrifuges, an ultracentrifuge is employed to collect sample directly into the NMR rotor using a specially designed funnel.[17]

2.1.3 Standard Solid-State NMR Experimental Setups and Parameters

All measurements are performed with an 11.75 T Bruker Avance III spectrometer with a 3.2 mm Bruker MAS probe unless otherwise specified. ^{1}H-^{13}C CPMAS measurements were run at 22 kHz magic angle spinning (MAS) with 100 kHz proton

decoupling and a cross-polarization (CP) contact time set to 2 ms.[18] NMR chemical shifts are referenced to tetramethyl silane, as calibrated using adamantane before each experiment. Quantitative ^{1}H-^{13}C CPMAS measurements were run at 22 kHz magic angle spinning (MAS) and 100 kHz proton decoupling.[19] Peptide nanofiber samples were run with 14 100μs CP periods to ensure equivalent cross-polarization.

Finite-pulse Radio-Frequency Driven Recoupling (fpRFDR) and dipolar assisted rotational resonance (DARR) measurements were performed at a sample-rotation rate of 22 kHz to produce 2D ^{13}C-^{13}C spectra.[20-23] The mixing period for 2D DARR experiments was set to 500ms. 2D ^{13}C-^{15}N TEDOR measurements were conducted with mixing times of 2.4 ms and 8 ms to observe intra-residue and inter-residue couplings, respectively.[24]

PITHIRDS-CT measurements were done at 12.5 kHz MAS with 26.7 μs π-pulses during ^{13}C dipolar recoupling. Total recoupling time was 61.44 ms, where k1 = 4 and k2 + k3 = 16.[14] Continuous wave proton decoupling at 100 kHz was applied during the PITHIRDS-CT pulse sequence and data acquisition, respectively. Sensitivity of PITHIRDS-CT measurements were improved by using pulsed spin locking.[25]

Both $^{13}C\{^{15}N\}$REDOR and $^{15}N\{^{13}C\}$REDOR measurements were performed at 10kHz sample rotation.[12, 13, 26, 27] Pulse imperfections were compensated using xy8 phase cycling of $^{15}N\{^{13}C\}$REDOR 6 and 10 μs rotor-synchronized ^{13}C and ^{15}N π pulses, respectively.[28] EXORCYCLE phase cycling of the final ^{13}C Hahn-echo refocusing pulse was applied with 95 kHz Spinal ^{1}H decoupling as well.[29-31]

2.2 Molecular Models and Nuclear Spin Simulations

Constructing a high-resolution molecular model of assembled peptide nanofibers involves an iterative process of developing models and testing models via solid-state NMR measurements. First, a series of speculative molecular models are drawn out by hand or simulated using molecular dynamics software. Second, an isotopic-labeling scheme and solid-state NMR experiment is devised to test a set of intermolecular interactions and distances predicted across the nanofiber models. Third, the isotopically labeled peptide nanofiber samples are prepared and solid-state NMR measurements are conducted. Fourth, NMR spectra are analyzed, and results are assessed against the molecular models ruling out some of the considered arrangements. This process is repeated until a singular molecular model remains or enough intermolecular constraints are identified to constrain the molecular model.

2.2.1 Idealized 3D Molecular Models

3D molecular models aid in the interpretation of solid-state NMR measurements on ^{13}C and ^{15}N isotopically labeled peptide nanofiber samples. The dipolar couplings probed by solid-state NMR decay by $1/r^3$ making measurements highly sensitive to the distance between ^{13}C and/or ^{15}N sites. To properly account for changes in these intermolecular distances between proposed 3D arrangements, MD simulations of peptide nanofiber structures are necessary. This molecular modeling is especially important for coassembling peptides given the increased complexity from the combinations of arrangements for two peptides versus a single peptide.

Each 3D molecular model of a coassembled β-sheet peptide nanofiber structure are constructed with the following assumptions. First, the two peptide molecules alternate perfectly along the nanofiber axis. Second, the peptide molecules are aligned to maximize the number of hydrogen bonds satisfied. Third, the amphipathic peptide molecules are arranged into a β-sheet such that there is a hydrophilic face and a hydrophobic face. Fourth, these two β-sheets are stacked with their hydrophobic faces pointing towards each other forming a hydrophobic core.

2.2.1.1 NAMD Simulation Details

Molecular models are constructed using a combination of custom code in Wolfram Mathematica, Nanoscale Molecular Dynamics (NAMD), and Visual Molecular Dynamics (VMD) software.[32, 33] First, each peptide molecule is built and configured into a straight β-strand conformation using the Molefacture plugin in VMD. Acetylation and/or amidation of the N- and C-termini are done during this step. The peptides are then manipulated and propagated along the nanofiber axis to form two β-sheets of 10 peptide strands each in Wolfram Mathematica. An initial protein databank (PDB) file of the peptide nanofiber structure is produced along with a separate file of dihedral angle and hydrogen bond constraints corresponding to an antiparallel or parallel β-strand orientation. These two files are used as the initial inputs to a series of NAMD simulations that assemble the peptide strands into the final hydrogen-bonded and stacked β-sheet nanofiber model in a stepwise fashion. More specific details on these simulations are included in each chapter. For each arrangement, 10 simulations are run to enhance statistical sampling of the distribution of distances created from slight variations in sidechain conformations.

2.2.2 Nuclear Spin Simulations of Solid-State NMR Experiments

The simplified ^{13}C and ^{15}N spin systems produced from partially labeled amino acids allows for numerical simulation of the dipolar recoupling NMR experiments, such as ^{13}C-^{13}C PITHIRDS-CT and ^{13}C-^{15}N REDOR, to be computationally feasible. Dipolar couplings between ^{13}C and ^{15}N labeled sites depend on distance and the relative geometry of isotopic labels. As previously shown in Figure 2.1, these distances differ between different 3D arrangements of peptide strands. Inputting the distances from MD-simulated peptide nanofiber structures into SpinEvolution simulations produces predictions for the PITHIRDS-CT decay and REDOR dephasing that can be compared to experimental results.[34] In this manner, dipolar recoupling NMR experiments can be analyzed in a quantitative way and differentiate between distinct molecular arrangements. In certain cases, Monte Carlo simulations are combined with SpinEvolution simulations to understand how isotopic dilution influences the measured PITHIRDS-CT decays. Monte Carlo simulations capture the statistical distribution of ^{13}C spins along the nanofiber axis resulting from isotopic dilution allowing us to better understand complex effects such as peptide self-association.

2.3 Complementary Structural Information from Coarse-Grained DMD Simulations and Optical Spectroscopy

Throughout this work, solid-state NMR measurements are complemented by coarse-grained DMD simulations and optical spectroscopy. PRIME20/DMD simulations were provided by Dr. Carol Hall's group at North Carolina State University. These coarse-grained DMD simulations report on early kinetic behavior of single-peptide and two-

peptide mixtures. The structure of peptide nanofibers coassembled in silico are analyzed and compared to experimental results to assess the ability for PRIME20 to predict structural features of two-component peptide nanofibers.

Thioflavin T fluorescence measurements were conducted by Dr. Greg Hudalla's group at University of Florida to monitor the change in β-sheet content over time. Thioflavin T is a fluorescent molecule that exhibits an increase in fluorescence emission upon binding to peptide β-sheets.[35-39] The degree of increase in ThT fluorescence emission varies from peptide to peptide. This variation is likely due to the manner in which ThT binds onto the grooved surface of peptide β-sheets.[37]

2.3.1 Coarse-grained DMD Simulations

In collaboration with Dr. Carol Hall's group at North Carolina State University, coarse-grained discontinuous molecular dynamics simulations were performed to observe early kinetic behavior during peptide coassembly. Discontinuous molecular dynamics is used as a fast alternative to traditional molecular dynamics.[40] These DMD simulations utilize the Hall group's custom implicit-solvent coarse-grained protein force field PRIME20 tailored to simulate peptide aggregation.[41-43] Exact details regarding simulations are found in the chapter-specific methods sections.

DMD/PRIME20 is among the most realistic of the protein coarse-grained models, does not build in any predetermined secondary structure or start from a pre-set ordered structure, provides a good representation of amyloid structure in comparison to experiment, and is fast enough to get to the fibrillar stage starting from the random coil state.[41, 42, 44] The DMD/PRIME20 combination allows us to explore in molecular detail the structure

and rearrangement of the oligomers that form along the aggregation/fibrilization pathway at time scales up to 672 μs at mM concentrations.[44] All of the simulations are carried out in the canonical (NVT) ensemble at a peptide concentration of 20 mM by varying the number of peptides and the volume of the simulation box. The Andersen thermostat is implemented to maintain the simulation system at a constant temperature.[45] The reduced temperature is defined to be $T^*=k_BT/\varepsilon_{HB}$, where ε_{HB}=12.47 kJ/mol is the hydrogen bonding energy.

2.3.2 The PRIME20 model

In the PRIME20 model, each of 20 residues contains three backbone spheres NH, Cα, CO and one sidechain sphere R as shown in Figure 2.3. The sidechain sphere R utilizes a unique set of geometric parameters: a hard sphere diameter (effective van der Waals radius), sidechain-to-backbone distances (R-Cα, R-NH, R-CO) for each sidechain. The potential function between two residue sidechain spheres is modeled as a square well potential. The parameter matrix for sidechain-sidechain interactions includes 210 different square well widths and 19 different square well depths to discriminate the polar, charge-charge and hydrophobic types of interactions.[43] The hydrogen-bonding interaction between backbone beads NH and CO is modeled as a directional square well potential. All the other non-bonded interactions are modeled as hard sphere potentials. For a detailed description of the geometric and energetic parameters of the PRIME20 model, please refer to the earlier work from the Hall group.[43, 44, 46]

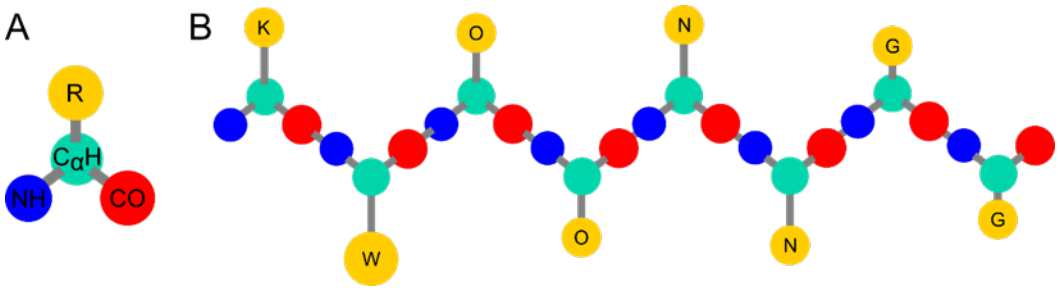

Figure 2.3 Cartoon depiction of the PRIME20 bead model. (A) Beads with corresponding chemical groups. (B) Demonstation of amino acid sidechain and bead size difference in the KWOONNGG peptide.

Structural analysis of the coarse-grained DMD simulations through custom code mostly in Wolfram Mathematica bridges the informational gap between predictions from simulations and experimental constraints from solid-state NMR measurements. Structures observed in simulations are identified and calculated to be compared against the experimental observations allowing a means for providing feedback for the protein force fields used in these molecular dynamics simulations.

2.3.3 Other Spectroscopic Measurements

2.3.3.1 Standard Fourier-Transformed Infrared Spectroscopy Details

The FTIR spectra were recorded on a Frontier FTIR spectrophotometer (PerkinElmer) equipped with a universal ATR sampling accessory. For aqueous samples, the FTIR spectrophotometer was blanked with ultrapure water prior to scanning. Samples were prepared at 10 mM and 1x PBS with 5 µl spotted onto the ATR accessory. Aqueous samples were scanned 50 times with the average of the spectra reported. Dry samples were

spotted and dried on the ATR accessory and then scanned 4 times with the average of the spectra reported.

2.3.3.2 Standard Thioflavin T (ThT) Assay Details

A stock solution containing 0.8 mg/mL of thioflavin T (ThT) (Acros) in water was filtered through a 0.22 μm syringe filter (Millex). Peptides in water, ThT, and PBS were added to a black 96-well plate (Corning) to obtain a final concentration of 500 μM total peptide, 0.08 mg/mL ThT, and 10x PBS. Samples were analyzed with a Molecular Devices SpectraMax M3 spectrophotometer (excitation 450 nm, emission 482 nm). All samples were run in triplicate, with the mean and standard deviation of these samples reported.

2.4 References

1. R. Sarroukh, E. Goormaghtigh, J.-M. Ruysschaert and V. Raussens, Biochim. Biophys. Acta, 2013, 1828, 2328-2338.

2. G. Zandomeneghi, M. R. H. Krebs, M. G. McCammon and M. Fändrich, Protein Sci., 2004, 13, 3314-3321.

3. E. F. Garman, Science, 2014, 343, 1102-1108.

4. K. R. Acharya and M. D. Lloyd, Trends Pharmacol. Sci., 2005, 26, 10-14.

5. K. Morris and L. Serpell, Chem. Soc. Rev., 2010,39, 3445-3453.

6. B. Li, P. Ge, K. A. Murray, P. Seth, M. Zhang, G. Nair, M. R. Sawaya, W. S. Shin, D. R. Boyer, S. Ye, D. S. Eisenberg, Z. H. Zhou and L. Jiang, Nature Communications, 9, 3609.

7. M. Kollmer, W. Close, L. Funk, J. Rasmussen, A. Bsoul, A. Schierhorn, M. Schmidt, C. J. Sigurdson, M. Jucker and M. Fandrich, Nature Communications, 10 , 4760.

8. D. Lyumkis, J. Biol. Chem., 2019, 294, 5181-5197.

9. D. S. Wishart, Prog Nucl Mag Res Sp, 2011, 58, 62-87.

10. E. L. Ulrich, H. Akutsu, J. F. Doreleijers, Y. Harano, Y. E. Ioannidis, J. Lin, M. Livny, S. Mading, D. Maziuk, Z. Miller, E. Nakatani, C. F. Schulte, D. E. Tolmie, R. K. Wenger, H. Y. Yao and J. L. Markley, Nucleic Acids Res., 2008, 36, D402-D408.

11. D. Wishart and B. Sykes, J. Biomol. NMR, 1994, 4, 171-180.

12. J. M. Goetz and J. Schaefer, J. Magn. Reson., 1997, 127, 147-154.

13. T. Gullion and J. Schaefer, Journal of Magnetic Resonance (1969), 1989, 81, 196-200.

14. R. Tycko, J. Chem. Phys., 2007, 126, 064506-064506.

15. D. T. Seroski, A. Restuccia, A. D. Sorrentino, K. R. Knox, S. J. Hagen and G. A. Hudalla, Cell. Mol. Bioeng., 2016, 9, 335-350.

16. K. Nagy-Smith, E. Moore, J. Schneider and R. Tycko, Proceedings of the National Academy of Sciences, 2015, 112, 9816-9821.

17. A. Mandal, J. C. Boatz, T. B. Wheeler and P. C. A. van der Wel, J. Biomol. NMR, 2017, 67, 165-178.

18. X. L. Wu and K. W. Zilm, Journal of Magnetic Resonance, Series A, 1993, 104, 154-165.

19. P. Duan and K. Schmidt-Rohr, J. Magn. Reson., 2017, 285, 68-78.

20. K. Takegoshi, S. Nakamura and T. Terao, Chem. Phys. Lett., 2001, 344, 631-637.

21. Y. Ishii, The Journal of Chemical Physics, 2001, 114, 8473-8483.

22. A. E. Bennett, C. M. Rienstra, J. M. Griffiths, W. Zhen, P. T. L. Jr. and R. G. Griffin, The Journal of Chemical Physics, 1998, 108, 9463-9479.

23. A. E. Bennett, R. G. Griffin, J. H. Ok and S. Vega, The Journal of Chemical Physics, 1992, 96, 8624-8627.

24. C. P. Jaroniec, C. Filip and R. G. Griffin, J. Am. Chem. Soc., 2002, 124, 10728-10742.

25. A. T. Petkova and R. Tycko, J. Magn. Reson., 2002, 155, 293-299.

26. G. M. Bernard, M. Miskolzie, G. Kotovych and R. E. Wasylishen, Can. J. Chem., 2004, 82, 1554-1563.

27. C. P. Jaroniec, B. A. Tounge, C. M. Rienstra, J. Herzfeld and R. G. Griffin, J. Magn. Reson., 2000, 146, 132-139.

28. T. Gullion, D. B. Baker and M. S. Conradi, Journal of Magnetic Resonance (1969), 1990, 89, 479-484.

29. N. Sinha, K. Schmidt-Rohr and M. Hong, J. Magn. Reson., 2004, 168, 358-365.

30. M. Rance and R. A. Byrd, Journal of Magnetic Resonance (1969), 1983, 52, 221-240.

31. B. M. Fung, A. K. Khitrin and K. Ermolaev, J. Magn. Reson., 2000, 142, 97-101.

32. J. C. Phillips, R. Braun, W. Wang, J. Gumbart, E. Tajkhorshid, E. Villa, C. Chipot, R. D. Skeel, L. Kalé and K. Schulten, J. Comput. Chem., 2005, 26, 1781-1802.

33. W. Humphrey, A. Dalke and K. Schulten, J. Mol. Graphics, 1996, 14, 33-38.

34. M. Veshtort and R. G. Griffin, J. Magn. Reson., 2006, 178, 248-282.

35. D. J. Lindberg, A. Wenger, E. Sundin, E. Wesén, F. Westerlund and E. K. Esbjörner, Biochemistry, 2017, 56, 2170-2174.

36. L. S. Wolfe, M. F. Calabrese, A. Nath, D. V. Blaho, A. D. Miranker and Y. Xiong, Proceedings of the National Academy of Sciences, 2010, 107, 16863-16868.

37. M. Biancalana and S. Koide, Biochim. Biophys. Acta, 2010, 1804, 1405-1412.

38. T. Ban, D. Hamada, K. Hasegawa, H. Naiki and Y. Goto, J. Biol. Chem., 2003, 278, 16462-16465.

39. H. Naiki, K. Higuchi, M. Hosokawa and T. Takeda, Anal. Biochem., 1989, 177, 244-249.

40. B. J. Alder and T. E. Wainwright, The Journal of Chemical Physics, 1959, 31, 459-466.

41. Y. Wang, S. J. Bunce, S. E. Radford, A. J. Wilson, S. Auer and C. K. Hall, Proceedings of the National Academy of Sciences, 2019, 116, 2091-2096.

42. S. J. Bunce, Y. Wang, K. L. Stewart, A. E. Ashcroft, S. E. Radford, C. K. Hall and A. J. Wilson, Science advances, 2019, 5, eaav8216-eaav8216.

43. M. Cheon, I. Chang and C. K. Hall, Proteins: Structure, Function, and Bioinformatics, 2010, 78, 2950-2960.

44. Y. Wang, Q. Shao and C. K. Hall, J. Biol. Chem., 2016, 291, 22093-22105.

45. H. C. Andersen, The Journal of Chemical Physics, 1980, 72, 2384-2393.

46. H. D. Nguyen and C. K. Hall, Proc. Natl. Acad. Sci. U.S.A., 2004, 101, 16180-16185.

CHAPTER 3. STRUCTURAL ANALYSIS OF COASSEMBLED KING-WEBB PEPTIDE NANOFIBERS[1]

3.1 Overview of Chapter

Despite the growth of coassembling β-sheet peptide designs, there has been limited structural characterization of the coassembling peptide pairs, and no atomistic model has been reported. In this chapter, the first of two existing coassembling β-sheet peptide designs, King-Webb peptides, is assessed to determine the molecular-level organization of the two components within the peptide nanofiber. This analysis is accomplished through a series of solid-state NMR measurements that are complemented by coarse-grained DMD simulations.

3.2 Introduction

Current selectively coassembling peptide designs rely on complementary electrostatic interactions between charged variants of well-known self-assembling peptides. An early example of complementary electrostatic sequences comes from Pandya et al. with the SAF-p1 and SAF-p2 peptides which form heteromeric coiled-coil peptide nanofibers via association of the "sticky-ends."[1] P_{11}-4 and P_{11}-5, one of the first coassembling β-sheet-forming pairs, were initially designed based off the self-assembling peptide DN1 created by Aggeli and coworkers to have opposing isoelectric points that

[1] Portions of this chapter have been adapted and reproduced from Wong, K. M., Wang, Y., Seroski, D. T., Larkin, G. E., Mehta, A. K., Hudalla, G. A., Hall, C. K., Paravastu, A. K. "Molecular complementarity and structural heterogeneity within co-assembled peptide β-sheet nanofibers" ***Nanoscale,*** 2020,**12**, 4506-4518 - Reproduced by permission of The Royal Society of Chemistry.

prevented their self-assembly at neutral pH.[2, 3] However, mixtures of the P_{11}-4 and P_{11}-5 peptides were found to readily form β-sheet rich nanofibers as observed by Fourier Transform Infrared (FTIR) and circular dichroism (CD) spectroscopy.[3] Other iterations built off the designs of the P_{11}-4 and P_{11}-5 peptides led to the P_{11}-14 and P_{11}-13 peptides by Kyle et al. and the p1 and p2 peptides by King, Webb, and coworkers.[4, 5] The latter is the focus of this Chapter which we herein refer to as the King-Webb peptides, comprised of KW+ (KKFEWEFEKK) and KW- (EEFKWKFKEE). As can be seen from the amino acid sequence, the KW+ and KW- peptides contain a mixture of positively and negatively charged residues that results in low net peptide charges of +1 and -1, respectively.

Prior structural characterization of coassembled KW+ and KW- peptide nanofibers by attenuated total reflectance FTIR spectroscopy suggests a coassembled antiparallel β-sheet structure.[4] While a lower amide I' maxima and presence of a low-intensity peak around 1685 cm^{-1} in FTIR spectra has often been attributed to antiparallel β-sheets, several experimental and theoretical studies have argued that this interpretation is not always true.[6] Our own work on RADA16-I revealed a parallel β-sheet structure with a 2-residue registry shift contradicting the proposed antiparallel β-sheet model.[7, 8] Included in this classification of a coassembled antiparallel β-sheet structure are three assumptions. First, KW+ and KW- peptides interact at the molecular level to form two-component nanofibers rather than self-sorting. Second, KW+ and KW- peptides arrange in a perfect alternation within a β-sheet. Third, nanofibers contain equal amounts of KW+ and KW- peptides. Currently, there is no direct biophysical evidence to support these assumptions and resolve these structural details.

In this Chapter, we assess the coassembled antiparallel β-sheet structural model and test the assumptions in the King-Webb peptide system through a combination of computer simulations, solid-state nuclear magnetic resonance (NMR) experiments and biophysical measurements. Solid-state NMR measurements indicate that KW+ and KW- peptide coassemble into near stoichiometric two-component β-sheet structures, and coarse-grained DMD simulations of 48 KW+ and 48 KW- chains support this observation of molecular-level coassembly. Although the experimental and computational results indicate some preference for an antiparallel β-sheet structure, a high percentage (31.7%) of β-strands are oriented parallel to at least one nearest neighbor. While the majority of β-sheets exhibit $(AB)_n$ alternation of KW+ and KW- strands, isotopic dilution NMR measurements reveal a significant amount of peptide self-association within the peptide nanofiber. The structural heterogeneity in the coassembled KW+ and KW- peptide nanofibers, which appears to occur within each coassembled peptide nanofiber, stands in contrast to typical behavior seen in self-assembling β-sheet peptides. In self-assembled peptide nanofibers, structure may vary between nanofibers in the same sample, but is believed to be consistent within individual nanofibers.[9-12]

3.3 Results

3.3.1 King-Webb Peptides Exhibit Molecular-Level Coassembly into β-Sheet-Rich Nanofibers.

Complementary interactions between KW+ and KW- peptides drive assembly into long β-sheet-rich nanofibers. Figure 3.1a shows a TEM image of a negatively stained nanofiber sample formed from an equimolar mixture of KW+ and KW- peptides at 10mM

concentration in 10X PBS. Fibers span microns in length and striations are visible indicating fiber bundling consistent with previous observations by the peptide designers.[4] Thioflavin T (ThT) fluorescence measurements of KW+, KW-, and an equimolar mixture of KW+/KW- shown in Figure 3.1b suggest complementary interactions are kinetically favored during assembly. ThT demonstrates enhanced fluorescence emission (Figure 3.1b) upon binding to β-sheet rich peptide nanofibers and increasing fluorescence corresponds to an increase in peptide nanofibers.[13, 14] Individual aqueous solutions of KW+ and KW- peptides in 10X PBS show little fluorescence at 1 hour while the equimolar mixture of KW+ and KW- shows a higher fluorescence intensity indicating assembly. The formation of β-sheet rich nanofibers in KW+ and KW- mixtures as shown by ThT fluorescence agrees with prior FTIR measurements by King et al.[4] Fluorescence of KW+ and KW- single-peptide solutions increases over a few days indicating self-assembly over time. King et al. previously observed the formation of weak gels after several hours indicative of self-assembly at room temperature.[4] In addition, the KW- peptide exhibits a higher propensity for self-assembly than the KW+ peptide. This observation agrees with prior FTIR measurements by King et al. on single-peptide solutions of KW- and KW+ in 50 mM NaCl in which the formation of β-sheets was only observed in the KW- solution after 20 minutes of incubation.[4] Coarse-grained DMD simulations of 48 KW+ or 48 KW- chains (Figure 3.1c-d and Figure A.1 in Appendix A) were performed to evaluate the propensity for self-assembly in silico. Formation of β-barrel-like oligomers and β-sheet nanofibers during simulation is observed in Figure 3.1d and Figure A.1. Remarkably, computational simulations qualitatively agree with the observation that the KW- peptide is more prone to self-assembly than the KW+ peptide, which remains as weakly associating random coils in

simulations. Simulations of mixtures of 48 KW+ and 48 KW- chains are also consistent with the experimental observation that the mixture assembles more quickly than either of the pure peptides (Figure 3.1c).

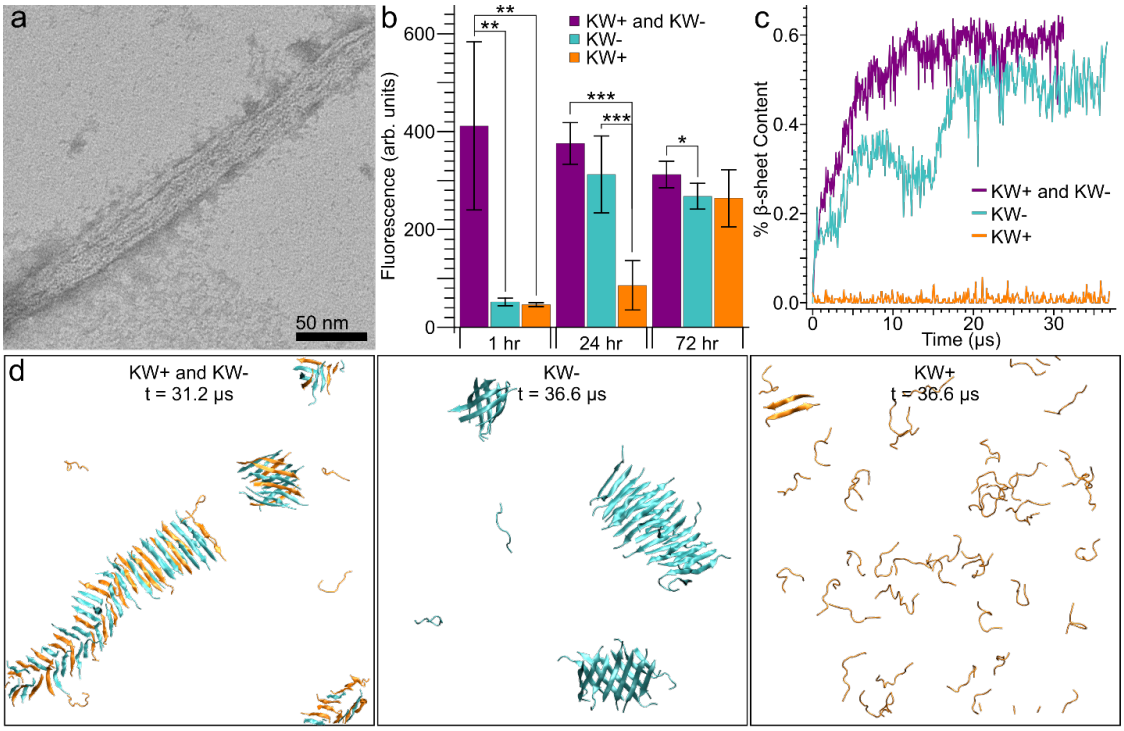

Figure 3.1 Complementary interactions are kinetically favored in KW co-assembly. a) TEM image of a negatively stained KW peptide nanofiber bundle. b) ThT fluorescence measurements of peptide solutions containing KW+ only, KW- only, and an equimolar mixture of KW+ and KW- at different assembly times. Error bars signify 95% confidence intervals, *p ≤ 0.05, **p ≤ 0.01, ***p ≤ 0.001 by Student's t-test. c) Percentage of β-sheet content over simulation time for 48 KW+ chains (orange), 48 KW- chains (cyan), and a mixture of 48 KW+ and 48 KW- chains (purple). d) Simulation snapshots of β-sheet nanofibers composed of KW+ strands (orange) and/or KW- strands (cyan) at specified times.

Solid-state NMR and computational results for equimolar mixtures of King-Webb peptides provide direct molecular-level evidence of a coassembled nanofiber structure. To

confirm this model, nearest-neighbor proximities between KW+ and KW- peptides were measured by 2-dimensional (2D) solid-state NMR. Nanofiber samples were prepared with uniform ^{13}C and ^{15}N isotopic enrichment at residue positions F3 and K9 on KW+ and E1 on KW- (Sample A). Table 1 lists samples investigated in this study with different residues isotopically labeled for NMR measurements. In Figure 3.2, 2D Dipolar Assisted Rotational Resonance (DARR) spectra of centrifuged and lyophilized nanofiber samples show measureable intermolecular contacts (off-diagonal "crosspeaks" between atoms on different residues) between KW+ and KW- peptides,[15] supporting coassembly at the molecular level. Solid colored lines in Figure 3.2 illustrate NMR peak assignments for the ^{13}C isotopically enriched amino acids determined from analysis of 1-bond correlations in the finite-pulse radio-frequency driven recoupling (fpRFDR) NMR spectra shown in Figure A.3.[16, 17] Contacts between E1 and K9 as well as E1 and F3, marked by red-blue and red-green bi-color circles, indicate inter-residue distances (distances between the closest pair of ^{13}C atoms on different residues) up to 0.6 nm between the specified amino acids. 1D slices of the DARR spectra are included in Figure A.2. Similarly, examination of the nanofibers in Figure 3.1d from a coarse-grained DMD simulation of a mixture of 48 KW+ (orange) and 48 KW- (cyan) chains shows mixing within resulting assemblies indicative of a coassembled structure.

Table 3.1 Isotopic labeling schemes for coassembled KW fibril samples

Sample	KW+ peptide	KW- peptide
A	U^{13}C and U^{15}N on F3 and K9	U^{13}C and U^{15}N on E1
B	U^{13}C and U^{15}N on F3 and K9	unlabeled
C	unlabeled	U^{13}C and U^{15}N on E1
D	unlabeled	unlabeled
E	^{13}C on CO of F3 and ^{15}N on K9	^{13}C on CO of F3
F	^{13}C on CO of F3 and ^{15}N on K9	unlabeled
G	unlabeled	^{13}C on CO of F3

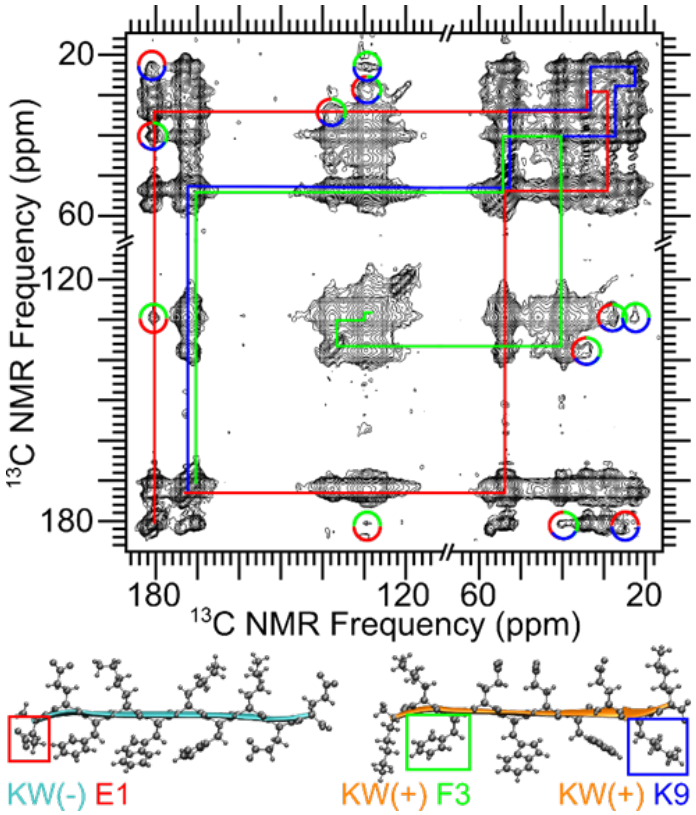

Figure 3.2 Molecular-level evidence of King-Webb peptide coassembly. 2D ^{13}C-^{13}C 500ms DARR spectrum of an isotopically enriched KW peptide nanofiber sample (Sample A). Colored lines indicate spectral assignments for isotopically enriched residues determined by 2D fpRFDR. Bi-colored circles highlight off-diagonal crosspeaks resulting from inter-residue ^{13}C-^{13}C couplings. Tri-colored circles indicate overlapping crosspeaks with signal contributions from 3 residues.

The coassembled nanofibers are composed of near stoichiometric amounts of KW+ and KW- peptides. Though equimolar solutions of the complementary peptides are mixed together to initiate assembly, it has not been previously shown whether the peptides are present in equal abundance within the final structure. To evaluate the relative amounts of each peptide incorporated into the coassembled nanofibers, a ^{13}C NMR spectrum was collected for Sample A using a method developed by Duan et. al. to produce a spectrum in which NMR peak intensities quantitatively represent relative numbers of underlying ^{13}C

sites.[18] In Figure 3.3a, peak positions (chemical shifts) uniquely attributable to the carboxyl carbon (Cδ) on glutamic acid and the γ-carbon (Cγ) on lysine sidechains are highlighted in red and blue, respectively.[19-21] The ratio of the peak areas (KW+ K9 Cγ to KW- E1 Cδ) was 1.12 ± 0.03 to 1. The presence of both peptide components at a near stoichiometric ratio further supports complementary interactions as a contributing factor in the coassembly of KW peptides.

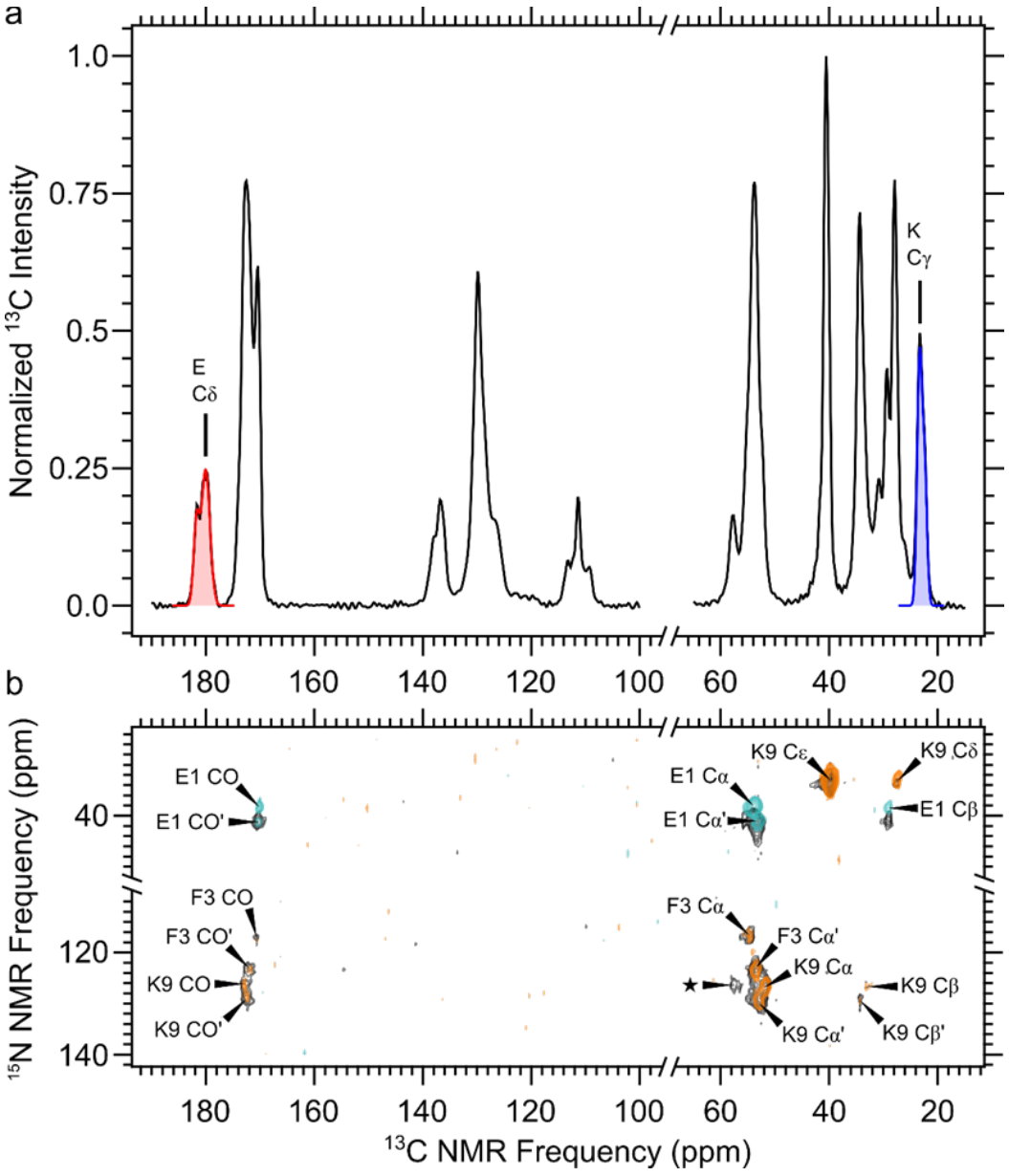

Figure 3.3 KW+ and KW- peptide coassemble stoichiometrically into β-sheet nanofibers. a) A quantitative ^{13}C spectrum of Sample A, which was isotopically labeled at E1 on KW- and F3 and K9 on KW+. Chemical shifts unique to KW+ and KW- are highlighted in blue and red, respectively. b) An overlay of 2D ^{13}C-^{15}N TEDOR spectra of Samples A, B, and C, corresponding to black, cyan, and orange contours, respectively. All three spectra were collected with 2.4 ms of ^{13}C-^{15}N mixing time. Chemical shift assignments indicated by arrows were determined by comparison with a 2D fpRFDR spectrum. Multiple assignments resulting from peak splitting are distinguished by an apostrophe (').

The NMR spectra show evidence of structural heterogeneity. The behavior is most clearly observed in NMR peak splitting, where more than one NMR peak is observed for individual isotopically enriched sites (Figure 3.3). Chemical shifts are sensitive to the local electronic environment surrounding ^{13}C sites (bond angles, arrangement of nearest-neighbor atoms) and differences in peptide nanofiber structure can result in distinct environments that produce different chemical shifts.[9, 11, 22] Figure 3.3b exhibits this behavior in ^{15}N chemical shifts, where 2D ^{13}C-^{15}N Transferred-Echo Double-Resonance (TEDOR) measurements were performed on Samples A, B, and C.[23] 2D TEDOR peaks arise because of magnetization transfer between $^{13}C/^{15}N$ that experience distance-dependent dipolar couplings.[23] Multiple spectral assignments were made for each of the enriched amino acids providing further evidence for structural heterogeneity in the coassembled King-Webb peptide nanofibers. As shown in Figure 3.3b, two peaks are observed for some near-backbone carbons and nitrogens suggesting at least 2 distinct chemical environments or structures exist. The starred NMR peak matches the peak position of a lysine α-carbon in a random coil configuration possibly indicating unassembled material in the sample.[19-21] However, other random coil signatures such as a lysine carbonyl carbon peak around 176.5ppm are not observed. Analysis of NMR peak linewidths in a ^{13}C NMR spectrum (Figure A.4) of a naturally abundant nanofiber sample, Sample D, indicate broad linewidths (~2.5 ppm). These broad linewidths are 5 times wider than those observed in protein crystals (0.5-0.6 ppm),[24] and while many factors contribute to line broadening, these linewidths are consistent with the presence of multiple local environments that would be expected from nanofibers having structural heterogeneity as indicated by the simulations.

3.3.2 Antiparallel and Parallel β-Sheets Are Detected in King-Webb Peptide Nanofibers.

Four distinct β-strand arrangements in coassembled peptide nanofibers were considered and compared using constrained 3D models of each arrangement. In Figure 3.4a, the 4 cross β-sheet structures considered consist of either parallel or antiparallel β-sheets that are stacked parallel or antiparallel to one another.[42] Each structure assumes a hydrophobic core such that the hydrophobic face of each peptide is shielded from water. In addition, each peptide component is assumed to be surrounded only by complementary peptides as nearest neighbors. We note that, when self-assembled antiparallel β-sheets stack, structures generated from different orientations of the individual sheets are typically indistinguishable. However, in the case of coassembling peptide β-sheets, the relative orientation of each peptide component between the two β-sheets is unique for antiparallel and parallel stacking leading to distinct arrangements; examine, for example, only the orange arrows for antiparallel β-sheets, stacked parallel and antiparallel, in Figure 3.4a. Figure 3.4b shows all-atom molecular models created from constrained MD simulations of 10 KW- peptides and 10 KW+ peptides arranged according to the cartoon illustrations in Figure 3.4a. Dihedral angles and hydrogen bonds were constrained according to expected angles and bond lengths for a cross-β nanofiber.

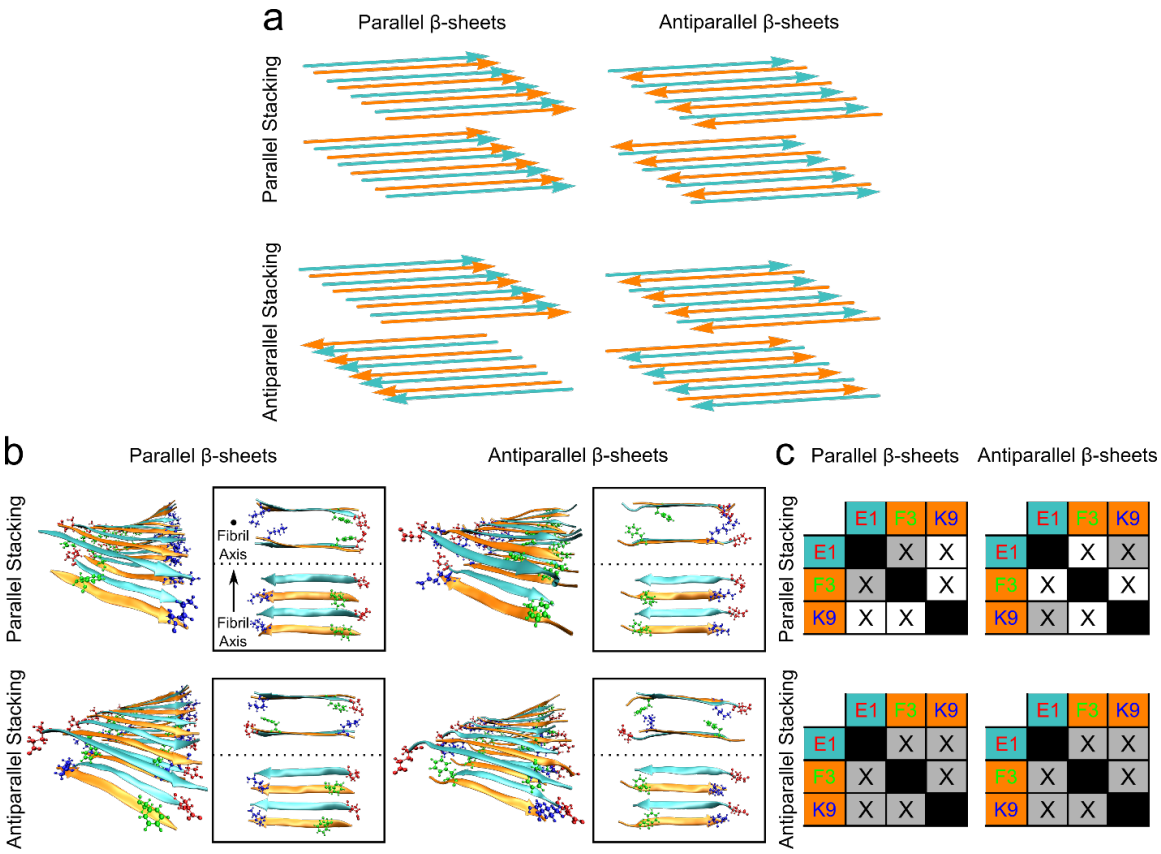

Figure 3.4 Multiple coassembled structures are possible as suggested by comparing experimental NMR results against predicted intermolecular contacts. a) Cartoon illustrations of 4 ideal coassembled β-sheet configurations considered. Colored arrows pointing from N-terminal to C-terminal represent KW+ (orange) and KW- (cyan). b) Images of all-atom molecular models for the 4 idealized coassembled β-sheet structures are shown. Cross-sectional and single sheet views are included to show predicted intermolecular contacts. c) Intermolecular contact tables based on the labeling scheme shown in part b. Gray squares depict computationally predicted intermolecular contacts. The symbol X marks experimentally observed intermolecular contacts from NMR measurements on labeled samples.

Comparison of observed 2D DARR contacts with those predicted from aforementioned molecular models suggest that the β-sheets stack antiparallel to one another. In Figure 3.4b, amino acid sidechains are drawn that correspond to the isotopically enriched amino acids in Sample A. Cross-sectional and single β-sheet views highlight the

relative orientation of isotopically enriched amino acids. Each structural arrangement produces a different set of predicted intermolecular contacts (gray squares) summarized in the DARR contact tables displayed in Figure 3.4c. NMR results indicate that all 3 intermolecular contacts (marked as 'X' in DARR contact tables) are observed. The presence of a contact between F3 and K9 labeled on the same peptide suggests that antiparallel stacking of the β-sheets occurs. Though antiparallel stacking must exist in the sample, observation of all 3 contacts does not rule out the existence of parallel stacked structures also existing because of the predicted parallel contacts are a subset of the antiparallel contacts. Thus, while the 2D DARR results provide some insight into the stacking in the nanofiber, more quantitative measurements are needed to discern between parallel and antiparallel β-sheet structures.

Dipolar recoupling NMR measurements suggest a preference toward antiparallel β-sheets, but surprisingly, a significant fraction of parallel β-sheets are present (Figure 3.5). By ^{13}C isotopically enriching only the carbonyl (CO) of F3 on KW+ and KW- peptides as shown in Figure 3.5a, we can measure distance-dependent ^{13}C-^{13}C dipolar couplings with PITHIRDS-CT to assess parallel β-sheet content in coassembled nanofiber samples.[25] In a parallel β-sheet, the ^{13}C-^{13}C interstrand spacing is expected to be 0.5 nm giving rise to a strong dipolar coupling and a strong ^{13}C signal decay in the PITHIRDS-CT experiment (Black solid line in Figure 3.5c). On the other hand, an antiparallel β-sheet structure increases the ^{13}C-^{13}C spacing to 1.0 nm leading to a weak dipolar coupling and a small decay in ^{13}C signal (Green solid line in Figure 3.5c). Results of PITHIRDS-CT experiments on Sample E suggest a mixture of strongly and weakly coupled spins. In Figure 3.5c, measurements of ^{13}C signal (black dots) rapidly decay at early recoupling times before

flattening out. Fitting by a linear combination of the solid green and black decays maps to 53.4% of the full signal decay. Therefore, the parallel β-sheet content is calculated to be 31.7% assuming each coupling is an independent event. In the same sample, KW+ peptides were isotopically enriched with ^{15}N at K9 to independently evaluate ^{15}N-^{13}C dipolar couplings. As demonstrated in Figure 3.5b, an antiparallel β-sheet arrangement results in a 0.5 nm ^{15}N-^{13}C interstrand spacing, creating a strong heteronuclear coupling. Consequently, a weak coupling is expected in the parallel β-sheet case. The $^{13}C\{^{15}N\}$REDOR experiment measures ^{13}C-^{15}N dipolar couplings, hence ^{13}C-^{15}N interstrand spacing.[26, 27] A ^{15}N-^{13}C distance of 0.5 nm is shown by the solid black curve in Figure 3.5d and generates a strong ^{13}C-^{15}N dipolar coupling. However, a ^{15}N-^{13}C distance of 1.0 nm has a weaker dipolar coupling resulting in a significantly smaller REDOR dephasing as depicted in Figure 3.5d as a solid green curve. Supporting the theory of a heterogeneous β-sheet structure, antiparallel β-sheet content is estimated to be between 56.4% and 62.2% from $^{13}C\{^{15}N\}$REDOR measurements on Sample E. While both antiparallel and parallel β-sheets are detected, it is unclear whether the two structures exist in the same nanofiber or self-sort into ideal parallel β-sheets and ideal antiparallel β-sheets.

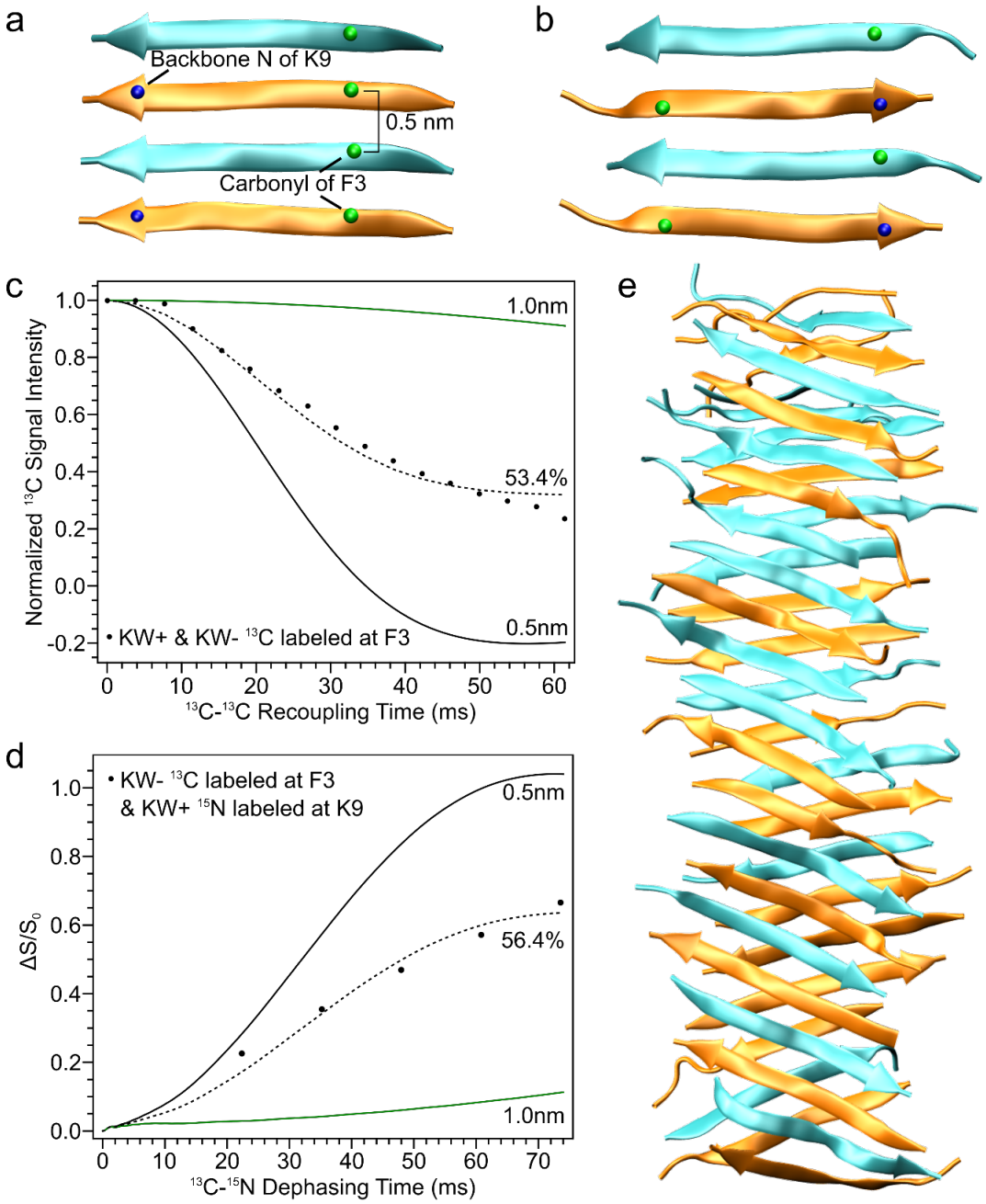

Figure 3.5 Dipolar recoupling experiments and coarse-grained DMD simulations of KW peptides show the presence of both parallel and antiparallel β-strands in coassembled nanofibers. a) Illustration of the Sample E labeling scheme in a parallel β-sheet configuration. b) Illustration of the Sample E ([1-^{13}C]F3 and [^{15}N]K9 of KW+ and [1-^{13}C]F3 of KW-) labeling scheme in an antiparallel β-sheet configuration. c) ^{13}C-^{13}C PITHIRDS-CT curves of Sample E. Solid curves represent SpinEvolution simulations of PITHIRDS-CT data from pairs of spins separated by the indicated distance. The dotted curves are a linear combination of the simulated curves corresponding to 1.0 and 0.5 nm ^{13}C-^{13}C distances, with 53.4% weighting of the 0.5nm

curve. d) $^{13}C\{^{15}N\}$REDOR spectra of Sample E. Solid curves represent calculated REDOR dephasing curves for pairs of atoms separated by the specified distance. The dotted curve represents a linear combination of the simulated REDOR curves using 56.4% weighting of the curves for 0.5nm. e) Representation of a β-sheet nanofiber observed in the coarse-grained DMD simulation.

Analysis of coarse-grained DMD simulations corroborates experimental observations of structural heterogeneity and unveils a possible minority population of out-of-register antiparallel β-sheets. Intermolecular distances between F3 CO sites on both KW+ and KW- peptides were examined in the final frames of the DMD simulations mimicking the experimental design of our PITHIRDS-CT measurements. In Figure A.5, we plot the relative distribution of F3 CO to F3 CO interstrand distances averaged over 6 simulation runs. In an ideal parallel β-sheet structure, a prominent peak would appear at 0.5 nm, whereas an antiparallel β-sheet would only show a peak at 1.0 nm or longer. The interstrand distance distribution between F3 CO sites shows a peak at 0.5 nm consistent with PITHIRDS-CT results indicating a measureable amount of parallel β-sheet structure. Calculation of the predicted parallel β-sheet content suggests 40.2% of KW peptides are oriented parallel which is higher than estimated from PITHIRDS-CT measurements. Similarly, analysis of the interstrand distance distribution between the F3 CO on KW- and K9 backbone N on KW+ qualitatively agrees with experimental REDOR results that predict antiparallel β-sheet content in the coassembled nanofiber. Simulations predict 54.0% antiparallel β-sheet content which is comparable to the experimentally measured value. Table 3.2 summarizes the computationally predicted and experimentally observed β-sheet structure content. Figure 3.5e shows a sample coassembled King-Webb nanofiber observed at the end of a DMD simulation. Computational simulations predict a preference

for the antiparallel orientation in agreement with the experimental results. Surprisingly, DMD simulations reveal the presence of out-of-register antiparallel β-sheets, which result in molecules that are not oriented perfectly perpendicular to the nanofiber axis (see Figure 3.5e). This feature is also exhibited in Figure A.5, with the peak near 0.8 nm. A small population of out-of-register antiparallel β-sheets could be consistent with the behavior observed at longer recoupling times in the PITHIRDS-CT and REDOR measurements: simulations predict plateaus in NMR intensity, which are not observed in the data. Lastly, the simulations predict that in-register parallel, in-register antiparallel, and out-of-register antiparallel β-sheets can coexist in the same nanofiber rather than self-sorting into structurally distinct fibers.

Table 3.2 Comparison of predicted and experimentally measured parallel and antiparallel β-sheet content

	DMD Simulations	NMR Measurements
Parallel β-sheets	40.2%	31.7%
Antiparallel β-sheets	54.0%	56.4%

3.3.3 Peptide Self-Association Observed in King-Webb Coassembled β-Sheets

Ideal coassembly produces a perfectly alternating $(AB)_n$ pattern within each β-sheet, where A and B correspond to KW+ and KW- peptide β-strands, respectively. In such a configuration, the β-sheet would be stabilized only through hydrogen bonding between

complementary peptide molecules. However, solid-state NMR measurements and DMD simulations show evidence of peptide self-association within the coassembled nanofiber. Specifically, self-association refers to AA or BB nearest-neighbor interactions within a β-sheet. To detect KW+ and KW- self-association, PITHIRDS-CT experiments were conducted on nanofiber samples prepared with the CO site of F3 ^{13}C-enriched on one but not both peptide components (Samples F and G). Coassembly of labeled and unlabeled peptides results in "isotopic dilution" and reduction of ^{13}C-^{13}C dipolar couplings. For coassembled nanofibers with ideal $(AB)_n$ alternation within β-sheets, the ^{13}C-labeled sites would be separated by at least 1 nm (see Figure 3.5b). Consequently, we would expect little detectable PITHIRDS-CT decays from Samples F or G. In contrast, peptide self-association would result in considerably stronger ^{13}C-^{13}C dipolar couplings and increased signal decay because nearest-neighbor ^{13}C spacing would decrease to 0.5 nm. In Figure 3.6a, an intermediate ^{13}C signal decay is observed over 61.44 ms of recoupling time for isotopically diluted samples in the PITHIRDS-CT experiment. Figure 3.6b shows a segment of coassembled nanofiber from the DMD simulation with noticeable peptide self-association along the β-sheet. In Figure A.6, we present the F3 CO to F3 CO interstrand distance distribution calculated for KW+ peptides from DMD simulations. This distribution reveals a small peak around 0.5 nm, indicating that some KW+ peptides are adjacent to other KW+ peptides in the β-sheets. Similarly, a peak near 0.5 nm is observed in the distribution for the KW- chains, indicating KW- are also found to self-associate in the peptide nanofiber. These predictions of KW- and KW+ self-association in the coassembled peptides align with experimental results detecting measureable peptide self-association in isotopically diluted nanofiber samples. These findings are consistent with

the Thioflavin T fluorescence measurements of β-sheet self-assembly in Figure 3.1b. Our measurements show that, while complementary peptide interactions between KW+ and KW- are kinetically favored, the peptides do have self-association tendencies.

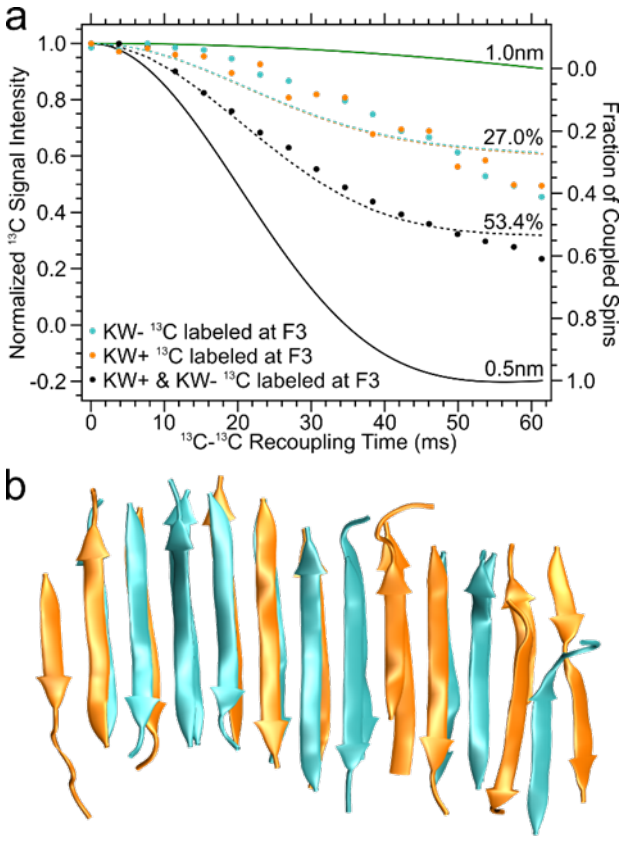

Figure 3.6 Self-association observed by NMR and coarse grained DMD simulations in coassembled King-Webb peptide nanofibers. a) ^{13}C-^{13}C PITHIRDS-CT decays measured for Sample F (orange) and Sample G (cyan). Solid curves represent SpinEvolution simulations of 2-spin PITHIRDS-CT experiments. Dotted curves represent linear combinations using 1.0 and 0.5 nm simulations. b) Representation of a β-sheet nanofiber exhibiting peptide self-association as predicted in the coarse-grained DMD simulation.

3.4 Discussion

In this work, we provide direct evidence for the molecular-level coassembly of KW+ and KW- peptides into β-sheet rich nanofibers. Although previous CD and FTIR measurements performed on King-Webb peptides indirectly indicated coassembly,[4] neither technique is capable of probing for molecular-level interactions between the two peptides within assembled nanofibers. Solid-state NMR experiments supported by computational simulations have shown molecular-level coassembly between KW+ and KW- peptides occurs. Even though individual peptides can self-assemble within days, coassembly is kinetically favored as observed by ThT fluorescence measurements and DMD simulations. Preference for coassembly results from the strong electrostatic attraction between the oppositely charged peptides. These results are consistent with previous studies of coassembling β-sheet systems based on enantiomeric peptides and oppositely charged Aβ(16-22) variants.[28, 29] Analysis of NMR chemical shift peak areas uniquely attributable to the KW+ and KW- peptides in a quantitative ^{13}C spectrum reveals a near stoichiometric ratio of the two components, emphasizing the role of complementary interactions. Electrostatic interactions are effective in promoting peptide coassembly at the molecular level while discouraging self-assembly. From our knowledge-based PRIME20 force field,[30] we know that the E sidechain has a strong electrostatic repulsion (sidechain-sidechain interaction strength, ε_{EE} = 3.15 kJ/mol) with other E sidechains. In contrast, the K sidechain, although positively charged, has a relatively weak repulsion (ε_{KK} = 0.91 kJ/mol) with other K sidechains; this behavior results from its large hydrophobic aliphatic sidechain. The KW+ peptide may have stronger resistance against self-assembly than the KW- peptide due to the stronger electrostatic repulsion from the 3 E residues in the middle of the KW+ peptide. We note that self-sorting could occur at different assembly conditions

and relative peptide ratios as shown by Webber et al. on DWDW and KWKW peptides.[31] Furthermore, the agreement between experimental results and computational predictions showcases the power of coarse-grained DMD simulations. Although simulations and experiments access different assembly timescales, it is interesting that there appears to be a basis for direct comparison of assembled structure.

Despite recent reports that peptide self-assemblies tend to be monomorphic, including recent work on RADA16-I and MAX1,[8, 12] coassembled King-Webb peptides seem to exhibit a fundamental lack of preference for a single structure. Dipolar recoupling NMR measurements designed to assess parallel and antiparallel β-strand alignments surprisingly reveal both alignments are present in coassembled samples. This mixture of β-sheet structures is supported by coarse-grained discontinuous molecular dynamics simulations. While the observation of antiparallel β-sheets matches the prediction from FTIR spectra by King et al.,[4] our site-specific measurements showed an abundance of parallel β-sheets that would be unresolved by FTIR. Estimation of the parallel and antiparallel β-sheet content from experimental results and computational predictions shows a preference for the expected antiparallel β-sheet structure (Table 3.2). Computational simulations show a mixture of β-strands aligned antiparallel and parallel along the same β-sheet, indicating that the addition of peptides in either orientation is favorable. Observation of this predicted behavior would be difficult to resolve by solid-state NMR. In addition, structure predictions from computational simulations reveal antiparallel β-sheets with a registry shift of 2 amino acids. Nanofibers produced from β-strands with a registry shift have a reduced number of hydrogen bonds, produce flexible peptide ends, and are skewed from the fiber axis (Figure 3.5e). Though there is no direct experimental evidence for this

structural feature, the presence of antiparallel β-sheets with a registry shift is consistent with the increased PITHIRDS-CT signal decay and REDOR dephasing observed at longer recoupling times. We note that the presence of multiple structures in a single sample is rather unique. Though many self-assembling peptides can be assembled into various structures, the resulting polymorphic peptides generally produce nanofibers of a single favored structure for a given set of assembly conditions.[19-21] In contrast, King-Webb peptide nanofibers surprisingly exhibit a mixture of several structures for a single assembly condition. Fast assembly kinetics may play a role in this structural heterogeneity though further studies would be needed. By combining computational simulations and experimental techniques, we have produced a detailed structural analysis of a highly heterogeneous coassembled peptide nanofiber that would be difficult to assess with a singular technique.

Remarkably, self-association of KW+ and KW- peptides occurs in the coassembled nanofiber samples. ThT fluorescence measurements showed that coassembly is kinetically favored over self-assembly, but self-assembly occurs over 72 hours consistent with the time scale that KW+ and KW- peptides can self-associate into β-sheets. Evidence of the peptide self-association tendency was observed in the coassembled nanofibers with dipolar recoupling NMR measurements on samples isotopically enriched on one peptide component at a time (Figure 3.6). These results are consistent with prior observations on coassembled nanotubes of Aβ(16-22) derivatives where NMR measurements indicated a mixture of self-associated and complementary peptide leaflets.[29] Given the high ionic strength of the assembly buffer (10X PBS), charge screening may facilitate KW+ and KW- self-association. Several self-assembling peptides have been shown to form gels upon

adjusting the solution's ionic strength.[32-34] Notably, the positively-charged MAX1 peptide forms β-hairpins that further assemble into β-sheet nanofibers in aqueous solution.[12] Also, P_{11}-4 and P_{11}-5 peptides, predecessors of the King-Webb peptides, exhibit a strongly pH-dependent self-assembly mechanism.[5] In context, it is not surprising that counterions modulate effective interactions between like-charged sidechains. Again, computational simulations are able to capture this non-ideal assembly behavior, providing an accurate view into the structural possibilities within coassembled peptide nanofibers.

While charge complementarity produces peptides that exhibit coassembly behavior, the King-Webb design does not produce well-controlled coassembled nanofiber structures. Long-range electrostatic interactions in charge-complementary peptide systems may reduce the energy difference in parallel and antiparallel β-sheet structures allowing peptides in either orientation to add to the fiber end. Electrostatic forces may also affect the assembly pathway of charge-complementary peptides. Hydrogen-bonding and hydrophobic interactions drive β-sheet formation in self-assembling peptides and contributions from charged residues can cause assembly to proceed along a different pathway dominated by charge complementarity.[10, 31] Coexistence of multiple peptide arrangements within the coassembled nanofiber alludes to the possibility that peptides similar to the King-Webb peptides as long as favorable electrostatic interactions are formed. This heterogeneity highlights the challenge in designing selectively coassembling β-sheet peptides. These peptides could belong to a family of coassembling peptides capable of coassembling with similarly patterned partners. While this lack of a strong preference for a specific arrangement may be desirable, we suggest that design of coassembling

peptides for more specific structures would aid in understanding the principles of creating coassembled nanofibers.

3.5 Conclusions

The peptides introduced by from King et al. represent a successful design of a primarily coassembled peptide nanofiber. Molecular-level coassembly was evaluated with computational simulations, biophysical measurements, and solid-state NMR spectroscopy. While charge-complementarity and the employed sidechain patterning do confer selective coassembly over self-assembly, analysis of the molecular-level structure reveals a lack of precise control over local intermolecular organization. This level of structural precision may be sufficient for certain biotechnological applications such as a cell-culture scaffold, but as we seek to increase our ability to manipulate biological systems with synthetic materials, higher molecular-level precision may be desired. Next-generation designs will need to turn towards hydrophobic interactions, lock-and-key mechanisms, and sidechain complementarity to introduce structural specificity as seen in many self-assembling peptide systems and folded proteins.[10, 35] Coarse-grained simulations may enable researchers to rapidly iterate through possible designs to identify well-controlled and highly selective coassembling peptide designs similar to the computational work by Baker et al. to produce orthogonal coiled-coil oligomers.[36, 37] Simulations can be combined with solid-state NMR techniques to reveal highly-resolved structural details to verify and validate new coassembling peptide designs as shown in this study. Structural insights from these combined studies refine our understanding of sequence to structure relationships necessary in the design process. The ability to exhibit fine control over peptide nanostructure will propel the design of supramolecular biomaterials beyond the designs in nature.

3.6 Materials and Methods

For general methods, please refer to Chapter 2. Content presented below indicate a deviation from the standard protocols previously mentioned.

3.6.1 King-Webb Peptide Material

Unlabeled KW+ and KW- peptides were purchased from CPC Scientific, Inc. (Sunnyvale, CA). Labeled peptides were also purchased from CPC Scientific, Inc. synthesized using uniformly or partially ^{13}C and/or ^{15}N enriched amino acids supplied by Cambridge Isotope Laboratories, Inc.

3.6.2 Standard Hydrogel Preparation

All hydrogel samples were prepared by initially dissolving KW+ and KW- peptides in 10X PBS to produce 10mM solutions of single peptides. Equimolar mixtures of the KW+ and KW- peptide solutions were vortexed for 1 min and allowed to assemble. Initial assembly occurred within a few minutes, but samples were allowed to mature overnight for all samples. Isotopically labeled peptide samples were prepared according to labeling schemes in Table 3.1. Samples were centrifuged at 17.0 x g for 5 min. Supernatant was removed and fresh DI water added before resuspension. This wash cycle was repeated 2 more times. Solutions were flash-frozen in liquid nitrogen before lyophilization overnight.

3.6.3 Solid-State NMR Measurements

REDOR measurements of lyophilized King-Webb peptide nanofibers were performed using a 14.1 T Bruker Avance spectrometer with a 4 mm Bruker HXY MAS

probe. To ensure MAS and RF heating did not denature the samples, the cooling and spinning air exit temperature was maintained below -1 °C. ^{13}C (150.8 MHz) and ^{15}N (60.8 MHz) CPMAS spectra before and after REDOR experiments sample integrity during the experiment. The sum of center and sideband peak heights is used to calculate REDOR data points.

3.6.4 Dipolar Recoupling Spin Simulations

Calculation of signal decay curves from PITHIRDS-CT experiments were produced by using SpinEvolution NMR simulation software.[42] Simulations were run with 2 nuclear spins set at 5.0 Å or 10.0 Å distances. Attenuated decay was quantified using linear combinations of simulated PITHIRDS-CT decay curves at 5.0 Å and 10.0 Å to fit experimental spectra.

A single ^{15}N spin in the presence of one ^{13}C spin spaced 0.5 or 1.0 nm apart were simulated for REDOR analysis.[27] Contributions from naturally abundant carbonyl carbons and ^{15}N dephasing from these carbons were included.[43]

3.6.5 Transmission Electron Microscopy (TEM)

Coassembled KW+ and KW- nanofibers were deposited onto 400 mesh lacey carbon-coated Cu electron microscopy grids (TED Pella, INC.) and strained with 1 wt% uranyl acetate. TEM images were taken using a Hitachi HT-7700 electron microscope at an accelerating voltage of 80 keV.

3.6.6 All-Atom Models of Ideal β-Sheet Structures

Idealized all-atom models of 4 possible β-sheet nanofiber structures were built to aid interpretation of intermolecular contacts observed by solid-state NMR. All β-sheet models were constructed using NAMD molecular dynamics and VMD software.[44-46] Initial models of the KW+ and KW- peptides were individually created in VMD with the molefacture plugin. KW+ and KW- monomers were manipulated depending on the β-sheet structure and stacking and repeated along the fiber axis using Mathematica to produce a 2 β-sheets with 10 units each (5 KW+ and 5 KW-) which were stacked to form a hydrophobic core. Using NAMD molecular dynamics software, artificial dihedral angle and hydrogen bond constraints were introduced and the constrained structure was energy minimized for 10 ps in implicit solvent. Then, the temperature was increased from 0 K to 500 K followed by cooling to 300 K in 10 K increments with 10 ps simulation time per step in implicit solvent. Following a 25 ps equilibration period, the two β-sheets were stacked into a 2-layer nanofiber by artificially constraining intersheet distances. The constrained bilayer nanofiber structure was energy minimized for 10 ps, heated from 0 to 300 K in 10 K per 10 ps increments before a final equilibration period of 20 ps.

3.6.7 Coarse Grained Discontinuous Molecular Dynamics Simulations

In this work, we performed large-scale DMD/PRIME20 simulations to evaluate the spontaneous aggregation propensities and coassembled structures of King-Webb peptides. All of the simulations are carried out for 30-36 μs in the canonical (NVT) ensemble at a peptide concentration of 20 mM. The Andersen thermostat is implemented to maintain the simulation system at a constant temperature.[47] For the peptide coassembly cases, 48 A and 48 B peptides are initially randomly placed in a cubic box with a length of 200.0 Å, corresponding to a peptide concentration of 20 mM. We set the reduced temperature T* of

the simulations to be 0.19, which corresponds to 319 K in real temperature unit.[48] For the peptide self-assembly cases, single peptide species system containing either 48 A or 48 B are kept at the same concentration as in the coassembly cases by reducing the cubic simulation box length to 159.0 Å. The simulation temperature is also kept the same as in the coassembled King-Webb simulations. We repeat the simulation three times for each of the systems mentioned above. Simulations are run at the previously specified temperature and concentration to reduce aggregation lag phases and nucleation barriers.

3.7 References

1. M. J. Pandya, G. M. Spooner, M. Sunde, J. R. Thorpe, A. Rodger and D. N. Woolfson, Biochemistry, 2000, 39, 8728-8734.

2. S. Baxter, Trans. Faraday Society, 1943, 39, 0207-0213.

3. A. Aggeli, M. Bell, L. M. Carrick, C. W. G. Fishwick, R. Harding, P. J. Mawer, S. E. Radford, A. E. Strong and N. Boden, J. Am. Chem. Soc., 2003, 125, 9619-9628.

4. P. J. King, M. Giovanna Lizio, A. Booth, R. F. Collins, J. E. Gough, A. F. Miller and S. J. Webb, Soft Matter, 2016, 12, 1915-1923.

5. S. Kyle, S. H. Felton, M. J. McPherson, A. Aggeli and E. Ingham, Advanced Healthcare Materials, 2012, 1, 640-645.

6. G. Zandomeneghi, M. R. H. Krebs, M. G. McCammon and M. Fändrich, Protein Sci., 2004, 13, 3314-3321.

7. S. Zhang, T. Holmes, C. Lockshin and A. Rich, Proc. Natl. Acad. Sci. U. S. A., 1993, 90, 3334-3338.

8. A. R. Cormier, X. Pang, M. I. Zimmerman, H. X. Zhou and A. K. Paravastu, ACS Nano, 2013, 7, 7562-7572.

9. B. H. Meier, R. Riek and A. Böckmann, Trends Biochem. Sci., 2017, 42, 777-787.

10. J. Park, B. Kahng and W. Hwang, PLoS Comp. Biol., 2009, 5, e1000492-e1000492.

11. R. Kodali and R. Wetzel, Curr. Opin. Struct. Biol., 2007, 17, 48-57.

12. K. Nagy-Smith, E. Moore, J. Schneider and R. Tycko, Proceedings of the National Academy of Sciences, 2015, 112, 9816-9821.

13. M. Biancalana and S. Koide, Biochim. Biophys. Acta, 2010, 1804, 1405-1412.

14. H. Naiki, K. Higuchi, M. Hosokawa and T. Takeda, Anal. Biochem., 1989, 177, 244-249.

15. K. Takegoshi, S. Nakamura and T. Terao, Chem. Phys. Lett., 2001, 344, 631-637.

16. Y. Ishii, The Journal of Chemical Physics, 2001, 114, 8473-8483.

17. A. E. Bennett, C. M. Rienstra, J. M. Griffiths, W. Zhen, P. T. L. Jr. and R. G. Griffin, The Journal of Chemical Physics, 1998, 108, 9463-9479.

18. P. Duan and K. Schmidt-Rohr, J. Magn. Reson., 2017, 285, 68-78.

19. D. S. Wishart, Prog Nucl Mag Res Sp, 2011, 58, 62-87.

20. E. L. Ulrich, H. Akutsu, J. F. Doreleijers, Y. Harano, Y. E. Ioannidis, J. Lin, M. Livny, S. Mading, D. Maziuk, Z. Miller, E. Nakatani, C. F. Schulte, D. E. Tolmie, R. K. Wenger, H. Y. Yao and J. L. Markley, Nucleic Acids Res., 2008, 36, D402-D408.

21. D. Wishart and B. Sykes, J. Biomol. NMR, 1994, 4, 171-180.

22. J. R. Lewandowski, P. C. A. van der Wel, M. Rigney, N. Grigorieff and R. G. Griffin, J. Am. Chem. Soc., 2011, 133, 14686-14698.

23. C. P. Jaroniec, C. E. MacPhee, V. S. Bajaj, M. T. McMahon, C. M. Dobson and R. G. Griffin, Proc. Natl. Acad. Sci. U.S.A., 2004, 101, 711-716.

24. S. G. Zech, A. J. Wand and A. E. McDermott, J. Am. Chem. Soc., 2005, 127, 8618-8626.

25. R. Tycko, J. Chem. Phys., 2007, 126, 064506-064506.

26. C. P. Jaroniec, B. A. Tounge, C. M. Rienstra, J. Herzfeld and R. G. Griffin, J. Magn. Reson., 2000, 146, 132-139.

27. J. M. Goetz and J. Schaefer, J. Magn. Reson., 1997, 127, 147-154.

28. R. J. Swanekamp, J. T. M. DiMaio, C. J. Bowerman and B. L. Nilsson, J. Am. Chem. Soc., 2012, 134, 5556-5559.

29. S. Li, A. K. Mehta, A. N. Sidorov, T. M. Orlando, Z. Jiang, N. R. Anthony and D. G. Lynn, J. Am. Chem. Soc., 2016, 138, 3579-3586.

30. M. Cheon, I. Chang and C. K. Hall, Proteins: Structure, Function, and Bioinformatics, 2010, 78, 2950-2960.

31. J. K. Sahoo, M. A. VandenBerg, E. E. Ruiz Bello, C. D. Nazareth and M. J. Webber, Nanoscale, 2019, 11, 16534-16543.

32. F. Koch, M. Müller, F. König, N. Meyer, J. Gattlen, U. Pieles, K. Peters, B. Kreikemeyer, S. Mathes and S. Saxer, Royal Society open science, 2018, 5, 171562-171562.

33. L. M. Carrick, A. Aggeli, N. Boden, J. Fisher, E. Ingham and T. A. Waigh, Tetrahedron, 2007, 63, 7457-7467.

34. M. R. Caplan, P. N. Moore, S. Zhang, R. D. Kamm and D. A. Lauffenburger, Biomacromolecules, 2000, 1, 627-631.

35. M. R. Sawaya, S. Sambashivan, R. Nelson, M. I. Ivanova, S. A. Sievers, M. I. Apostol, M. J. Thompson, M. Balbirnie, J. J. W. Wiltzius, H. T. McFarlane, A. O. Madsen, C. Riekel and D. Eisenberg, Nature, 2007, 447, 453-457.

36. S. E. Boyken, Z. Chen, B. Groves, R. A. Langan, G. Oberdorfer, A. Ford, J. M. Gilmore, C. Xu, F. DiMaio, J. H. Pereira, B. Sankaran, G. Seelig, P. H. Zwart and D. Baker, Science, 2016, 352, 680-687.

37. Z. Chen, S. E. Boyken, M. Jia, F. Busch, D. Flores-Solis, M. J. Bick, P. Lu, Z. L. VanAernum, A. Sahasrabuddhe, R. A. Langan, S. Bermeo, T. J. Brunette, V. K.

Mulligan, L. P. Carter, F. DiMaio, N. G. Sgourakis, V. H. Wysocki and D. Baker, Nature, 2019, 565, 106-111.

38. T. Gullion and J. Schaefer, Journal of Magnetic Resonance (1969), 1989, 81, 196-200.

39. M. Rance and R. A. Byrd, Journal of Magnetic Resonance (1969), 1983, 52, 221-240.

40. N. Sinha, K. Schmidt-Rohr and M. Hong, J. Magn. Reson., 2004, 168, 358-365.

41. B. M. Fung, A. K. Khitrin and K. Ermolaev, J. Magn. Reson., 2000, 142, 97-101.

42. M. Veshtort and R. G. Griffin, J. Magn. Reson., 2006, 178, 248-282.

43. G. M. Bernard, M. Miskolzie, G. Kotovych and R. E. Wasylishen, Can. J. Chem., 2004, 82, 1554-1563.

44. M. T. Nelson, W. Humphrey, A. Gursoy, A. Dalke, L. V. Kalé, R. D. Skeel and K. Schulten, The International Journal of Supercomputer Applications and High Performance Computing, 1996, 10, 251-268.

45. J. C. Phillips, R. Braun, W. Wang, J. Gumbart, E. Tajkhorshid, E. Villa, C. Chipot, R. D. Skeel, L. Kalé and K. Schulten, J. Comput. Chem., 2005, 26, 1781-1802.

46. W. Humphrey, A. Dalke and K. Schulten, J. Mol. Graphics, 1996, 14, 33-38.

47. B. J. Alder and T. E. Wainwright, The Journal of Chemical Physics, 1959, 31, 459-466.

48. H. C. Andersen, The Journal of Chemical Physics, 1980, 72, 2384-2393.

CHAPTER 4. STRUCTURAL ANALYSIS OF COASSEMBLED CATCH PEPTIDE NANOFIBERS*[2]

4.1 Overview of Chapter

In the previous chapter, the coassembling King-Webb peptide nanofibers were evaluated by solid-state NMR and DMD simulations revealing a heterogeneous mixture of β-sheet structures. It is unclear whether other charge-complementary peptide pairs exhibit this structural heterogeneity as well. In this Chapter, we consider a related peptide pair, CATCH peptides, based on a different approach towards the concept of charge-complementary amino acid sequences. The same combined experimental and computational approach used in Chapter 3 is applied here.

4.2 Introduction:

Within the class of selectively coassembling β-sheet peptides, two distinct approaches to charge-complementary sequences have emerged. In general, peptides will disfavor self-assembly as long as the molecules have an overall net charge, but complementary electrostatic attraction between oppositely charged peptide chains will promote coassembly. King-Webb peptides have a mixture of positively and negatively residues, but an imbalance of the two residue types results in an overall net charge preventing self-assembly. The King-Webb peptide's predecessors, the P_{11}-4 and P_{11}-5,

[2] Portions of this chapter have been adapted and reproduced from Shao, Q., Wong, K. M., Seroski, D. T., Wang, Y., Liu, R. Paravastu, A. K., Hudalla, G. A., Hall, C. K. "Anatomy of a selectively coassembled β-sheet peptide nanofiber" *Proceedings of the National Academy of Sciences,* 2020, **9**, 4710-471. Copyright 2020 National Academy of Sciences.

peptides follow this principle.[1] In contrast, "CATCH+" (Ac-QQKFKFKFKQQ-Am) and "CATCH-" (Ac-EQEFEFEFEQE-Am) developed by Seroski et al. are patterned with only positive residues or only negative residues resulting in a high overall charge.[2] This sequence design follows another charge-complementary pair, the P_{11}-13 and P_{11}-14 peptides.[3] As shown in the previous chapter, King-Webb peptides align in both parallel and antiparallel orientations and exhibit significant peptide self-assembly within a single β-sheet. It is not known whether this behavior is inherent to all coassembling β-sheet designs. Thus, we apply the same solid-state NMR and coarse-grained DMD analysis to evaluate coassembled CATCH peptide nanofibers to better understand structural heterogeneity in the charge complementary peptide sequences.

Prior studies on the CATCH+ and CATCH- peptides focused on installing superfolding green fluorescent protein (GFP) onto β-sheet rich nanofibers with limited structural characterization the peptide nanofiber structure.[2] Circular dichroism of single-peptide solutions of CATCH- and CATCH+ indicate the peptides resist self-assembly. Equimolar mixtures of CATCH+ and CATCH- show a strong β-sheet signal at total peptide concentrations above 320 μM in 1X PBS solutions.[2] These results are corroborated by a strong increase in thioflavin T fluorescence emission. When CATCH- peptides covalently fused to the GFP are incorporated into mixtures of CATCH+ and CATCH- peptides, β-sheet-rich nanofibers form with the protein of interest immobilized onto the surface of the peptide nanofibers without any noticeable change in structure.[2] These results suggest that CATCH+ and CATCH- peptides coassemble into β-sheet-rich nanofibers and the proteins covalently attached to the peptides are successfully fixed onto the nanofibers. However, there is no evidence that these peptide pattern into the hypothesized coassembled

antiparallel β-sheet structure. Similar to the King-Webb peptides, CATCH+ and CATCH- peptides are assumed to pattern into $(AB)_n$ alternating β-sheets though there is no direct evidence for this patterning.

Here we present a comprehensive investigation into the alignment and patterning of CATCH+ and CATCH- peptides within coassembled amyloid-like β-sheet nanofibers. Solid-state nuclear magnetic resonance (NMR) measurements are used to determine secondary structure and inter-strand contacts between peptides within coassembled nanofibers. Experimental evidence of molecular-level coassembly into β-sheet-rich nanofibers are corroborated by discontinuous molecular dynamics (DMD) simulations of a large (96-peptide) system of CATCH+ and CATCH- peptides. Off-center ^{13}C and ^{15}N isotopic labeling of the CATCH+ and CATCH- peptides indicate a conglomerate of antiparallel and parallel aligned β-strands within the coassembled peptide nanofibers. CATCH nanofibers assembled *in silico* show this mixture of β-sheet alignments can exist within a single β-sheet. ^{13}C-^{13}C PITHIRDS-CT measurements of isotopically diluted nanofiber samples reveal a significant amount of AA and BB peptide self-association. Lyophilization of single-peptide CATCH solutions produces β-sheet-rich samples that exhibit strong ^{13}C-^{13}C couplings in PITHIRDS-CT measurements demonstrating that self-association is possible despite the high overall charges of each peptide. The structural heterogeneity observed in coassembled CATCH peptide nanofibers is similar to that observed in King-Webb nanofibers suggesting this behavior is inherent to charge-complementary β-sheet peptide pairs.

4.3 Results:

4.3.1 CATCH(+) and CATCH(-) exhibit molecular-level coassembly

Data from simulations and experiments in Figure 4.1 demonstrate molecular-level coassembly of CATCH(+) and CATCH(-) peptides into β-sheets. Here, we refer to the CATCH(+) peptide as "A" and the CATCH(-) peptide as "B" for simplicity. Ten DMD simulations were run at T* = 0.2 (equivalent to 342 K) for 16 μs, using the PRIME20 model. Each simulation started with a mixture of 48 A and 48 B molecules in random coil configurations at a concentration of 20 mM. Representative snapshots of the simulations at 0, 3.2, 6.4, and 16 μs depict the coassembly process (Figure 4.1A). Ordered aggregates containing both A and B emerge as early as 3.2 μs, but they are β-barrel structures not amyloid-like structures. As the simulation progresses, more and more peptides join the ordered aggregates. At 6.4 μs, an amyloid-like structure can be seen in addition to several β-barrel structures. The amyloid-like structure grows with time and by 8 μs (not shown) differentiates itself significantly from the β-barrel structures. By 16 μs, nearly 90% of peptides have aggregated into two-component amyloid or β-barrel structures. The simulation kinetics for this run is described in APPENDIX B and shown in Fig. B.1. The β-barrel structures do not convert to amyloid or serve as seeds for amyloid formation, suggesting that they are off-pathway for fibril formation. However, the simulation time scale of 16 μs is orders of magnitude smaller than the experimental time scale, so simulations cannot be used to predict whether or not the β-barrels are a kinetically trapped metastable state or transient in real-world settings.

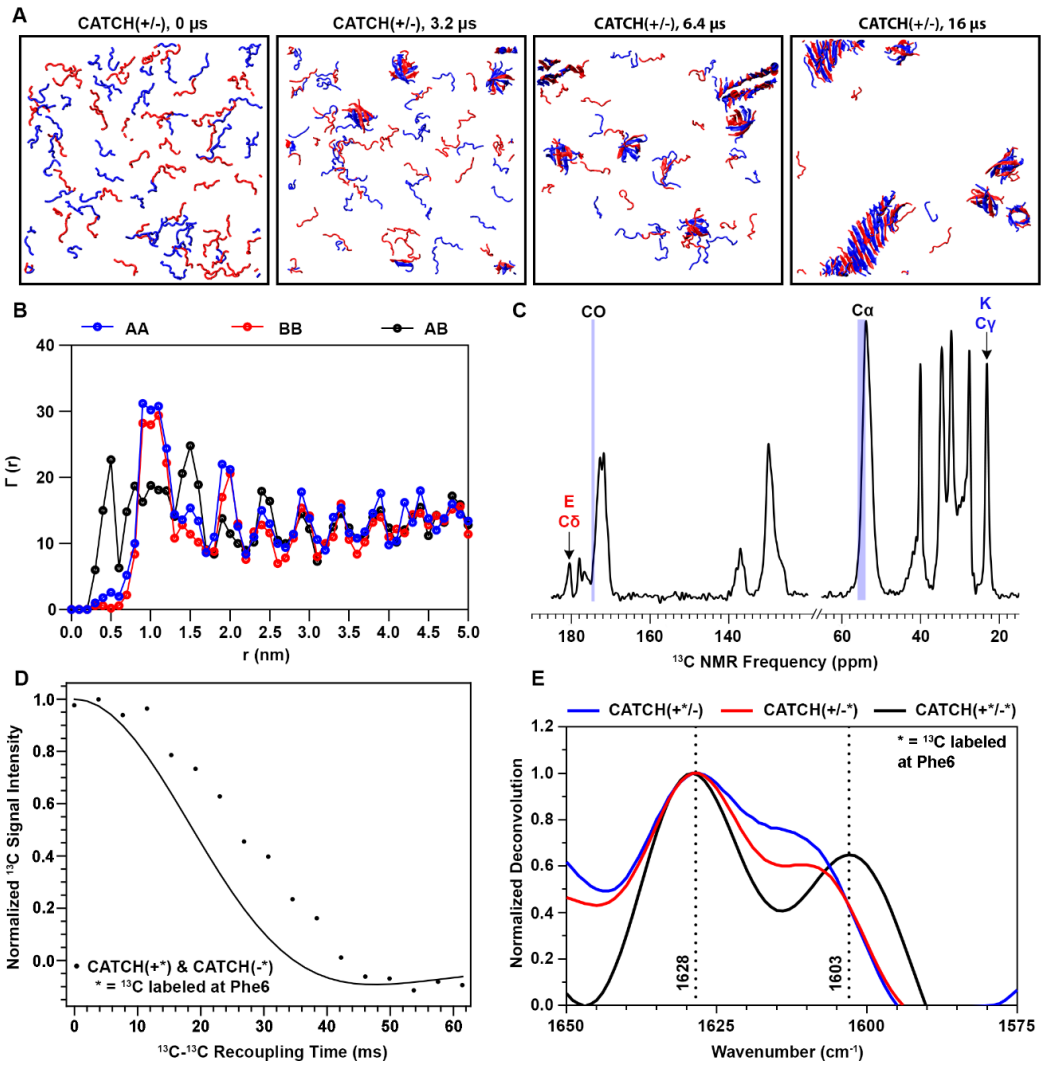

Figure 4.1 Computational simulations and biophysical measurements of an equimolar CATCH(+) and CATCH(-) mixture show coassembly. (A) DMD/PRIME20 simulations of a mixture of 48 CATCH(+) and 48 CATCH(-) peptides at 20mM concentration. Snapshots at 0, 3.2, 6.4, and 16 μs are presented. (B) Γ_AB (r), Γ_AA (r), and Γ_BB (r), defined in the text as computationally-predicted average distributions of A or B central atoms as a function of distance r from centrals atoms within peptide A or B. (C) ^{1}H-^{13}C CPMAS spectra of a CATCH(+/-) nanofiber sample. (D) PITHIRDS-CT decay curve of a CATCH nanofiber sample ^{13}C labeled on both CATCH(+) and CATCH(-) on the carbonyl C of Phe6. The solid black curve corresponds to the predicted signal decay in the PITHIRDS-CT experiment from a nuclear spin simulation of eight ^{13}C atoms along an ideal coassembled antiparallel β-sheet. (E) FTIR spectra of equimolar mixtures of labeled CATCH(+) and CATCH(-) (black), labeled CATCH(+) and unlabeled CATCH(-) (blue), and unlabeled CATCH(+) and CATCH(-) (red) at 10 mM in 1x PBS.

Quantitative analysis of the organization of A and B in the final configurations of the DMD simulations indicates that the majority of the peptides are arranged in an ordered alternating ABAB pattern. Figure 4.1B shows the numbers of AB, AA, and BB neighbors, Γ_AB (r), Γ_AA (r), and Γ_BB (r), as a function of the distance r between the Phe6 carbonyl C atoms (central atoms) on the peptides in the final aggregated structure averaged over the 10 independent simulations. Choosing the central atom as a reference makes analysis of peptide organization insensitive to the relative directions of adjacent β-strands (parallel or antiparallel) within each β-sheet. The high intensity peak for Γ_AB (r) at r = 0.5 nm (the first-neighbor distance between peptides) demonstrates that the majority of A molecules are next to B molecules, and vice versa, in the final aggregated structures. Further, the peaks for Γ_AA (r) and Γ_BB (r) at r = 1.0 nm (the second-neighbor distance) demonstrate that the peptides are primarily organized into ABA or BAB configurations. The non-zero values for Γ_AA and Γ_BB when r < 1.0 nm indicate, however, that some of the A and B molecules do sit next to their own kind in the final structure, as will be discussed in a later section.

FTIR and solid-state NMR measurements demonstrate that structures rich in β-sheets are formed in equimolar mixtures of A and B at comparable concentrations to those used in simulations. We observed up-field shifts in ^{13}C natural abundance solid-state NMR peak frequencies for the carbonyl carbon (CO) and α-carbon (Cα) of Gln, Lys, Glu, and Phe relative to reference peptides in random-coil configurations (Figure 4.1C), which indicate that A and B aggregate into a β-sheet secondary structure.[5, 6] A centrifuge pellet of coassembled A and B in which each peptide was labeled with ^{13}C at its central atom (CO site of Phe6) yielded a strong ^{13}C decay in PITHIRDS-CT NMR measurements (Figure

4.1D), which indicates dipolar couplings between ^{13}C labeled site.[7] This decay maps to simulations of 8 ^{13}C spins spaced as predicted by an antiparallel β-sheet structure, with ^{13}C-^{13}C distances of either 0.49 nm or 0.65 nm. Likewise, the FTIR spectrum of an equimolar mixture of A and B has a strong maximum at 1620 cm^{-1} (Figure B.2), which is within the amide I region and indicative of peptides in a β-strand conformation.

FTIR and solid-state NMR measurements also indicate that A and B are coassembled. In a centrifuge pellet of coassembled A and B, we observed ^{13}C natural abundance solid-state NMR signals that are uniquely attributable to the Lys and Glu residues which are exclusive to CATCH(+) or CATCH(-), respectively (Figure 4.1C), indicating that both peptides are present in the sample.[5] Likewise, in the deconvoluted FTIR spectrum of an equimolar mixture of ^{13}C-labeled A and B, the amide I peak was split into maxima at 1628 and 1603 cm^{-1} (Figure 4.1E), similar to a prior report of enantiomeric peptide mixtures with a single ^{13}C label on each peptide4. In contrast, the deconvoluted FTIR spectra of equimolar mixtures of labeled A and unlabeled B, as well as unlabeled A and labeled B, had maxima at 1628 and 1610 cm^{-1}. The maximum at 1603 cm^{-1} in mixtures of labeled A and B is attributed to vibrational coupling between ^{13}C atoms in neighboring hydrogen-bonded β-strands, whereas the higher frequency maximum at 1610 cm^{-1} in mixtures of labeled and unlabeled peptides is likely due to the presence of ^{13}C labeled strands with interspersed ^{12}C strands. The latter would only occur if unlabeled A is coassembled with labeled B, or vice versa, as has been reported recently for mixtures of $^{12}C/^{13}C$-labeled amyloid-β.[8] Collectively, these experimental results validate the computational observations that A and B coassemble into two-component β-sheet structures rather than self-sort.

4.3.2 CATCH(+) and CATCH(-) peptides resist self-assembly

DMD/PRIME20 simulations of single-component systems of CATCH(+) or of CATCH(-) peptides show little evidence of aggregation. Representative snapshots depict DMD/PRIME20 simulations of 96 CATCH(+) and of 96 CATCH(-) peptides at 16 μs (Figure 4.2A). The peptides are in random coil configurations at this time point. CATCH(-) peptides remain dispersed throughout the entire simulation run, whereas some instances of unstable interactions are observed in snapshots of CATCH(+) peptide simulation runs (Figure B.3). These computational observations are consistent with prior experimental data demonstrating that individual CATCH peptides resist self-assembly, albeit at much lower concentrations than those used in the models reported herein.[9]

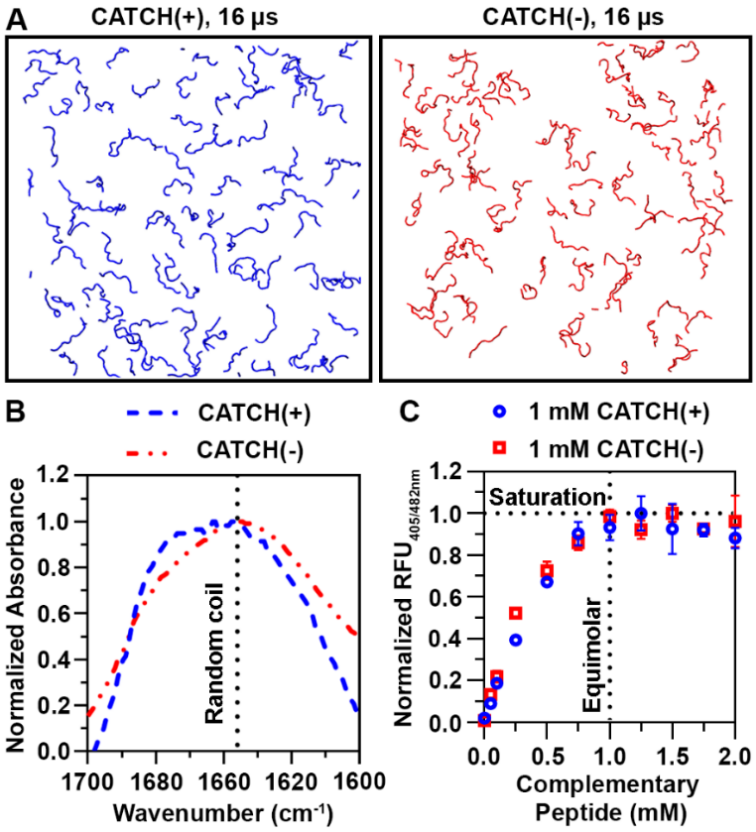

Figure 4.2 Complementary interactions are necessary for assembly. (A) Snapshots of DMD/PRIME20 simulations of a system containing 96 CATCH(+) peptides (blue) and a system containing 96 CATCH(-) peptides (red) at 16 µs. (B) FTIR spectra of 20 mM CATCH(+) and CATCH(-). (C) Thioflavin T fluorescence measurements at varying CATCH(+):CATCH(-) ratios indicating saturation at equimolar mixtures.

Biophysical measurements demonstrate that CATCH(+) and CATCH(-) do not self-associate in solution at comparable concentrations to those used in simulations. FTIR spectra of solutions containing only CATCH(+) or CATCH(-) have broad peaks at ~1645 cm^{-1} that are consistent with an unstructured and predominantly random coil state (Figure 4.2B). Likewise, solutions containing only CATCH(+) or CATCH(-) did not increase the fluorescence emission of Thioflavin T (ThT) a dye that emits increased fluorescence when bound to β-sheet structures (Figure B.4A). In contrast, adding increasing amounts of

CATCH(-) to a 1 mM CATCH(+) solution increased ThT fluorescence emission until the molar ratio of CATCH(+) to CATCH(-) approached unity (Figure 4.2C). CATCH(+) present in a molar excess relative to CATCH(-) produced no further increase in ThT fluorescence suggesting that coassembly of CATCH peptides proceeds until molar equivalency is reached, at which point excess peptide remains unassembled (Figure 4.2). Similar behavior was observed when the concentration of CATCH(-) was held constant and the concentration of CATCH(+) was varied. Collectively, computational models and experimental data demonstrate that CATCH(+) and CATCH(-) only assemble into β-sheets when the complementary peptide is present, and at a near-stoichiometric ratio.

4.3.3 Mixtures of coassembled antiparallel and parallel β-sheets are detected

Solid-state NMR measurements on isotopically enriched CATCH peptide nanofibers indicate that peptide strands align in both parallel and antiparallel orientations within coassembled β-sheets. Centrifuged and lyophilized peptide nanofiber samples were prepared with CATCH(+) and CATCH(-) peptides isotopically labeled with ^{13}C at the carbonyl carbon on F4. Formation of parallel β-sheets would bring the ^{13}C labeled sites within 0.5 nm of each other resulting in strong ^{13}C-^{13}C dipolar couplings. PITHIRDS-CT measurements are sensitive to this distance-dependent ^{13}C-^{13}C dipolar coupling resulting in a change in the ^{13}C signal decay and report on the parallel β-sheet content within the coassembled peptide nanofibers.[7] As shown in Figure 4.3A moderate ^{13}C signal decay is observed during the PITHIRDS-CT experiment which indicates some parallel β-sheets are detected. However, the ^{13}C signal decay does not match that expected for a homogeneous parallel β-sheet nanofiber sample. Therefore, other β-sheet structures must also exist in the sample.

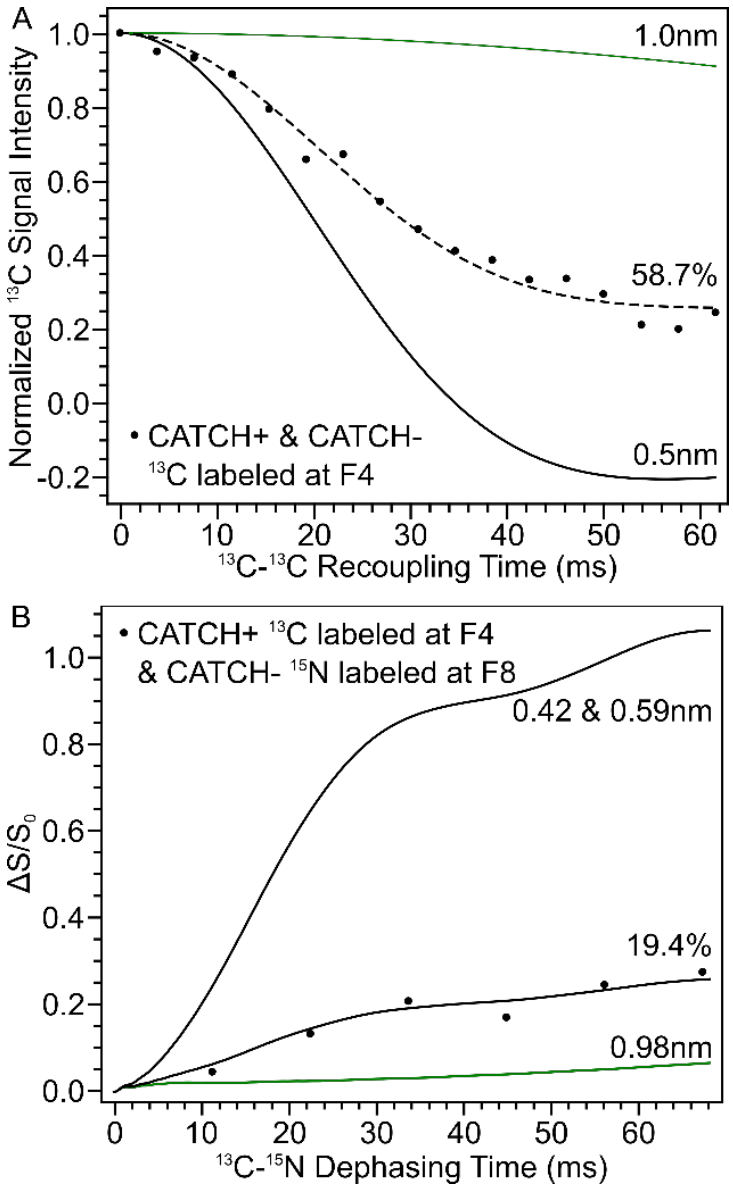

Figure 4.3 CATCH(+) and CATCH(-) peptides coassemble into a mixture of parallel and antiparallel β-sheets. (A) ^{13}C-^{13}C PITHIRDS-CT curves of ^{13}C isotopically enriched CATCH nanofiber samples. Solid curves correspond to SpinEvolution simulations of PITHIRDS-CT data from pairs of spins separated by the indicated distance. The dotted curves are a linear combination of the simulated curves corresponding to 1.0 and 0.5 nm ^{13}C-^{13}C distances. (B) ^{15}N{^{13}C}REDOR spectra of ^{13}C and ^{15}N isotopically enriched CATCH nanofiber samples. Solid curves represent calculated REDOR dephasing curves for pairs of atoms separated by the specified distance.

Within the same nanofiber sample, the F8 residue on the CATCH(+) peptide was isotopically labeled with ^{15}N on the backbone nitrogen. This ^{15}N labeling along with the ^{13}C sites allow for the measurements of ^{13}C-^{15}N couplings that are enhanced when the CATCH(+) and CATCH(-) peptides are aligned antiparallel to one another. An antiparallel alignment would place the ^{13}C site on the CATCH(-) peptide between 0.42 and 0.59 nm to the ^{15}N site on the complementary CATCH(+) peptide. As a result, a strong ^{13}C-^{15}N dipolar coupling occurs between the two nuclei that shows up as an increase in $\Delta S/S_0$ during $^{15}N\{^{13}C\}$REDOR NMR experiments.[9, 10] In Figure 4.3B, the value of $\Delta S/S_0$ increases with mixing time indicating that antiparallel β-sheets also exist within the sample. This observation is consistent with the partial decay observed in the PITHIRDS-CT measurement and our prior studies on the arrangement of King-Webb peptides within β-sheet-rich nanofibers.

Structural analysis of nanofibers formed in DMD simulations of 48 CATCH(+) and 48 CATCH(-) peptides support the observation of both parallel and antiparallel β-sheets in coassembled nanofiber samples. The percentage of parallel and antiparallel β-sheets from DMD simulation predictions are quantified and compared to the values estimated from the PITHIRDS-CT and $^{15}N\{^{13}C\}$REDOR spectra. Summarized in Table 4.1, both the DMD simulations and NMR measurements suggest a slight preference for antiparallel β-sheets. However, the DMD simulations predict a higher amount of antiparallel β-sheets than experimentally observed. The sum of the antiparallel and parallel β-sheet content from NMR measurements is less than 100% suggesting that out-of-register β-strands exist within the nanofiber sample. This result is again consistent with observations in the King-Webb peptide system.

Table 4.1 Comparison of predicted and experimentally measured parallel and antiparallel β-sheet content in CATCH peptide nanofibers

	DMD Simulations	NMR Measurements
Parallel β-sheets	39.1%	24.5%
Antiparallel β-sheets	60.9%	38.8%

4.3.4 CATCH nanofibers contain detectable AA and BB nearest neighbors

Simulations and experimental measurements identified a significant number of AA and BB neighbors within CATCH β-sheet assemblies; this behavior was unexpected based on the charge state of the peptides in neutral aqueous conditions. In the final configuration of the 10 DMD simulations, the percentage of AA (i.e., CATCH(+)) neighbors is 12.5 + 6.9%, while that of BB (i.e., CATCH(-)) neighbors is 5.1 + 4.3%. We probed for the presence of AA and BB neighbors using PITHIRDS-CT NMR experiments on nanofiber samples produced with ^{13}C labeling of peptide A or peptide B, but not both. As illustrated in Figure 4.4A, β-sheets with ideal alternation of A and B β-strands would correspond to a 1.0 nm ^{13}C-^{13}C nearest-neighbor distance if only the central atom of one peptide were ^{13}C-labeled. Figure 4.4B shows that the presence of some like-peptide nearest neighbors results in a fraction of ^{13}C atoms having 0.5 nm nearest-neighbor distances. Centrifuge pellets of "isotopically diluted" equimolar mixtures of ^{13}C-labeled A with unlabeled B (Figure 4.4C, red data points) or ^{13}C-labeled B with unlabeled A (blue data points) yielded reduced decays of ^{13}C signal intensity in PITHIRDS-CT NMR measurements when compared to

the decay observed for the "isotopically pure" mixture containing both labeled A and labeled B (Figure 4.1D, black data points). Reduction of PITHIRDS-CT decay with this kind of isotopic dilution indicates that A and B are coassembled into the same β-sheets. As explained next, however, the degree of observed reduction in the decays with isotopic dilution is less than what would be anticipated with ideal AB alternation in the β-sheet structure.

To understand the effects of isotopic dilution in the presence of deviation from ideal AB-alternation, we performed Monte Carlo simulations to generate the many possible arrangements of β-sheets that can form by coassembling two complementary peptides and combined this analysis with an analysis of the ^{13}C-^{13}C dipolar coupling during PITHIRDS-CT NMR experiments on the various arrangements. These simulations, described in detail in the APPENDIX B and illustrated in Figure B.5, predict the relationship between the arrangements of A and B β-strands and the probabilities of having like-peptide (AA or BB) nearest neighbors within each β-sheet. The results of this analysis are the green dashed curves in Figure 4.4C, which are PITHIRDS-CT decays predicted for the probabilities of like-neighbors indicated by black arrows of the ^{13}C-labeled peptide (AA or BB) for experiments in which only one peptide is ^{13}C-labeled. The experimental data lie in between the predicted curves corresponding to the two extreme cases. The weakest predicted decay in Figure 4.4C, corresponding to a 0 probability for AA or BB nearest neighbors, is the prediction for ideal alternation of A and B peptides within each β-sheet (Figure 4.4A). The strongest predicted PITHIRDS-CT decay in Figure 4.4C, corresponding to a 1.0 probability for AA/BB neighbors, is the prediction for the case in which the isotopically labeled peptide self-assembles into β-sheets that contain no unlabeled peptide. Intermediate

predicted curves correspond to the illustration in Figure 4.4B, in which some AA/BB neighbors occur in coassembled β-sheets. As illustrated in Figure B.6A and B.6B, shapes of PITHIRDS-CT decays are sensitive to small changes in relative positions of ^{13}C atoms within reasonable models of β-sheet structure, but this sensitivity is low for ^{13}C-^{13}C recoupling times below 30 ms. At short ^{13}C-^{13}C recoupling times, we expect decays to be more sensitive to nearest-neighbor ^{13}C-^{13}C interactions and less affected by longer-range interactions. Figure B.6C shows that PITHIRDS-CT curves on isotopically diluted samples exhibit linear dependence on like-peptide nearest-neighbor probability (AA or BB) for ^{13}C-^{13}C recoupling times below 30ms. Based on comparison of measured and simulated PITHIRDS-CT decays at recoupling times less than 30 ms, we estimate that the percentage of like-peptide nearest-neighbor pairs is between 9.4% and 32.8% in the coassembled nanofiber. Although there is significant sample-to-sample variation (Figure B.7, like-peptide neighbors of CATCH(+) appear more likely than like-peptide neighbors of CATCH(-), consistent with the simulation predictions. This observation is also consistent with the smaller net charge of +4 for CATCH(+) in comparison to -6 for CATCH(-).

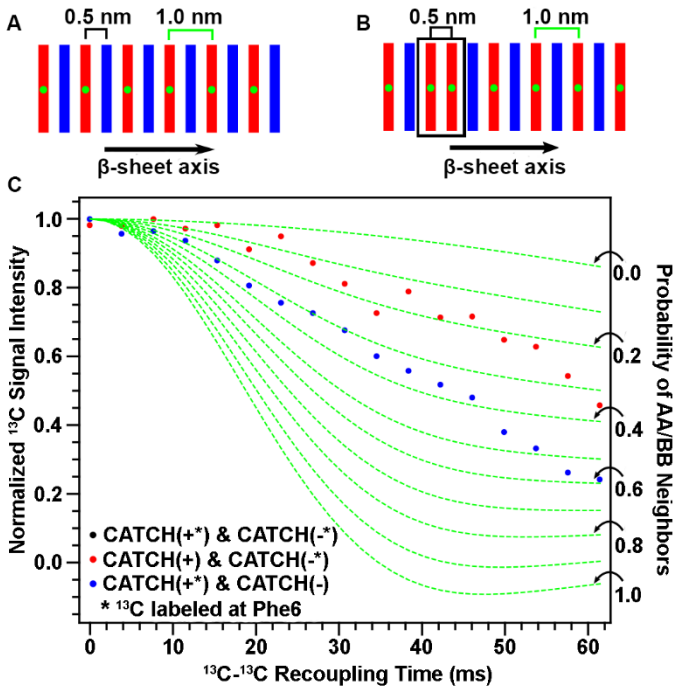

Figure 4.4 Evaluating the propensity for CATCH(+) and CATCH(-) to self-associate. (A,B) Schematics of possible peptide organization within the nanofiber, green dots represent ^{13}C labeling. (C) Isotopic dilution PITHIRDS-CT measurements of coassembled CATCH(+/-) nanofibers where only one peptide is ^{13}C labeled at a time. The asterisks in the plot legend indicate which peptide was isotopically labeled with ^{13}C at the central atom. The dashed green curves correspond to simulations that account for the probabilities of like-neighbors for the ^{13}C-labeled peptide as indicated by black arrows along the right vertical axis. Details describing these simulations can be found in APPENDIX B.

There are several possible explanations for the apparent discrepancy in the estimates of the numbers of AA and BB neighbors from PITHIRDS-CT experiments and simulations. First, the number of peptides assessed in simulations is orders of magnitude smaller than those present in samples analyzed using NMR; thus the probability will change significantly if the number of like-neighbors changes by only 1 or 2 in simulations (see Figures B.8 and B.9). Second, the apparent discrepancies could be due to inaccuracies in the PRIME20 potential energy function. Third, variability in the PITHIRDS-CT

measurements could result from errors introduced during sample preparation. Uncertainties associated with measuring peptide concentration could cause sample-to-sample variation in measured ^{13}C signal decays as shown in Figure B.7. Lyophilization of CATCH(+/-) samples for ssNMR analysis may induce residual unassembled peptide to self-associate into β-sheet structures upon dehydration as described in APPENDIX B and demonstrated in Fig. S16. Fourth, our efforts to correct for naturally abundant ^{13}C, which accounts for ~1% of the carbon in the sample, may be inadequate. This is especially complicating at longer recoupling times where natural abundance plays a larger role as signal decays. Nonetheless, despite reasonable differences in the probabilities estimated from simulations and experiments, these observations collectively demonstrate a non-negligible frequency of like-neighbors in CATCH β-sheet coassemblies.

4.4 Discussion:

This work reports on the molecular-level coassembly of CATCH(+) and CATCH(-) peptides into two-component amyloid-like β-sheet nanofibers. When kept alone in aqueous solution, CATCH(+) and CATCH(-) largely resist self-assembly, although CATCH(+) demonstrates propensity for weak, transient association in DMD simulations, possibly due to its lower net charge compared to CATCH(-). When combined in aqueous solution, the two peptides co-organize into a bilayer of β-sheet tapes. Each tape has a predominant alternating -ABABAB- type β-strand pattern. Bilayer formation is a result of hydrophobic collapse; the tapes have opposing hydrophilic and hydrophobic faces conferred by the alternating sequence of hydrophilic and hydrophobic amino acids in CATCH(+) and CATCH(-), and these hydrophobic faces are packed into the core of the bilayer. This general architecture is not surprising, as it is consistent with the structure hypothesized for

the self-assembling zwitterionic Q11 peptide from which CATCH(+) and CATCH(-) were designed,[4] as well as the closely related P_{11} variant.[11-13] Taken together, these observations support the general hypothesis that electrostatic attraction and repulsion can encode molecular-level organization of β-strands within coassembled β-sheets.

The CATCH peptides are charged variants of a well-known self-assembling peptide Q11 that is hypothesized to preferentially form antiparallel β-sheets to favor interactions between oppositely charged amino acids either end of the peptide.[4] The designs of the CATCH(+) and CATCH(-) peptides lose this electrostatically driven alignment preference through the replacement of charged residues on either peptide that make the sequence palindromic. This sequence design may explain the lack of preference for the antiparallel or parallel orientation though the lack of programming towards an arrangement does not inhibit the MAX1 peptide from aligning in a specific manner within nanofibers.[14] Another possible cause for the mixture of β-sheet structures is the fast kinetics which result in gelation within mixing times. Either of the β-sheet structures could be a kinetically trapped state. Thus, these results stand in contrast to the prevailing thought that peptides form a singular nanofiber structure for a given set of assembly conditions as observed in self-assembling peptides.[15-18]

The resultant assemblies are not, however, perfectly alternating. Rather, some CATCH(-):CATCH(-) and CATCH(+):CATCH(+) neighbors were found in DMD simulations and observed in ssNMR measurements. Not surprisingly, the tendency for CATCH(+):CATCH(+) mismatches appears greater than that for CATCH(-):CATCH(-) mismatches, presumably due to the lower net charge of the former. This tendency for like-charge mismatches in CATCH nanofibers may be due in part to charge-shielding by

counterions present in buffered aqueous solutions. Here, instances may exist in which favorable hydrophobic interactions between the Phe residues on a free peptide and those in the core of a CATCH bilayer can overcome weakened Coulombic repulsion associated with peptide-ion complexation, thereby leading to like-charge peptide pairing within the growing amyloid. Similar results have been observed in ferricytochrome c fibrillization, where hydrophobic interactions can outweigh electrostatic repulsion in alkaline conditions even in the absence of counterions,[19] as well as thermally induced assembly of the cationic MAX3 peptide.[20] Thus, although electrostatic attraction and repulsion can encode peptide organization in general, our results suggest that achieving exquisite molecular-level precision in coassembled amyloid-like structures will require more sophisticated designs that incorporate other types of specific interactions between complementary β-strands. Such precision may ultimately be important in coassembling peptides systems finding use as biomaterials for medical or biotechnological applications because like-charged neighbor "defects" could act as fracture points or facilitate fiber remodeling via strand-swapping.

Our experimental observations suggest that hydration is an important determinant of CATCH peptide self-association versus coassembly propensity. CATCH(+) and CATCH(-) adopted random-coil configurations when kept alone in aqueous conditions, yet each peptide aggregated into β-sheet rich structures when dehydrated (Figure B.10). Consistent with this result, a previous report demonstrated that dehydration of amyloid-forming peptides can increase their fibrillization kinetics.[21] Likewise, studies based on computational models have identified peptide dehydration as a key event in Aβ aggregation and self-assembly.[22, 23] One plausible explanation for the role of water in preventing erroneous, "off-pathway" (AA) or (BB) self-association is rooted in observations that

hydrophilic molecules that tightly bind water molecules experience a repulsive steric-hydration force that leads them to repel each other at small separations (<1 nm). Here, we postulate that it is the combination of long-range electrostatic repulsion plus the energy needed to dehydrate two CATCH(+) or two CATCH(-) molecules as they approach each other that limits (AA) or (BB) interactions in aqueous conditions. When CATCH(+) and CATCH(-) are combined in solution, though, Coulombic attraction between oppositely charged E and K residues coupled with hydrophobic collapse involving Phe residues is sufficient to overcome the dehydration energy barrier. Ultimately, coulombic interactions favor formation of β-sheets with an alternating (AB) strand arrangement over (AA) or (BB) pairings.

4.5 Conclusions

Coassembly of charge-complementary peptide pairs into amyloid-like β-sheet nanofibers is an emerging area of biophysics that is gaining increasing interest as the basis for fabricating new nanomaterials for medical and biotechnological applications. It is often suggested that charge-complementary peptides precisely coassemble into β-sheets with an alternating -ABABAB- strand pattern based on intuition and inferences drawn from biophysical measurements, yet such molecular-level order has not previously been validated. Here, we demonstrate that a combination of computational modeling and biophysical measurement methodologies can close this gap. In particular, we observed that an alternating strand pattern does indeed predominate upon coassembly of CATCH(+) and CATCH(-), yet some CATCH(+):CATCH(+) and CATCH(-):CATCH(-) neighbors do occur. Thus, charge-complementarity alone is insufficient to encode precise β-strand order in two-component amyloid-like nanofibers. The charge patterning on the CATCH(+) and

CATCH(-) peptides also neglect to bias the alignment of β-strands within the nanofiber resulting in a mixture of arrangements. Collectively, these examples demonstrate the power of our computational-experimental framework to provide previously inaccessible views of the process of peptide coassembly from initiation to equilibrium. Such insights are expected to yield advances in our understanding of the molecular-level interactions that drive peptide coassembly, which in turn will lead to guiding principles for a priori design of new peptide pairs demonstrating exquisite molecular-level organization. We envision that achieving fine control of coassembled β-strand structure will afford unprecedented opportunities to design new nanomaterials with precisely defined organization of integrated functional biomolecule components, such as cell binding peptides, enzymes, or antigens. As a result, we may ultimately be able to realize supramolecular designs or patterns that are not possible with conventional self-assembling systems, thereby greatly expanding the range of functional nanomaterials available to medicine and biotechnology.

4.6 Materials and Methods

For general methods, please refer to Chapter 2. Content presented below indicate a deviation from the standard protocols previously mentioned.

4.6.1 DMD simulations

Discontinuous Molecular Dynamics (DMD) simulations are used to investigate spontaneous aggregation of complementary charged peptides. For DMD simulations with both CATCH(+) and CATCH(-) peptide chains, the initial configuration was prepared by randomly placing 48 CATCH(+) and 48 CATCH(-) peptide chains in a 200.0×200.0×200.0

nm^3 box (20 mM). For DMD simulations with only CATCH(+) or CATCH(-) peptides, 96 peptide chains were placed in the simulation box with a concentration of 20 mM.

Canonical-ensemble (NVT ensemble) DMD simulations were conducted using our in-house code. DMD is an alternative to classical MD simulations. Instead of solving Newton's equation of motion at regularly spaced time steps, DMD simulations proceed by solving the dynamics after each event between any two interacting sites. The temperature of the simulation system was controlled at T*=0.20 using the Andersen thermostat and is equivalent to temperature (342 K) with the PRIME20 model.[24] Ten independent DMD simulations were conducted for each system; and each DMD simulation contains 500 billion collisions, equivalent to 16 μs. The criteria for determining when pairs of peptides adjacent to each other are in a β-barrel or a β-sheet are the following. Any two peptide chains are considered to form a pair if they form >5 hydrogen bonds between them. Two peptides are in the same cluster if they form either >5 hydrogen bonds or >1 hydrophobic association. The tail and head amino acid resides are excluded from either calculation.

4.6.2 PITHIRDS-CT nuclear spin simulations

To understand the effects of isotopic dilution in the presence of deviation from ideal AB-alternation, we performed Monte Carlo simulations of β-sheets formed by coassembly of complementary peptides A and B. Each β-sheet pattern is symbolized by a string sequence of A's and B's. The addition of a peptide to the end of a β-sheet sequence in the Monte Carlo simulations is determined by the identity of the current peptide at the end and a probability of AA or BB nearest neighbors. The β-sheet length was set to 2000 peptide

units to approximate steady state. Then, the β-sheet sequence patterns were used to create spin simulations to examine dilutions effects on PITHIRDS-CT measurements.

Due to computational limitations of spin simulations, the Monte Carlo predicted β-sheet sequence pattern was sampled in 8-unit long segments at 50 random and distinct locations. Each 8-unit long letter sequence was then mapped to central sites on an ideal antiparallel β-sheet to produce sets of isotopically diluted spin systems. Simulations of PITHIRDS-CT decay curves are then produced using SpinEvolution NMR simulation software on each spin system.[25] The series of simulations are summed across all 50 locations. This procedure was performed 10 times on each Monte Carlo sequence to eliminate sampling artifacts to produce an averaged PITHIRDS-CT decay simulation. Finally, PITHIRDS-CT decays were produced by averaging over 10 Monte Carlo sequences at each simulated percentage of self-association propensity to again reduce sampling bias.

4.7 References

1. A. Aggeli, M. Bell, L. M. Carrick, C. W. G. Fishwick, R. Harding, P. J. Mawer, S. E. Radford, A. E. Strong and N. Boden, J. Am. Chem. Soc., 2003, 125, 9619-9628.

2. D. T. Seroski, A. Restuccia, A. D. Sorrentino, K. R. Knox, S. J. Hagen and G. A. Hudalla, Cell. Mol. Bioeng., 2016, 9, 335-350.

3. S. Kyle, S. H. Felton, M. J. McPherson, A. Aggeli and E. Ingham, Advanced Healthcare Materials, 2012, 1, 640-645.

4. J. H. Collier and P. B. Messersmith, Bioconj. Chem., 2003, 14, 748-755.

5. E. L. Ulrich, H. Akutsu, J. F. Doreleijers, Y. Harano, Y. E. Ioannidis, J. Lin, M. Livny, S. Mading, D. Maziuk, Z. Miller, E. Nakatani, C. F. Schulte, D. E. Tolmie, R. K. Wenger, H. Y. Yao and J. L. Markley, Nucleic Acids Res., 2008, 36, D402-D408.

6. D. S. Wishart, Prog Nucl Mag Res Sp, 2011, 58, 62-87.

7. R. Tycko, J. Chem. Phys., 2007, 126, 064506-064506.

8. C. M. Baronio, M. Baldassarre and A. Barth, PCCP, 2019, 21, 8587-8597.

9. T. Gullion and J. Schaefer, Journal of Magnetic Resonance (1969), 1989, 81, 196-200.

10. C. P. Jaroniec, B. A. Tounge, C. M. Rienstra, J. Herzfeld and R. G. Griffin, J. Magn. Reson., 2000, 146, 132-139.

11. A. Aggeli, M. Bell, N. Boden, L. M. Carrick and A. E. Strong, Angew. Chem., 2003, 115, 5761-5764.

12. A. Aggeli, M. Bell, N. Boden, J. N. Keen, P. F. Knowles, T. C. B. McLeish, M. Pitkeathly and S. E. Radford, Nature, 1997, 386, 259-262.

13. A. Aggeli, I. A. Nyrkova, M. Bell, R. Harding, L. Carrick, T. C. B. McLeish, A. N. Semenov and N. Boden, Proceedings of the National Academy of Sciences, 2001, 98, 11857-11862.

14. K. Nagy-Smith, E. Moore, J. Schneider and R. Tycko, Proceedings of the National Academy of Sciences, 2015, 112, 9816-9821.

15. R. Kodali, A. D. Williams, S. Chemuru and R. Wetzel, J. Mol. Biol., 2010, 401, 503-517.

16. J. R. Lewandowski, P. C. A. van der Wel, M. Rigney, N. Grigorieff and R. G. Griffin, J. Am. Chem. Soc., 2011, 133, 14686-14698.

17. B. H. Meier, R. Riek and A. Böckmann, Trends Biochem. Sci., 2017, 42, 777-787.

18. J. Park, B. Kahng and W. Hwang, PLoS Comp. Biol., 2009, 5, e1000492-e1000492.

19. D. Ramakrishna, M. D. Prasad and A. K. Bhuyan, Arch. Biochem. Biophys., 2012, 528, 67-71.

20. D. J. Pochan, J. P. Schneider, J. Kretsinger, B. Ozbas, K. Rajagopal and L. Haines, J. Am. Chem. Soc., 2003, 125, 11802-11803.

21. S. Mukherjee, P. Chowdhury and F. Gai, The Journal of Physical Chemistry B, 2009, 113, 531-535.

22. M. G. Krone, L. Hua, P. Soto, R. Zhou, B. J. Berne and J.-E. Shea, J. Am. Chem. Soc., 2008, 130, 11066-11072.

23. B. Tarus, J. E. Straub and D. Thirumalai, J. Mol. Biol., 2005, 345, 1141-1156.

24. H. C. Andersen, The Journal of Chemical Physics, 1980, 72, 2384-2393.

25. M. Veshtort and R. G. Griffin, J. Magn. Reson., 2006, 178, 248-282.

CHAPTER 5. CHARGE-DEPENDENCE OF SELECTIVE COASSEMBLY INTO B-SHEET NANOFIBERS

5.1 Overview of Chapter

In Chapter 3 and 4, we evaluated two existing coassembling peptide pairs that represent two distinct approaches towards charge-complementary sequences. The amino acid sequences and overall peptide charges differ significantly from peptide pair to peptide pair. Even within the CATCH peptides design, the number of charged residues to promote selective coassembly ranges from 4 to 6 charged amino acids. As a result, it is not known how many negatively and positively charged amino acids are necessary to prevent self-assembly and consequently, how this charge density affects peptide coassembly behavior. In this chapter, we evaluate the assembly behavior and composition of a series of designs incorporating an increasing number of lysine or glutamic acid residues to elucidate the role electrostatic repulsion plays in selective coassembly.

5.2 Introduction

Among the design of coassembling β-sheet peptides, there are two classes of sequences; selective coassembly versus nonselective coassembly. Peptides exhibiting selective coassembly behavior resist self-assembly in single-peptide solutions but form two-component β-sheets when combine. In contrast, we consider nonselective coassembly to include peptide pairs that self-assemble in addition to coassembly. Selective coassembly offers a method for triggered peptide assembly that does not rely on common stimuli such as temperature, pH, and salt to induce β-sheet formation. Many biological systems are

sensitive to such environmental factors and could result in unintended effects thereby limiting the application of peptide materials fabricated in this manner.[1, 2] In addition, resistance to self-assembly prevents the formation of inclusion bodies in E. coli when recombinantly expressed with proteins of interest enabling its use for protein immobilization.[3, 4] Understanding how to create peptide pairs that selectively coassemble into β-sheet nanofibers would broaden the form and function of peptide-based biomaterials.

Charge-complementarity has been the prevalent method for creating peptide pairs exhibiting selective coassembly behavior, but there are no design rules on how to promote this behavior. In contrast, the alternation of hydrophilic and hydrophobic residues $(HP)_n$ has been shown to promote the formation of β-sheet nanofibers.[5] The existing peptide pairs shown in Table 1.1 differ significantly with regards to the amino acid sequences making it difficult to conclude how electrostatic repulsion and attraction contributes to selective coassembly behavior. Peptide-peptide interactions involves an interplay of interactions such as van der Waals, hydrogen bonding, and electrostatic forces. These interactions create an energetic landscape that give rise to the hierarchy of structures for a specific amino acid sequence. Early studies relating the periodicity of polar and nonpolar residues to promote α-helical or β-strand conformations showcase the importance of these sequence-to-structure relationships.[5] However, there has not been a systematic study of the charge necessary to prevent self-assembly and promote coassembly.

In this Chapter, we investigate the propensity for coassembly over self-assembly in a series of peptides with increasing overall charge through a combination of experimental measurements and computational simulations. The three peptide pairs were designed by systematically incorporating an increasing number of lysine (K) or glutamic acid (E)

residues into an 11-amino acid sequence based off the well-known Q11 peptide. Equimolar mixtures of each charge-complementary pair successfully produce two-component β-sheet-rich nanofibers as observed in TEM images and 1D ^{13}C NMR spectra. Of these 3 pairs, only the CATCH(4+/4-) and CATCH(6+/6-) pairs qualify as selectively coassembling designs based on FTIR measurements of single-peptide solutions. The kinetics of coassembly was evaluated by thioflavin T (ThT) fluorescence measurements and DMD simulations highlighting the role of complementary electrostatic interactions in promoting coassembly. Comparison of the relative abundance of the two components from quantitative ^{13}C NMR spectra reveals that the positively charged peptide is more prevalent than the negatively charged peptide in all cases. Altogether, these results begin to shed light on the complex sidechain-sidechain interactions that result in selective coassembly behavior.

5.3 Results

5.3.1 Charge-complementarity peptides assemble into β-sheet-rich nanofiber

Each equimolar mixture of charge-complementary CATCH peptides produces long nanofibers with distinct morphological features dependent on charge. Nanofiber samples were prepared at 10 mM total peptide concentration in 1X phosphate-buffered saline (PBS) and allowed to incubate for 24 hours before preparing TEM grids. CATCH(2+) and CATCH(2-) peptides assemble into long, straight nanofibers that seem to bundle and twist together as shown in Figure 5.1. Fibrils from coassembled CATCH(4+) and CATCH(4-) form long, thin and wiry nanofibers that sometimes associate and bundle into thicker and more rigid regions. This partial fiber bundling is similar to that observed in TEM

micrographs of coassembled King-Webb peptide nanofibers. Finally, mixtures of CATCH(6+) and CATCH(6-) peptides assemble into relatively uniform nanofibers that do not exhibit the same bundling observed in CATCH(2+/2-) and CATCH(4+/4-) mixtures. Similar differences in morphology have been reported for one- and two-component peptide nanofibers suggesting differences in the nanofiber compositions.[6] However, we also note that differences may arise as a result of drying artifacts associated with TEM samples preparations.

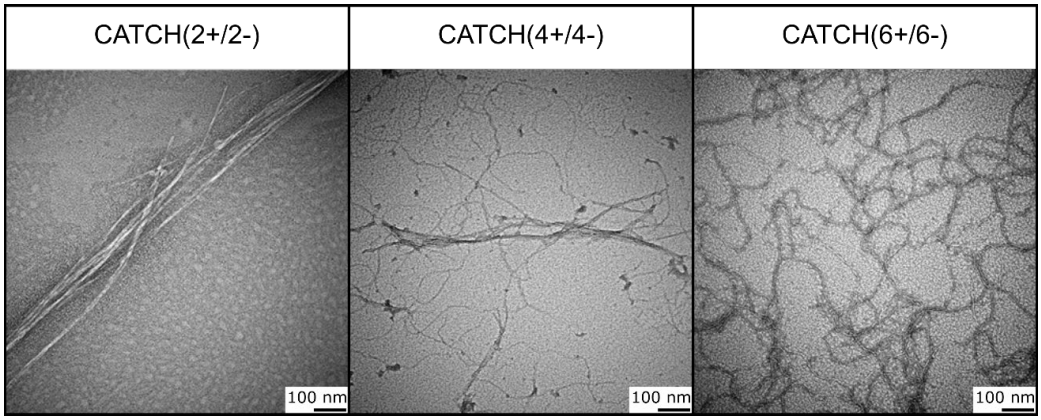

Figure 5.1 Coassembled CATCH peptides exhibit charge-dependent differences in nanofiber morphologies. TEM images of nanofibers produced from 10 mM mixtures of CATCH(2+/2-), CATCH(4+/4-), and CATCH(6+/6-)

Solid-state NMR analysis of CATCH(2+/2-), CATCH(4+/4-), and CATCH(6+/6-) nanofiber samples point to the formation of highly ordered two-component β-sheets. ^{13}C NMR spectra were collected for centrifuged and lyophilized CATCH(2+/2-), CATCH(4+/4-), and CATCH(6+/6-) mixtures. The chemical shift peak centered at 53.4

ppm can be attributed to the α-carbons (Cα) of Gln, Lys, Glu, and Phe while the peak centered around 171.8ppm is assigned to the carbonyl carbons (CO) of the same residues.[7, 8] Comparison the measured chemical shifts for near-backbone carbon sites to values at the same sites in random coil structures can report on the secondary structure.[7, 8] As illustrated in 97, the majority of the Cα and CO peaks are shifted upfield consistent with a β-strand conformation. The presence of shifts corresponding to the Cϵ of lysine and Cδ of glutamic acid at ~23 and ~181 ppm, respectively, indicated that both peptides were abundant in CATCH(4+/4-) and CATCH(6+/6-) samples.[9] The abundance of both peptides suggest coassembly is strongly promoted by charge complementary partners. In contrast, a relatively smaller peak around 181 ppm is observed in the CATCH(2+/2-) suggesting that a smaller fraction of the total CATCH(2-) coassembled with the CATCH(2+) peptide. Narrow linewidths observed in the aliphatic region of the 1D ^{13}C spectra ranged from 1.1 ppm to 1.8 ppm (Table 5.1) and are close to linewidths found in protein crystals (0.5 – 0.6 ppm).[10] These results suggest that the nanofibers are highly ordered. Surprisingly, CATCH(2+/2-) peptide nanofibers seem to be less ordered despite the observation of long, straight nanofibers in TEM micrographs.

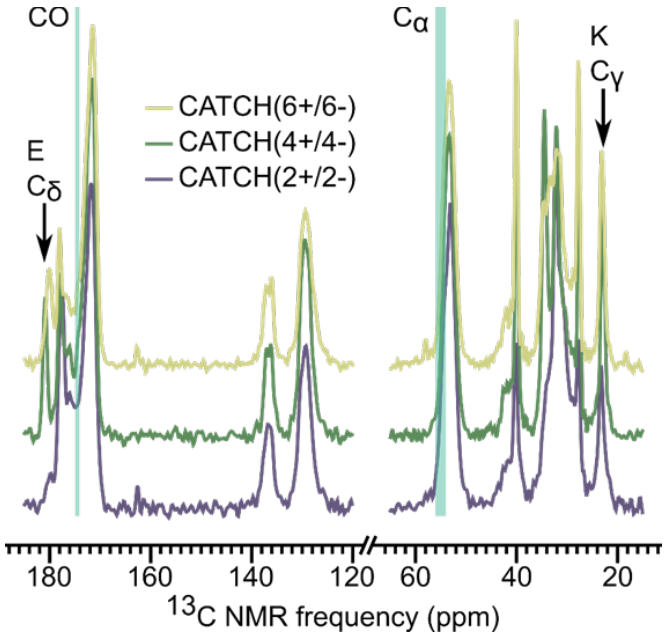

Figure 5.2 CATCH peptides coassemble into β-sheets as shown by 1D ^{13}C NMR spectra of CATCH(2+/2-), CATCH(4+/4-), and CATCH(6+/6-) pairs

Table 5.1 Comparison of Linewidths for the Lysine Cϵ Peak

	FWHM in ppm
CATCH(2+/2-)	1.82
CATCH(4+/4-)	1.09
CATCH(6+/6-)	1.18

5.3.2 Resistance to self-assembly depends on sidechain-sidechain interactions

The minimum charge density necessary to prevent self-assembly in the CATCH peptides depends on the amino acid. Single-peptide solutions of CATCH(2-), CATCH(4+), CATCH(4-), CATCH(6+), and CATCH(6-) remain as random coils as shown by a broad maximum between 1642-1645 cm^{-1} in FTIR spectra as shown in Figure 5.3. FTIR spectra of CATCH(2+) solutions exhibit a maximum at 1621 cm^{-1} consistent with a β-sheet secondary structure indicating that CATCH(2+) readily self-assembles. The propensity for self-assembly of CATCH(2+) peptides corroborates the higher ratio of CATCH(2+) peptides to CATCH(2-) peptides observed in the 1D ^{13}C NMR spectra. Thus, a minimum of at least 4 lysine residues are needed to disfavor peptide self-assembly while only 2 glutamic acid residues are required in the negatively charged CATCH peptides. Altogether, the FTIR spectra indicate that only CATCH(4+/4-) and CATCH(6+/6-) peptide pairs meet our criteria for selective peptide coassembly.

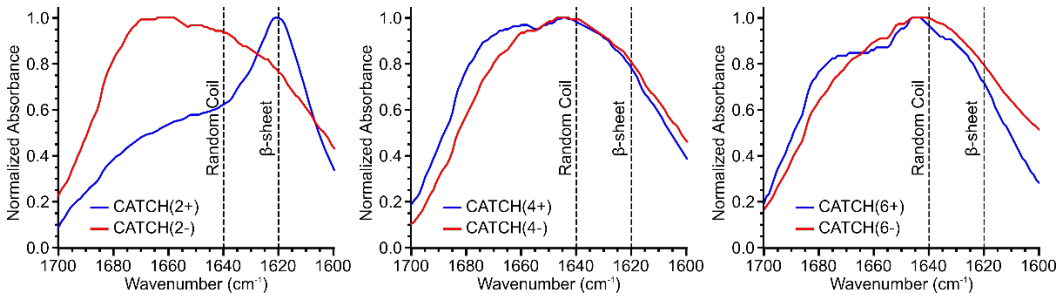

Figure 5.3 Most charged CATCH peptides remain as random coils as indicated by FTIR of single-peptide solutions.

5.3.3 The rate of coassembly increases with charge density

CATCH(6+/6-) mixtures assemble more rapidly than the CATCH(4+/4-) solutions call attention to the role of electrostatic attraction plays in fibrillization kinetics. To probe coassembly kinetics, ThT fluorescence emission was monitored over 48 hours of assembly time. ThT binds to the grooved surface of β-sheets causing a shift in fluorescence excitation and an increase in ThT fluorescence corresponds to an increase in β-sheet content.[11, 12] A large initial increase in ThT fluorescence in both CATCH(4+/4-) and CATCH(6+/6-) mixtures with no noticeable lag phase indicates rapid coassembly into β-sheets. The signal of the latter pair appears to saturate sooner suggesting a faster rate of coassembly. This rapid assembly behavior is consistent with our prior studies on the CATCH(4+/6-) and King-Webb peptides. Assembly kinetics of the CATCH(4+/4-) and CATCH(6+/6-) pairs were also assessed in PRIME20/DMD simulations to probe early timescales inaccessible by experiments. Each simulation run consisted of 48 positively charged chains and 48 negatively charged chains within a 200 nm^3 box. Analysis of the hydrogen bonds formed in DMD simulations qualitatively agrees with the faster coassembly of CATCH(6+/6-) pairs.

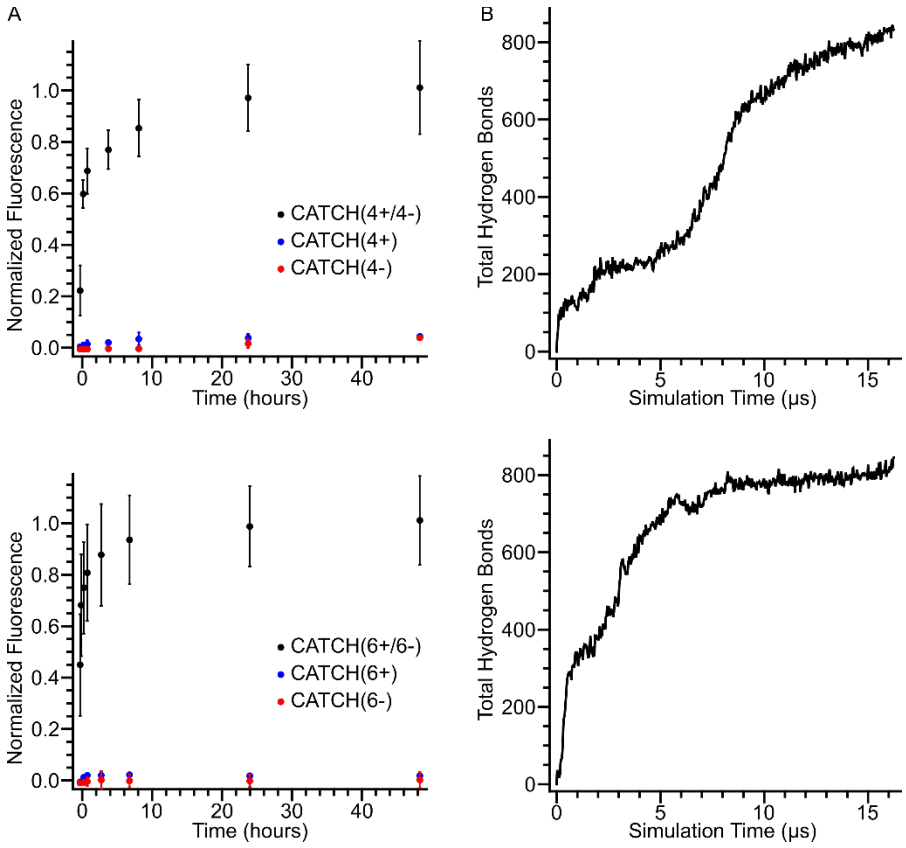

Figure 5.4 CATCH(6+/6-) coassembles more rapidly than CATCH(4+/4-) peptides as observed by kinetics analysis. (A) ThT kinetics measurements (B) Hydrogen bond analysis of DMD simulations.

5.3.4 Composition of Coassembled β-sheet Nanofibers

The positively charged CATCH peptide is more abundant than the negatively charged CATCH peptide within all coassembled peptide pairs. Analysis of chemical shift peaks in 1D ^{13}C NMR spectra collected in a quantitative manner allow for a direct comparison of the relative amounts of a ^{13}C site.[13] As previously mentioned, the peak at ~23 ppm can be attributed to the Cϵ of lysine residues within the positively charged CATCH peptides while the peak at ~181 ppm can be assigned to the Cδ of glutamic acid

residues in the negatively charged CATCH peptide sequences as shown in 102.[9] Within each peptide pair, the number of positively and negatively charged residues in the complementary sequences is equivalent. Thus, the ratio of the peak areas directly corresponds to the relative amount of each peptide component within the coassembled β-sheet nanofibers. Table 5.2 summarizes the ratio of the two peak areas highlighted in 102 for each of the peptide pairs. The CATCH(2+) peptide is 4 times more abundant than the CATCH(2-) peptide within coassembled nanofibers produced from equimolar mixtures. The higher amount of CATCH(2+) peptides is not surprising given the propensity for self-assembly shown by FTIR. Remarkably, the CATCH(4+) peptide is 2 times more abundant than the CATCH(4-) peptides. CATCH(6+/6-) peptide nanofibers are similarly proportioned. Though we would expect increasing the charge of the peptide molecules to promote a 1-to-1 assembly, the ratio of the two peptides seems to plateau as noted by the similar composition of CATCH(4+/4-) and CATCH(6+/6-) nanofibers. In each case, the ratio of the K Cϵ peak area to the E Cδ peak area is greater than 1 for all pairs despite the expectation that peptides would assemble into charge neutral nanofibers.

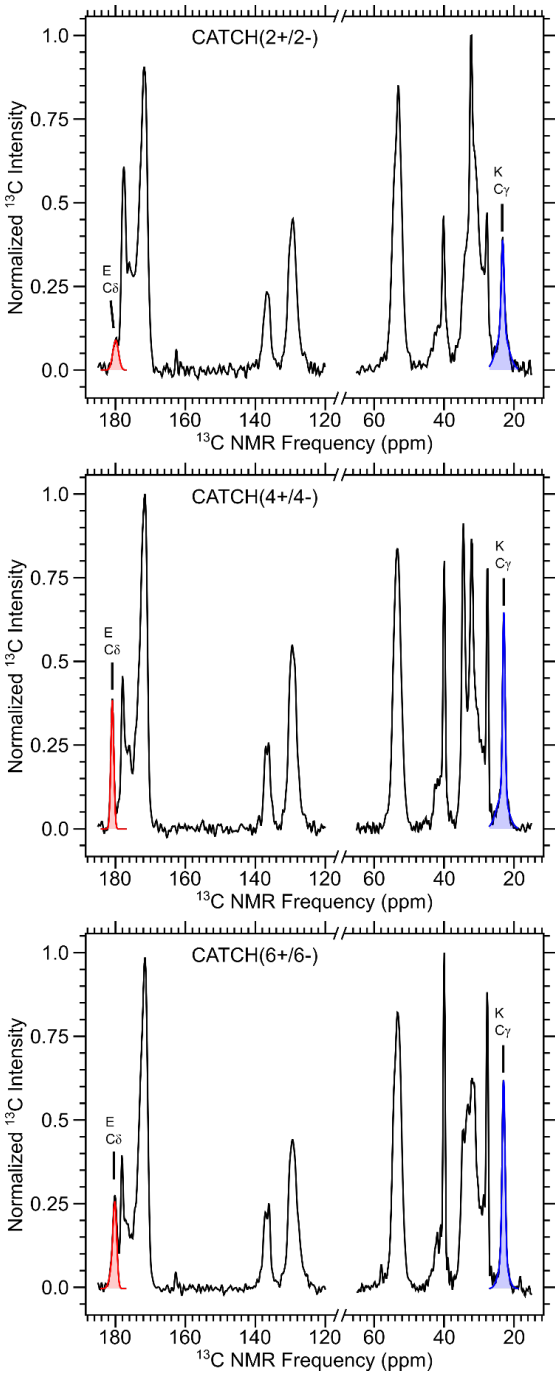

Figure 5.5 Quantitative 1D 13C NMR spectra of CATCH(2+/2-), CATCH(4+/4-), and CATCH(6+/6-) pairs. Peak areas for Cδ of E and Cγ of K residues are highlighted in red and blue, respectively.

Table 5.2 Composition of Coassembled CATCH Nanofibers

	Ratio of Peak Areas Lys Cϵ/Glu Cδ
CATCH(2+/2-)	4.33
CATCH(4+/4-)	2.22
CATCH(6+/6-)	2.07

5.4 Discussion

Our studies show that the minimum charge density necessary to prevent peptide self-assembly depends on the sidechain-sidechain repulsion of the chosen amino acid. Several charge-complementary peptide sequences have been reported to exhibit selective coassembly behavior.[4, 14-16] Despite the variety of peptide sequence designs, no systematic study has been conducted to determine the net charge density necessary to prevent self-assembly. CATCH(2-) peptides remained as random coils within 10mM single-peptide solutions suggesting that 2 glutamic acid residues is sufficient to resist self-assembly in an 11-residue amphiphilic peptide. In contrast, CATCH(2+) peptides are prone to self-assemble into β-sheets as observed in FTIR measurements. For the positively charged CATCH peptides, a minimum density of at least 4 lysine residues was required to prevent self-assembly. This discrepancy in minimum net charge density to deter peptide self-assembly may be rationalized by analysis of sidechain-sidechain interactions. The E

sidechain has a strong electrostatic repulsion as determined from the sidechain-sidechain interaction strength (εEE = 3.15 kJ/mol) computed from the knowledge-based PRIME20 force field.[17] In constrast, the K sidechain has a lower sidechain-sidechain interaction strength of εKK = 0.91 kJ/mol with other K sidechains. The relatively weaker repulsion results from its large hydrophobic aliphatic sidechain. Therefore, the CATCH(2+) peptide exhibits relatively weaker repulsion compared to the CATCH(2-) peptide. The weak repulsion is evidenced in the peptide nanofibers produced from mixtures of CATCH(2+) and CATCH(2-) which were primarily composed of CATCH(2+) peptides.

Increasing the charge density disfavors self-assembly in single-peptide solutions, however, self-association still occurs in all cases. In all cases, the positively charged CATCH peptides were more abundant than the negatively charged CATCH peptides. Therefore, the peptide nanofibers likely grow and elongate through a kinetic competition between peptide self-assembly and coassembly. This kinetic competition is evidenced by the fact that CATCH(6+) peptides self-associate despite their high overall charge. The self-association of the positively charged CATCH peptides can be rationalized by the sidechain-sidechain interactions previously mentioned. On the other hand, a significant percentage of the CATCH(2+/2-) must be coassembled given that 20% of the peptide nanofiber is composed of CATCH(2-) peptides even though the CATCH(2+) peptides show a high propensity for self-assembly. Thus, oppositely charged peptides do favorably coassemble into two-component β-sheets echoing our previous findings. The competitive addition of peptide molecules to the β-sheet nanofibers is similar to the behavior of random copolymer growth.[18] As such, it may be possible to tune the kinetic rate at which the peptide

"monomers" add to the nanofiber ends and thereby control the nanoscale patterning of peptide strands along the coassembled β-sheet nanofibers.

Another consequence of increasing the overall charges of the two peptide components is the increase in the rate of fibrillization. ThT fluorescence kinetic measurements and hydrogen bond analysis of DMD simulations of CATCH(4+/4-) and CATCH(6+/6-) mixtures indicate a faster nanofiber formation in the latter pair. This behavior would suggest that the higher overall charges increase the rate of coassembly and complementary interactions should dominate, but the amount of self-association in the two charge-complementary pairs is similar. Instead, the long-range electrostatic interactions may promote aggregation and nucleation of peptide nanofibers. The DMD simulations show the formation of a peptide nanofiber occurs sooner in the CATCH(6+/6-) pair than the CATCH(4+/4-) pair possibly supporting this theory.

5.5 Conclusion

The design of two-component β-sheet peptide nanofibers has been predominated by experimentally derived sequences that utilize charge complementarity to confer coassembly behavior. This study has shown that electrostatic repulsion can be effective in preventing peptide self-assembly and consequently, it can confer selective coassembly behavior in charge complementary systems. Closer examination of the composition of the β-sheet rich peptide nanofibers reveals an imbalance in the stoichiometry that is consistent with FTIR measurements and analysis of the relative repulsion forces from the PRIME20 force-field. Coassembling peptides were previously assumed to assemble stoichiometrically to form neutral β-sheets. Instead, the composition of the peptide

nanofibers follows the difference in repulsion between glutamic acid and lysine residues with the latter observing weaker like-sidechain repulsions due to the longer aliphatic sidechain. The non-stoichiometric assembly of the peptides highlights the complexity of interactions that contribute to the self-assembly and coassembly of peptides. As a result, it is challenging to develop two peptide sequences that selectively coassemble in a finely controlled manner. Designs of coassembling β-sheet peptides should attempt to account for sidechain-sidechain interactions in a more detailed manner. Computational simulations provide one route to factoring in this complexity. By tuning these sidechain-sidechain interactions, the competition between self-association and complementary addition to the fiber end may be manipulated to produce assemblies with exquisite control over the patterning of the β-sheet peptide nanofibers.

5.6 Materials and Methods

For general methods, please refer to Chapter 2. Content presented below indicate a deviation from the standard protocols previously mentioned.

5.6.1 Discontinuous Molecular Dynamics Simulations

Discontinuous Molecular Dynamics (DMD) simulations are used to investigate spontaneous aggregation of complementary charged peptides. DMD simulations were performed in a 200.0×200.0×200.0 nm^3 simulation box using either 48 chains for peptides alone or 48 of both the cationic and anionic peptides. The simulation temperature was maintained at T*=0.20 (~310 K) using the Andersen thermostat. Ten independent DMD simulations were conducted for each DMD simulation containing 500 billion collisions, equivalent to 16 μs.

5.7 References

1. D. Ramakrishna, M. D. Prasad and A. K. Bhuyan, Arch. Biochem. Biophys., 2012, 528, 67-71.

2. D. J. Pochan, J. P. Schneider, J. Kretsinger, B. Ozbas, K. Rajagopal and L. Haines, J. Am. Chem. Soc., 2003, 125, 11802-11803.

3. X. Wang, B. Zhou, W. Hu, Q. Zhao and Z. Lin, Microbial Cell Factories, 2015, 14, 88.

4. D. T. Seroski, A. Restuccia, A. D. Sorrentino, K. R. Knox, S. J. Hagen and G. A. Hudalla, Cell. Mol. Bioeng., 2016, 9, 335-350.

5. H. Xiong, B. L. Buckwalter, H. M. Shieh and M. H. Hecht, Proceedings of the National Academy of Sciences, 1995, 92, 6349-6353.

6. Y. Hu, R. Lin, P. Zhang, J. Fern, A. G. Cheetham, K. Patel, R. Schulman, C. Kan and H. Cui, ACS Nano, 2016, 10, 880-888.

7. D. Wishart and B. Sykes, J. Biomol. NMR, 1994, 4, 171-180.

8. D. S. Wishart, Prog Nucl Mag Res Sp, 2011, 58, 62-87.

9. E. L. Ulrich, H. Akutsu, J. F. Doreleijers, Y. Harano, Y. E. Ioannidis, J. Lin, M. Livny, S. Mading, D. Maziuk, Z. Miller, E. Nakatani, C. F. Schulte, D. E. Tolmie, R. K. Wenger, H. Y. Yao and J. L. Markley, Nucleic Acids Res., 2008, 36, D402-D408.

10. S. G. Zech, A. J. Wand and A. E. McDermott, J. Am. Chem. Soc., 2005, 127, 8618-8626.

11. M. Biancalana and S. Koide, Biochim. Biophys. Acta, 2010, 1804, 1405-1412.

12. H. Naiki, K. Higuchi, M. Hosokawa and T. Takeda, Anal. Biochem., 1989, 177, 244-249.

13. P. Duan and K. Schmidt-Rohr, J. Magn. Reson., 2017, 285, 68-78.

14. A. Aggeli, M. Bell, L. M. Carrick, C. W. G. Fishwick, R. Harding, P. J. Mawer, S. E. Radford, A. E. Strong and N. Boden, J. Am. Chem. Soc., 2003, 125, 9619-9628.

15. P. J. King, M. Giovanna Lizio, A. Booth, R. F. Collins, J. E. Gough, A. F. Miller and S. J. Webb, Soft Matter, 2016, 12, 1915-1923.

16. S. Kyle, S. H. Felton, M. J. McPherson, A. Aggeli and E. Ingham, Advanced Healthcare Materials, 2012, 1, 640-645.

17. Y. Wang, Q. Shao and C. K. Hall, J. Biol. Chem., 2016, 291, 22093-22105.

18. N. A. Boulding, J. M. Millican and L. R. Hutchings, Polymer Chemistry, 2019, 10, 5665-5675.

CHAPTER 6. A COMBINED COMPUTATIONAL AND EXPERIMENTAL FUNNEL FOR COASSEMBLING PEPTIDE DISCOVERY

6.1 Overview of Chapter

Existing coassembling β-sheet peptide pairs were discovered by an iterative experimental approach using a well-known self-assembling peptide as the starting point. This iterative approach has been successful in discovering several selectively coassembling peptide pairs including those identified in Chapter 5. Thus far, current designs have employed a limited set of residues ignoring the wealth of sidechain-sidechain interactions afforded by all 20 naturally occurring amino acids. This lack of sequence diversity is in part due to the intractability of exploring the full sequence space for two 11-residue peptides. Here, we propose a combined computational and experimental pipeline for the efficient discovery of selectively coassembling β-sheet peptides. In addition, we compare the computationally designed peptide pairs with previous designs.

6.2 Introduction

Coassembly is rare in nature requiring insights from de novo designs to inform the discovery of synthetic peptide pairs. A simple scan through the sequences of existing coassembling β-sheet peptides reveals that a small portion of the possible sequence space has been explored thus far. As a result, we have little direct knowledge of the molecular-level interactions that cause two distinct peptides to coassemble into amyloid-like structures. Subsequently, the discovery of coassembling peptide pairs has relied on an

iterative approach beginning with the peptide sequences of well-known self-assembling peptides.[1-5] The King-Webb and CATCH peptides were developed in this manner.[2, 5] This iterative approach requires significant labor and cost; peptide synthesis and purification along with structural characterization can take several weeks. Even so, the process does not guarantee selective coassembly behavior as evidenced by the results in Chapter 5. Therefore, it is desirable to create a design framework that efficiently identifies coassembling β-sheet peptide sequences.

One of difficulties in designing of β-sheet-forming peptides comes from the challenge of effectively searching the enormous amino acid sequence space to identify peptides with the desired properties. For this reason, systematic investigation of peptide assembly has been limited to short peptides within two to three residues.[6, 7] The design problem becomes even more challenging for two distinct peptides that selectively coassemble into β-sheet nanofibers. Algorithms such as WALTZ, TANGO, and Zyggregator predict the self-aggregation propensities of sequences by correlate amyloidogenic tendencies of individual amino acids.[8] No such algorithm exists for the prediction of peptide coassembly. Even with a design algorithm, these sequence designs need to be validated by experiments. Thus, evaluation by FTIR spectroscopy and solid-state NMR are necessary to determine self-assembly propensity and molecular-level coassembly. A combined computational and experimental funnel would expedite the discovery of new peptide pairs yielding insights into the design rules for selective coassembly and the broader protein folding problem.

In this Chapter, we describe a combined computational and experimental design funnel to efficiently identify new coassembling peptide pairs for a targeted nanofiber

structure. Initially, candidate selectively coassembling peptide designs are identified through a Monte Carlo-type computational algorithm. This algorithm builds off prior work from Xiao et al. to design peptide sequences that bind to biomolecular targets with high affinity.[9, 10] Potential peptide pairs are then screened by discontinuous molecular dynamics (DMD) simulations and FTIR spectroscopy for the likelihood of selectively coassembling into β-sheet-rich nanofibers. Of the 6 peptide pairs, only 4 of the peptides are observed to resist self-assembly in single-peptide solutions and form β-sheets in two-component mixtures. Finally, centrifuged and lyophilized nanofiber samples were prepared, and solid-state NMR measurements were conducted testing molecular coassembly by detecting chemical signatures from each peptide component within the assembled β-sheet nanofibers. Further analysis of the 1D ^{13}C NMR spectra suggest the computationally identified peptide nanofibers are more highly ordered than previous designs, but peptide self-association still occurs and may be unavoidable in charge-complementary designs.

6.3 Results

6.3.1 The computational algorithm identifies 6 potential pairs

Six coassembling peptide sequences are evolved from the Monte Carlo-based search algorithm that exhibit high binding energies and low intrinsic self-aggregation propensities. The computational algorithm runs were initiated from a randomly generated sequence following the same hydrophobic and hydrophilic residue patterning as the CATCH(4+) and CATCH(6-) peptides. Peptide molecules with this sequence pattern are arranged into a two-component β-sheet nanofibril structure derived from the CATCH(4+/6-) peptides. In this arrangement, the peptide strands are aligned antiparallel

to one another to form two perfectly alternating β-sheets. These two coassembled β-sheets are then stacked with their hydrophobic faces pointing towards each other forming a hydrophobic core. Additional details regarding this initial structural model are described in Appendix D. Once initiated, the Monte Carlo-based algorithm proceeds through 3 possible sequence moves for 1000 steps as described in the methods section. For each of six runs (3 runs with $\lambda = 3.0$ and 3 runs with $\lambda = 4.0$), the sequence with the lowest score was selected producing six candidate pairs. All of the peptide pairs show negative values for the binding free energy and low values for self-assembly propensities summarized in Table 6.1.

Table 6.1 Sequences of 6 computationally identified coassembling peptide pairs

Designs		Sequences and Sites											Scores (kcal/mol)	Binding free energy	Aggregation propensity
		1	2	3	4	5	6	7	8	9	10	11			
1	**A**	K	K	K	M	K	V	K	V	N	T	T	-203.20	-200.56	-0.88
	B	T	N	T	A	D	F	E	F	E	E	D			
Starting sequences for design 1: DRKLEFRATQS, EQHFDYNVKRE. (Initial score: 62.34 kcal/mol)															
2	**A**	K	K	K	V	K	V	K	F	T	T	N	-202.74	-199.43	-1.11
	B	T	N	T	V	D	F	E	Y	E	E	D			
Starting sequences for design 2: ETSYDFKAREQ, RSEIQWNLDEE. (Initial score: 70.82 kcal/mol)															
3	**A**	K	K	K	W	K	M	K	A	T	N	T	-214.69	-206.95	-2.58
	B	T	N	T	V	E	V	E	L	D	D	D			
Starting sequences for design 3: HREWRLRITRQ, ESNFEMRWKQK. (Initial score: 212.12 kcal/mol)															

Table 6.1 continued

4	A	K	K	K	V	K	V	K	V	N	T	T	-204.90	-201.26	-0.91
	B	T	N	T	A	E	F	E	F	E	E	D			
Starting sequences for design 4: DRKLEFRATQS, EQHFDYNVKRE. (Initial score: 62.34 kcal/mol)															
5	A	K	K	K	V	K	V	K	V	N	T	T	-206.44	-204.95	-0.37
	B	T	N	T	M	D	F	E	Y	E	E	D			
Starting sequences for design 5: ETSYDFKAREQ, RSEIQWNLDEE. (Initial score: 70.82 kcal/mol)															
6	A	K	K	K	V	K	Y	T	F	K	N	T	-207.40	-201.63	-1.44
	B	T	N	T	M	E	V	D	F	D	E	D			
Starting sequences for design 6: HREWRLRITRQ, ESNFEMRWKQK. (Initial score: 212.12 kcal/mol)															

*Designs 1-3 result from setting λ=3.0, while Designs 4-6 result from setting λ =4.0. The starting sequences for the six pairs of the peptides A and B are listed after each design.

6.3.2 DMD simulations and FTIR measurements screen for β-sheet-rich Nanofibers

Computationally identified peptides are screened through a series of DMD simulations to observe coassembly and self-assemlby behavior in silico reducing the pool to 5 peptide pairs. Final snapshots of PRIME20/DMD simulations of peptides are shown in Figure 6.1. Four of the peptide designs (1, 2, 4, and 5) form multilayer β-sheet fibrils during the simulations. While unintended, the computational observation of multilayer β-sheet suggests this structural feature can be programmed into peptide sequences. Peptide design 3 remains as random coils throughout the simulation time suggesting a low

propensity for coassembly. As a result, we exclude design 3 from further testing. Of the 6 original designs, only design 6 assembles into the desired two-layer β-sheet nanofibers within DMD simulations. Subsequently, designs 1, 2, 4, 5, and 6 were synthesized and purified.

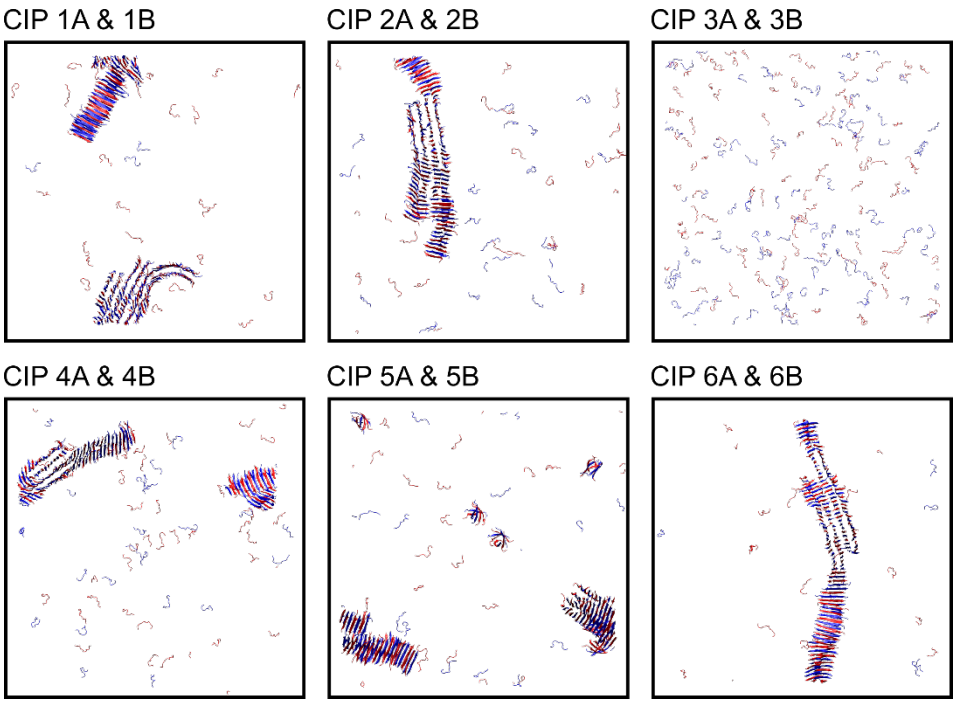

Figure 6.1 PRIME20/DMD simulations of all 6 candidate pairs identified by the computational search algorithm

Experimentally, all of the synthesized designs resist self-assembly and four out of the 5 candidates successfully assemble into β-sheets. FTIR spectra were collected on each of the peptides individually as well as in equimolar mixtures at a total peptide concentration of 10 mM in 1X PBS. Figure 6.2 shows FTIR spectra for the 5 candidate pairs that were

synthesized. Individually, all synthesized peptides remained as random coils as suggested by the broad peak at 1640 cm^{-1}. FTIR spectra of design pairs 1, 2, 4, and 5 exhibited peaks at 1620 cm^{-1} consistent with the formation of β-sheets. These results are consistent with our prior studies on charge complementary peptides indicating that complementary interactions drive assembly in charge-complementary peptides. Further analysis by solid-state NMR is required to assess peptide coassembly.

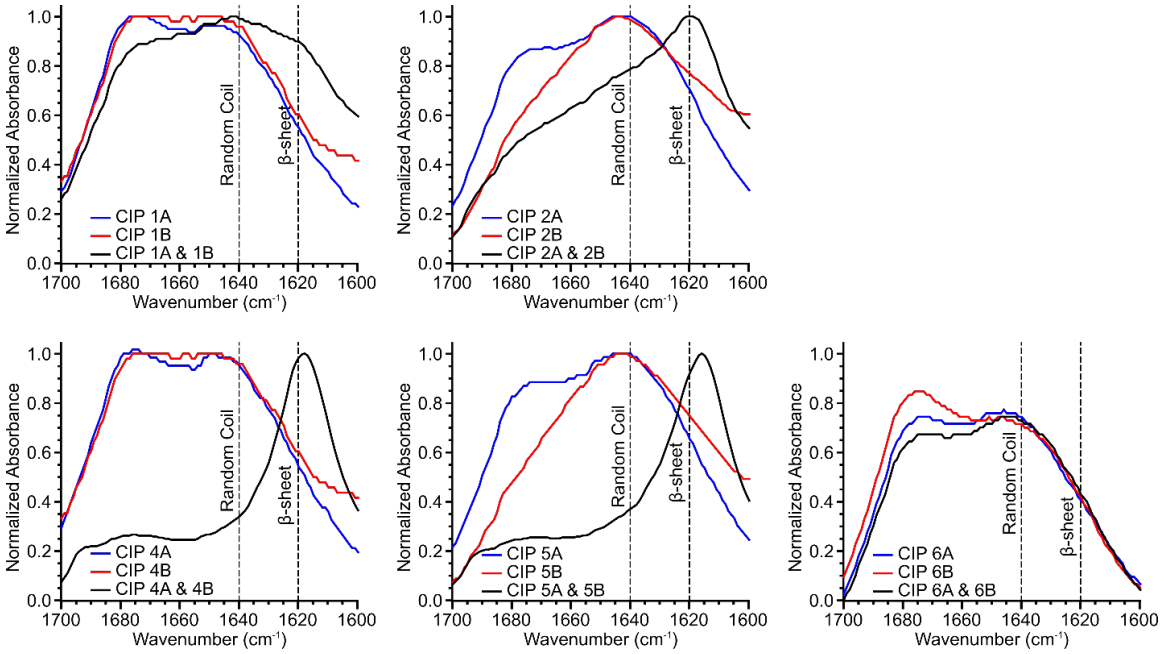

Figure 6.2 All candidate pairs resist self-assembly and form β-sheets through complementary interactions as shown by FTIR spectra of the computationally identified pairs 1, 2, 4, 5, and 6.

6.3.3 Computationally identified pairs coassemble into β-sheet nanofibers

Remarkably, the remaining 4 computationally identified pairs coassemble into β-sheet-rich nanofibers. The positively charged, A, peptide features 5 lysine residues in each of the designs providing an abundant and distinct chemical shift around 23 ppm corresponding to the Cϵ site on the lysine sidechain. Similarly, the negatively charged, B, peptides all contain 3-4 glutamic acid residues. As we have previously demonstrated, the δ-carbon of the Glu sidechain provides a well-separated chemical shift peak at ~181ppm. In 1D ^{13}C NMR spectra of centrifuged and lyophilized nanofiber samples, the Glu Cδ peak and Lys Cϵ peaks are well resolved and are present in all 4 cases.[11] This result suggests that each of the computationally identified pairs coassemble into nanofibers. Comparison of the measured carbonyl carbons (CO) chemical shifts against the value for the same sites in a random coil configuration in Figure 1.1 shows a decrease in the upfield shift in the peak consistent with a β-sheet-rich structure.[12, 13] This result corroborates the analysis from FTIR spectra of equimolar mixtures. After the computational and experimental testing, four out of the six evolution runs successfully produced sequences that meet the criteria for selective coassembly.

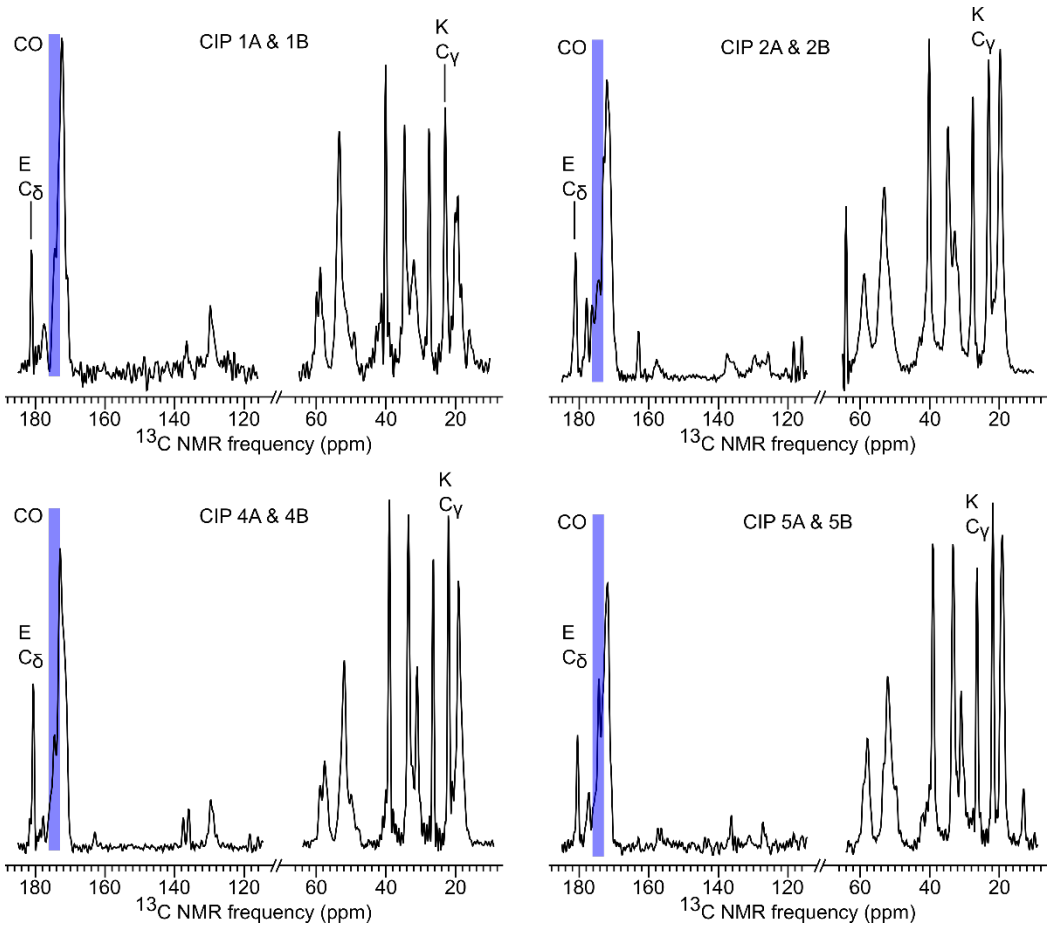

Figure 6.3 1D 13C NMR spectra of computationally identified peptide pairs 1, 2, 4 and 5 show signatures of coassembled β-sheets.

6.3.4 Computationally Designed Pairs are more ordered than previous designs

Measurements of the peak linewidths in 1D ^{13}C NMR spectra of the coassembled peptide pairs show that the nanofibers are exceptionally well ordered. Linewidths (full width at half maximum) are reported in Table 6.2 for the Glu Cδ and Lys Cϵ chemical shift peaks. The sensitivity of chemical shift values to the chemical environment surrounding a ^{13}C site can result in broad linewidths for a disordered structure or multiple structures though other factors can contribute to broad linewidths. On the other hand, narrow

linewidths would suggest a highly ordered structure. The linewidths observed in the computationally identified pairs are comparable to those observed in protein crystals indicating a very highly ordered structure.[14] Compared to linewidths in the family of CATCH peptides and King-Webb peptides, the linewidths of the computationally identified pairs are almost 2X smaller suggesting the new peptide pairs may be better behaved and structurally homogeneous.

Table 6.2 Peak linewidth and area analysis computationally identified peptides (CIP)

	Peptide A FWHM in ppm	Peptide B FWHM in ppm	Peak Area Lys Cϵ/Glu Cδ
CIP 1	0.682	0.430	1.73
CIP 2	0.775	0.687	1.55
CIP 4	0.522	0.526	1.53
CIP 5	0.553	0.553	1.78

In each of the pairs, the two peptides are almost equally abundant though the amount of the positively charged peptide (peptide A) is slightly higher as observed in other charge-complementary peptide systems. As previously detailed, the chemical shift peaks assigned to the Glu Cδ and the Lys Cϵ sites are unique to peptide B and peptide A, respectively. The

ratio of the peak areas is normalized for the number of Glu and Lys residues within the sequence and reported in Table 6.2. In all cases, the Lys Cϵ peak area is larger than the Glu Cδ peak area consistent with our prior observations in the CATCH and King-Webb systems. Surprisingly, the computationally identified pairs form coassembled β-sheet-rich nanofibers that are significantly closer to stoichiometric as compared to the family of CATCH peptides investigated in Chapter 5.

6.4 Discussion

Computational tools can successfully explore the vast amino acid sequence space to identify sequences that selectively coassemble into β-sheet-rich nanofibers. From six evolution runs, four peptide pairs were shown to resist self-assembly and coassemble into β-sheets experimentally. This computational algorithm combined with FTIR and solid-state NMR spectroscopy represent a shift in the paradigm of discovering selectively coassembling peptide pairs. Prior to this work, peptides were designed through an iterative process that systematically replaced residues within a well-characterized self-assembling peptide to produce two peptides that remained in a random coil configuration in single-peptide solutions but formed coassembled β-sheet nanofibers when combined.[1-3, 5] It is important to note that one of the designs failed to coassemble into β-sheets. Until simulations can capture the full complexity of protein folding and interactions, experimental validation is necessary. Successful application of coassembling β-sheet peptides as functional biomaterials will inevitably require different peptide sequences with different material properties. This design framework reduces the labor and cost in expanding the breadth of literature on coassembling β-sheet peptides enabling their application to a variety of challenges.

Despite the simplicity in the score function used in evolving the peptide sequences, the computational algorithm identifies coassembling peptide sequences that may be more structurally homogeneous than previously reported peptide sequences. The score function accounts only for the self-assembling propensities and the binding energy of the peptide sequence. These two factors were sufficient in producing sequences that had exceptionally narrow linewidths and that were coassembled into near stoichiometric β-sheets as compared to our investigations of the CATCH and King-Webb peptides. These results highlight the utility in including computational tools that can better capture the complexities of sidechain-sidechain interactions.[15] In addition, the high-resolution of the 1D NMR spectra and the diversity of residues used in the sequence encodes more structural information into the nanofiber structure that can be easily probed by 2D solid-state NMR measurements. Nanofibers produced from the computationally identified pairs may exhibit less structural heterogeneity than that observed in the CATCH and King-Webb aggregates potentially yielding insights into the design of complementary sequences for a targeted structure.

Similarities between the sequence pairs may indicate design considerations for peptides that coassemble into β-sheet-rich nanofibers. It is important to note that the algorithm was initiated from a random sequence that obeyed the hydrophilic/hydrophobic patterning of the CATCH peptides. In addition, the amino acids were restricted to 3 hydrophobic residues, 5 charged residues, and 3 hydrophilic residues to ensure sufficiently solubility in aqueous solutions. The evolution of the sequences led to the clustering of lysine (K) residues to the N-terminus of Peptide A while glutamic acid (E) and aspartic acid (D) residues are clustered at the C-terminus of the Peptide B in all complementary

pairs. Similar "sticky ends" have been shown to be effective the coassembly of the SAF p1 and p2a peptides into highly ordered coiled-coil nanofibers.[16] Asparagine (N) and threonine (T) amino acids appear frequently in the sequences due to their low intrinsic self-aggregation propensities and favorable sidechain-sidechain interactions between the carboxamide group ($CO\text{-}NH_2$) on the asparagine sidechain and the hydroxyl group (OH) on the threonine sidechain.[15] As expected, the arrangement of the amino acids likely accounts for the preference for a certain arrangement within the coassembled nanofiber and could explain the mixed β-strand alignments seen in the more palindromic King-Webb and CATCH peptides.

6.5 Conclusions

The discovery of coassembling peptides has commonly relied on an iterative experimental approach requiring significant labor and cost. Through a combined computational and experimental funnel, the identification of selectively coassembling peptides can be facilitated. The utility of this framework has been shown to successfully produce four new coassembling peptide pairs significantly increasing the number of designs in literature. The peptide nanofibers produced from these computationally identified pairs appear to be more ordered and structurally homogeneous than previously reported coassembling β-sheet peptides. As it stands, the computational algorithm only factors in two design parameters, self-aggregation propensity and binding energy, and has several constraints to the sequence pattern. Most notably, it constrains the sequence to an alternating hydrophobic/hydrophilic patterning derived from earlier work sequence patterning to promote secondary structure reducing the possible designs. Releasing the sequence constraints could identify design motifs that promote selectively coassembly

behavior not currently known. Increasing the complexity of the computational algorithm could produce nanofibers with exquisite control over the molecular-level organization of the peptide strands.

6.6 Materials and Methods

For general methods, please refer to Chapter 2. Content presented below indicate a deviation from the standard protocols previously mentioned.

6.6.1 Peptide design algorithm

A Monte Carlo-based search is used to design peptides A and B that can coassemble into a predetermined molecular architecture, such as a β-sheet or a β-barrel. This architecture, hereafter referred to as the "peptide scaffold", can be of any type, e.g., a single or multiple β-sheet fibril (flat or twisted, parallel or antiparallel, in-register or out-of-register), a β -barrel oligomer, or an α-helix bundle, and can contain any number of assembling peptides. Figure 6.4 shows a flowsheet of the computational search algorithm. Classification used by the algorithm for the 20 natural amino acids is provided in Table 6.3.

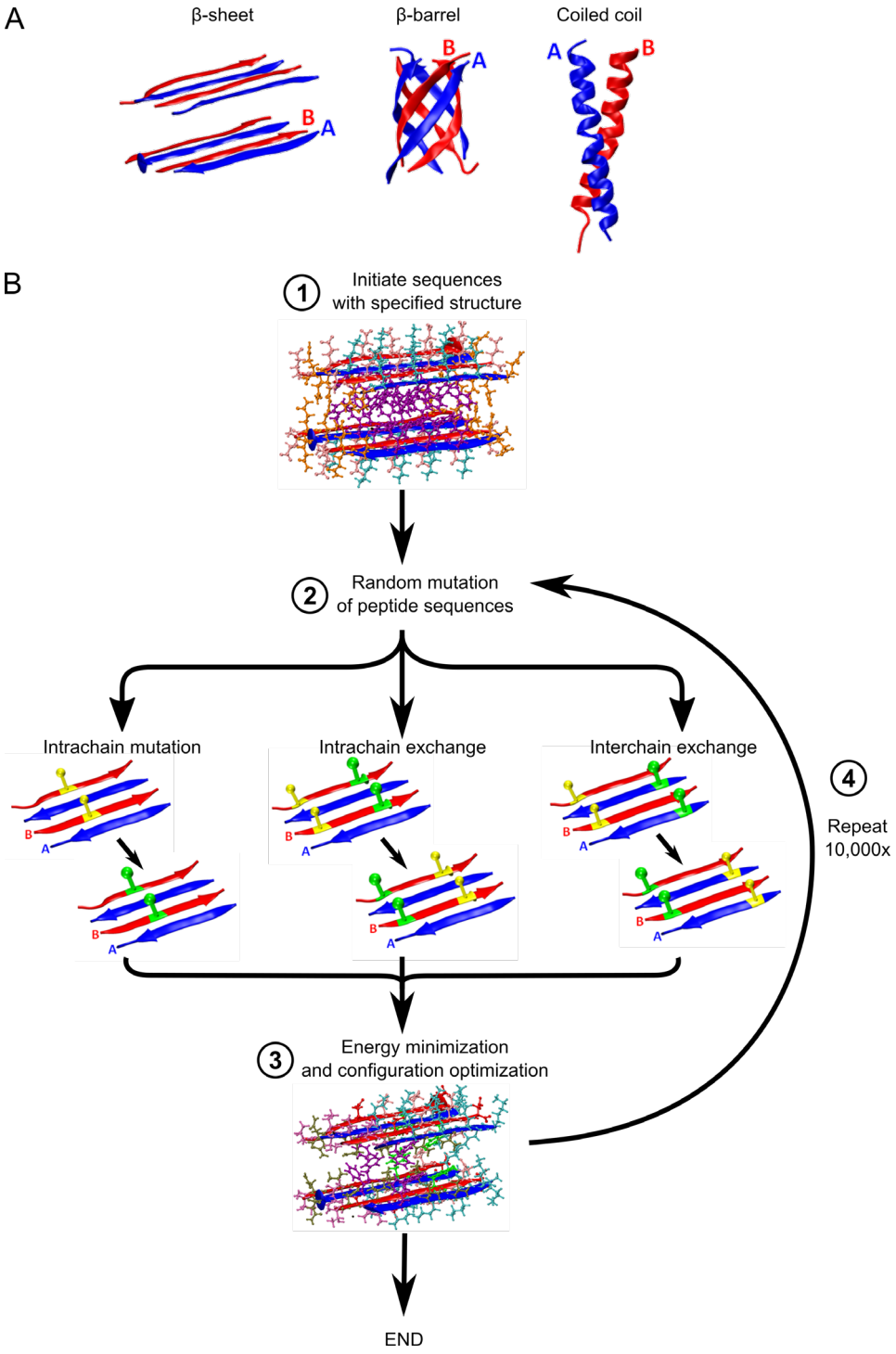

Figure 6.4 Workflow for the MC-based search algorithm. A) Different possible initial structures including β-sheet fibril, β-barrel oligomer, and α-helix bundle. B) Schematic depicting the design process for coassembling peptide sequences.

Table 6.3 Classification of the 20 natural amino acids

Hydrophobic Residues	Ala(A), Leu(L), Val(V) Ile(I), Met(M) Phe(F), Tyr(Y), Trp(W)	3	**H**
Charged Residues	Arg(R), Lys(K) Glu(E), Asp(D)	5	**P**
Hydrophilic Residues	Asn(N), Gln(Q) Ser(S), Thr(T), His(H)	3	
Other Residues	Cys(C), Pro(P), Gly(G)	0	

6.6.2 Discontinuous molecular dynamics (DMD) simulation and PRIME20 model

In this work, we performed large-scale DMD/PRIME20 simulations to evaluate the spontaneous aggregation and coassembled structures of the best six peptide pairs designed from our computational algorithm. In addition, we also perform simulations on the CATCH peptide pair designed by Seroski et al.[5] All the simulations are carried out for 5 μs in the canonical (NVT) ensemble. For the peptide coassembly cases, 100 A and 100 B peptides are initially randomly placed in a cubic box with a length of 321.0 Å, corresponding to a peptide concentration of 10 mM. We set the reduced temperature T* of the simulations to be 0.195, which corresponds to 330 K in real temperature units.[23] For the peptide self-assembly cases, single peptide species system containing either 40 A or 40 B that originate from the six designed peptide pairs are kept at the same concentration and temperature as

in the coassembly cases. We repeat the simulation three times for each of the systems mentioned above.

6.7 References

1. A. Aggeli, M. Bell, L. M. Carrick, C. W. G. Fishwick, R. Harding, P. J. Mawer, S. E. Radford, A. E. Strong and N. Boden, J. Am. Chem. Soc., 2003, 125, 9619-9628.

2. P. J. King, M. Giovanna Lizio, A. Booth, R. F. Collins, J. E. Gough, A. F. Miller and S. J. Webb, Soft Matter, 2016, 12, 1915-1923.

3. S. Kyle, S. H. Felton, M. J. McPherson, A. Aggeli and E. Ingham, Advanced Healthcare Materials, 2012, 1, 640-645.

4. J. K. Sahoo, M. A. VandenBerg, E. E. Ruiz Bello, C. D. Nazareth and M. J. Webber, Nanoscale, 2019, 11, 16534-16543.

5. D. T. Seroski, A. Restuccia, A. D. Sorrentino, K. R. Knox, S. J. Hagen and G. A. Hudalla, Cell. Mol. Bioeng., 2016, 9, 335-350.

6. P. W. J. M. Frederix, G. G. Scott, Y. M. Abul-Haija, D. Kalafatovic, C. G. Pappas, N. Javid, N. T. Hunt, R. V. Ulijn and T. Tuttle, Nat. Chem., 2015, 7, 30-37.

7. F. Li, J. Han, T. Cao, W. Lam, B. Fan, W. Tang, S. Chen, K. L. Fok and L. Li, Proceedings of the National Academy of Sciences, 2019, 116, 11259-11264.

8. B. P. Roland, R. Kodali, R. Mishra and R. Wetzel, Peptide Science, 2013, 100, 780-789.

9. X. Xiao, P. F. Agris and C. K. Hall, J. Chem. Theory Comput., 2015, 11, 740-752.

10. X. Xiao, C. K. Hall and P. F. Agris, J. Biomol. Struct. Dyn., 2014, 32, 1523-1536.

11. E. L. Ulrich, H. Akutsu, J. F. Doreleijers, Y. Harano, Y. E. Ioannidis, J. Lin, M. Livny, S. Mading, D. Maziuk, Z. Miller, E. Nakatani, C. F. Schulte, D. E. Tolmie, R. K. Wenger, H. Y. Yao and J. L. Markley, Nucleic Acids Res., 2008, 36, D402-D408.

12. K. J. Fritzsching, Y. Yang, K. Schmidt-Rohr and M. Hong, J. Biomol. NMR, 2013, 56, 155-167.

13. D. Wishart and B. Sykes, J. Biomol. NMR, 1994, 4, 171-180.

14. S. G. Zech, A. J. Wand and A. E. McDermott, J. Am. Chem. Soc., 2005, 127, 8618-8626.

15. Y. Wang, Q. Shao and C. K. Hall, J. Biol. Chem., 2016, 291, 22093-22105.

16. M. J. Pandya, G. M. Spooner, M. Sunde, J. R. Thorpe, A. Rodger and D. N. Woolfson, Biochemistry, 2000, 39, 8728-8734.

17. H. Gohlke, C. Kiel and D. A. Case, J. Mol. Biol., 2003, 330, 891-913.

18. K. F. DuBay, A. P. Pawar, F. Chiti, J. Zurdo, C. M. Dobson and M. Vendruscolo, J. Mol. Biol., 2004, 341, 1317-1326.

19. A. P. Pawar, K. F. DuBay, J. Zurdo, F. Chiti, M. Vendruscolo and C. M. Dobson, J. Mol. Biol., 2005, 350, 379-392.

20. G. G. Tartaglia, A. P. Pawar, S. Campioni, C. M. Dobson, F. Chiti and M. Vendruscolo, J. Mol. Biol., 2008, 380, 425-436.

21. G. G. Tartaglia and M. Vendruscolo, Chem. Soc. Rev., 2008, 37, 1395-1401.

22. J. A. Maier, C. Martinez, K. Kasavajhala, L. Wickstrom, K. E. Hauser and C. Simmerling, J. Chem. Theory Comput., 2015, 11, 3696-3713.

23. H. C. Andersen, The Journal of Chemical Physics, 1980, 72, 2384-2393.

CHAPTER 7. CONCLUSIONS

Coassembling β-sheet peptides emerged as a new frontier in functional biomaterials that expand the portfolio of accessible nanostructures.[1] These materials were assumed to behave as programmed, but there has been no evidence to support this claim.[2, 3] Through the structural analysis presented here, we show that the peptides coassemble into the proposed arrangements, but remarkably, a significant proportion of the nanofibers form off-target structures. While this level of heterogeneity may suffice for some biotechnological applications, these results highlight the challenge in designing complementary peptides with exquisite control. Subsequently, we investigated a series of new peptide pairs discovered through two different methods, a systematic experimental approach and a combined computational and experimental pipeline. Coassembling peptides developed through these two methods provided insights into the sidechain-sidechain interactions governing the formation of two-component β-sheet-rich nanofibers. Altogether, these results begin to chip away at the complexities underlying peptide sequence to structure relationships.

7.1.1 Charge Complementarity: an Imperfect Tool for Selective Coassembly

While several coassembling β-sheet peptides exist, only a handful coassemble in a selective manner meaning the peptides only form β-sheets when combined rather. The only reported method for imparting selective coassembly behavior is through the concept of charge complementarity. Each peptide exhibits an overall charge that reduces the likelihood of self-assembly via electrostatic repulsion, but the oppositely charged peptides attract each other and arrange into two-component β-sheets. It was assumed that these

complementary peptides alternate along the β-sheet due to electrostatic repulsion of like-peptides.[2, 3] However, our solid-state NMR measurements indicate that like-peptides can neighbor each other forming self-associated pairs within the peptide nanofiber. Depending on the amino acid sequence, abundance of self-associated peptide pairs can be significant as shown in Chapter 4.

Direct and indirect observations of like-peptide pairs in all charge-complementary β-sheet peptides investigated leads to two possibilities. First, charge complementarity alone is insufficient in preventing self-association in mixtures of the two peptide components. A number of self-assembling peptides have an overall charge, yet, self-assemble in ionic solutions. Most notably, the lysine-rich MAX1 peptide folds into β-hairpins and assembles into highly ordered β-sheet-rich nanofibers.[4] Several of the P_{11} peptides developed by Aggeli and Boden have an overall negative or positive charge but self-assemble into β-sheet ribbons and fibrils beyond a critical concentration.[5] Charge-screening from salts and the complementary peptides may facilitate the addition of a like-peptide to the fiber end to form a self-associated pair. Second, the alternating polar and nonpolar residue patterning $(HP)_n$ promotes self-association driven by hydrophobic interactions and hydrogen bonding. β-sheet oligomers were shown to be promoted by sequence patterning despite the individual amino acid's propensity for β-sheet formation.[6] One solution to this problem is exploring the sequence space for new amino acid patterns that promote selective coassembly into β-sheets.

7.1.2 Sequence Symmetry and Structural Heterogeneity in Peptide Designs

Existing coassembling β-sheet peptides are derived from well-known self-assembling peptides that are believed to arrange into antiparallel β-sheets. By extension, the charge-complementary variants of these parent sequences are hypothesized to also form antiparallel β-sheets.[2, 3] Limited FTIR measurements provide some support for this claim. However, solid-state NMR measurements along with coarse-grained DMD simulations revealed that complementary β-strands can orient into both parallel and antiparallel positions within a β-sheet. Looking at the amino acid sequences of the CATCH and King-Webb peptides, these findings are not surprising. Symmetry in the amino acid sequence may be aesthetically pleasing but the palindromic patterning of the sidechains may permit peptides to add onto the fiber end in either orientation. Simulations also predict the out-of-register alignment of peptide strands that could result from lack of programming for a given 3D arrangement. Sequences generated by the combined computational and experimental framework in Chapter 6 exhibit a patterning that may bias towards antiparallel β-sheets. With linewidths in 1D ^{13}C NMR spectra comparable to protein crystals, the computationally identified peptides are more likely to form a single structure. The computational algorithm produced sequences that used a wider variety of amino acids that could aid preferential arrangement into antiparallel β-sheets.

7.1.3 Combining Computational Simulations with Solid-State NMR

By combining computational simulations with experiments, a deeper understanding of peptide coassembly was achieved. These two approaches complement each other and can make up for the limitations of the other. Computational tools allow us to observe

peptide coassembly at timescales inaccessible by conventional experimental methods. Probing these timescales provides insight into possible mechanisms that cannot be easily observed by solid-state NMR. Furthermore, the use of predictions from simulations and the use of 3D molecular models aides in the design of solid-state NMR measurements and the interpretation of NMR results. On the other hand, computational cost restricts the size and length of simulations. These constraints make it difficult to truly sample all thermodynamic states and has been shown in our studies could lead to a gap in the predictive capabilities of computations on the final structure of coassembled peptide nanofibers. Experimental techniques capture these final states and can report on behavior from a true statistical distribution. Computational tools such as the PRIME20 force-field[7] provide insight into these intermolecular interactions and could enable the future design of sequences with a specific nanoscale organization important in the use of these peptide-based fibers as functional biomaterials.

7.2 Future work:

Broadly speaking, peptide coassembly is a novel route to expanding the portfolio of nanostructured biomaterials with the possibility of incorporating functional motifs in a reproducible and controlled manner. Further development of coassembled peptides as functional biomaterials will be enabled by a better understanding of the coassembly pathway, refining the computational algorithms to design novel coassembled nanostructures, and characterizing the effects of covalently attached biomolecules on the peptide nanofiber structure.

7.2.1 Uncovering the Peptide Coassembly Pathway

Self-assembling peptides are considered to fold and organize into their thermodynamically favored state. Coassembling peptides are less well characterized and have fast assembly kinetics within mixing times. This difference in behavior raises the question whether or not the structural defects in the coassembled King-Webb and CATCH peptides are kinetically trapped states. Further study along this pathway is needed to test this hypothesis. Lowering the total peptide concentration can slow down the assembly times of the peptides. Solid-state NMR analysis of nanofiber samples prepared through this method would make progress toward answering this question. Another consideration is the assembly pathway in which the charge-complementary coassembling peptides proceed. Rapid formation of peptide aggregates has been observed in TEM micrographs of CATCH peptides at low concentration and lower temperatures. The strong electrostatic attraction between the oppositely charged peptides may facilitate this rapid oligomer formation. The oligomers may then slowly reorganize into bi-layer β-sheets that grow by oligomer addition or by monomer addition.[8-10] If these mixtures can be trapped in the oligomeric state, further study by solid-state NMR or cryo-EM may be possible. Recent advancements in dynamic nuclear polarization NMR and high-resolution magic-angle-spinning NMR have benefitted the related fields, such as metabolomics and protein folding, and could also aid in the study of oligomeric species.[11, 12] However, these methods are relatively new and not widely used in characterizing self-assembling and co-assembling peptides possibly requiring adaptation to these systems. Understanding the cause of this mixture in β-strand arrangements and peptide self-association will enable us to develop next generation coassembled β-sheets with exquisite control. Furthermore, control over the arrangement and patterning of

peptides in the nanofiber may be desirable to intentionally promote self-association to co-localize biomolecules. These designed defects are reminiscent of the implantation of defects in crystalline materials to effect change in its physical properties.

One of the changes necessary in developing a mechanistic understanding of the assembly pathway is the characterization of non-ideal samples. Commonly, the field of biomolecular NMR focuses on the analysis of highly ordered protein and peptide samples.[13-16] While the highly ordered structures provide high quality and high resolution data that facilitate the study of biological systems, these systems and samples neglect the more nuanced effects of off-pathway structures and the presence of structural defects. These deviations deepen our knowledge on the ensemble of interactions that govern peptide assembly and protein folding. Minor structures that form in these assembly conditions may also be ignored in the same manner.[17] Evaluating these heterogeneities will also benefit from the further refinement of nuclear spin simulations that capture some of their complex effects on different NMR measurements. By studying peptide assemblies holistically in different conditions we can better capture the complex interactions involved in the process.

7.2.2 Structures: Oligomers and Computationally Aided Design

The ability to computationally identify new coassembling β-sheet peptides is a promising step forward in the design of these materials. However, the designs produced from the algorithm rely on the same sequence pattern found in the CATCH peptide pair which consequently results in charge-complementary peptides. Materials with highly charged surfaces are unattractive in certain cell applications that are sensitive to

interactions between the cell membrane, which has a negative resting membrane potential, and the material scaffold.[2, 18-20] Creating peptides that do not only rely on electrostatic repulsion and attraction to confer coassembly behavior is the next challenge in designing functional peptide-based biomaterials for a broader range of biotechnological applications. Insights from the design of peptides beyond the experimentally based sequences could unveil novel design motifs that promote β-sheets and deepen our understanding of protein folding and misfolding. Coassembling β-sheet segments that react orthogonally could also further our ability to design more complex geometries and nanoarchitectures beyond those found in nature similar to efforts in DNA origami.[21]

Computational simulations revealed the possibility of β-barrel-like oligomers forming along the coassembly pathway. These β-sheet rich oligomers could be a desirable structure for developing functional biomaterials. These β-sheet rich oligomers would offer a higher density of functional ligands in soluble nanoparticles. Through our combined computational and experimental approach, characterization of the organization of these oligomeric aggregates observed by TEM and DLS in the CATCH systems may provide insights into the targeted design of these structures. The design and study of β-sheet rich oligomers would inform the active research on disease-related amyloids which are often though to form toxic oligomers.[22]

7.2.3 Towards Functional Use

Ultimately, our interest in coassembled peptides is rooted in the desire to create biomaterials with specific properties for use in a variety of biomedical and biotechnological applications. Towards this end, assessing the influence of covalently attached biomolecules

on peptide coassembly is necessary to develop fine control of nanoscale organization. Experimental measurements and computational simulations have highlighted the significant heterogeneity present in current coassembling peptide designs. Subsequently, it is likely that covalently attached biomolecules will influence the structure of coassembled peptide nanofibers especially if the ligands have negatively and positively charged functional groups. Despite the prevalence of self-assembling peptides as biomaterial scaffolds, there has not been any systematic studies on the structural changes that could arise from the additional functional motifs onto these self-recognizing peptides. The attachment of glycans to well-known self-assembling peptide Q11 has been shown to produce to hierarchical structures similar to collagen.[23] On a more applied side, the organization of these functional segments may be important in the type and degree of response they elicit when interacting with cells in applications such as immunoengineering and regenerative medicines.[24-28]

Zooming out from the nanoscale, macroscopic material properties are often important in determining the choice of material for a targeted application. The field of biocompatible polymers has benefitted from the polymer theory that bridges this gap in molecular-level design to macroscopic material properties enabling their prevalent use in biomedical and biotechnological applications. Similarly, peptide-based biomaterials research should develop a functional theory of how sequence design can influence physical properties of the assembled material. Ultimately, an engineer should be able to search through a library of materials to identify a subset of peptide designs that have the desired elastic, thermal, and optical properties. Work from the Barone lab has begun to characterize the material properties of β-sheet inducing additives to produce structurally engineered

peptide materials.[29] This work while promising falls short of understanding the structure. A common example of proteinaceous material with exceptional physical properties is silk. Characterization of the composition and structure of silk has led to the development of synthetic silk as well as the creation of silk-like materials for other applications.[30]

7.3 References

1. C. J. Wilson, A. S. Bommarius, J. A. Champion, Y. O. Chernoff,, D. G. Lynn, A. K. Paravastu, C. Liang, M-C. Hsieh. *Chemical Reivews*, 2018, **118**, 11519-11574.

2. P. J. King, M. Giovanna Lizio, A. Booth, R. F. Collins, J. E. Gough, A. F. Miller and S. J. Webb, Soft Matter, 2016, 12, 1915-1923.

3. D. T. Seroski, A. Restuccia, A. D. Sorrentino, K. R. Knox, S. J. Hagen and G. A. Hudalla, *Cell. Mol. Bioeng.*, 2016, **9**, 335-350.

4. K. Nagy-Smith, E. Moore, J. Schneider and R. Tycko, Proceedings of the National Academy of Sciences, 2015, 112, 9816-9821.

5. C. J. Bowerman and B. L. Nilsson, Peptide Science, 2012, 98, 169-184.

6. H. Xiong, B. L. Buckwalter, H. M. Shieh and M. H. Hecht, Proceedings of the National Academy of Sciences, 1995, 92, 6349-6353.

7. M. Cheon, I. Chang and C. K. Hall, Proteins: Structure, Function, and Bioinformatics, 2010, 78, 2950-2960.

8. H.-S. Liao, J. Lin, Y. Liu, P. Huang, A. Jin and X. Chen, Nanoscale, 2016, 8, 14814-14820.

9. W. Hwang, S. Zhang, R. D. Kamm and M. Karplus, Proc. Natl. Acad. Sci. U.S.A., 2004, 101, 12916-12921.

10. S. Zhang, K. Iwata, M. J. Lachenmann, J. W. Peng, S. Li, E. R. Stimson, Y. Lu, A. M. Felix, J. E. Maggio and J. P. Lee, J. Struct. Biol., 2000, 130, 130-141.

11. A-H. Emwas, R. Roy, R. T. McKay, L. Tenori, E. Saccenti, G. A. N. Gowda, D. Raftery, F. Alahmari, L. Jaremko, M. Jaremko, D. S. Wishart, Metabolites, 2019, 9, 123.

12. Y. Su, L. Andreas, R. G. Griffin, Annu. Rev. Biochem., 2015, 84, 465-497.

13. A. Goldbourt, Curr. Opin. Biotechnol., 2013, 24, 705-715.

14. B. Habenstein and A. Loquet, Biophys. Chem., 2016, 210, 14-26.

15. B. H. Meier, R. Riek and A. Böckmann, Trends Biochem. Sci., 2017, 42, 777-787.

16. R. Tycko, Curr. Opin. Chem. Biol., 2000, 4, 500-506.

17. E. K. Roberts, K. M. Wong, E. J. Lee, M. M. Le, D. M. Patel and A. K. Paravastu, Soft Matter, 2018, accepted for publication.

18. J. P. Jung, A. K. Nagaraj, E. K. Fox, J. S. Rudra, J. M. Devgun and J. H. Collier, Biomaterials, 2009, 30, 2400-2410.

19. E. C. Wu, S. G. Zhang and C. A. E. Hauser, Adv. Funct. Mater., 2012, 22, 456-468.

20. S. G. Zhang, T. C. Holmes, C. M. Dipersio, R. O. Hynes, X. Su and A. Rich, Biomaterials, 1995, 16, 1385-1393.

21. P. Wang, T. A. Meyer, V. Pan, P. K. Dutta and Y. Ke, Chem, 2017, 2, 359-382.

22. M. P. Lambert, A. K. Barlow, B. A. Chromy, C. Edwards, R. Freed, M. Liosatos, T. E. Morgan, I. Rozovsky, B. Trommer, K. L. Viola, P. Wals, C. Zhang, C. E. Finch, G. A. Drafft and W. L. Klein, Proc. Natl. Acad. Sci. U. S. A., 1998, 95, 6448-6453.

23. A. Restuccia and G. A. Hudalla, Biomaterials Science, 2018, 6, 2327-2335.

24. J. Chen, R. R. Pompano, F. W. Santiago, L. Maillat, R. Sciammas, T. Sun, H. Han, D. J. Topham, A. S. Chong and J. H. Collier, Biomaterials, 2013, 34, 8776-8785.

25. R. R. Pompano, J. Chen, E. A. Verbus, H. Han, A. Fridman, T. McNeely, J. H. Collier and A. S. Chong, Advanced Healthcare Materials, 2014, 3, 1898-1908.

26. J. S. Rudra, S. Mishra, A. S. Chong, R. A. Mitchell, E. H. Nardin, V. Nussenzweig and J. H. Collier, Biomaterials, 2012, 33, 6476-6484.

27. J. S. Rudra, Y. F. Tian, J. P. Jung and J. H. Collier, Proceedings of the National Academy of Sciences, 2010, 107, 622-627.

28. P. D. Tatman, E. G. Muhonen, S. T. Wickers, A. O. Gee, E.-S. Kim and D.-H. Kim, Biomaterials Science, 2016, 4, 543-554.

29. D. M. Ridgley, E. C. Claunch and J. R. Barone, Appl. Spectrosc., 2013, 67, 1417-1426.

30. T. Scheibel, Microbial Cell Factories, 2004, 3, 14.

APPENDIX A.SUPPLEMENTARY INFORMATION FOR CHAPTER 3

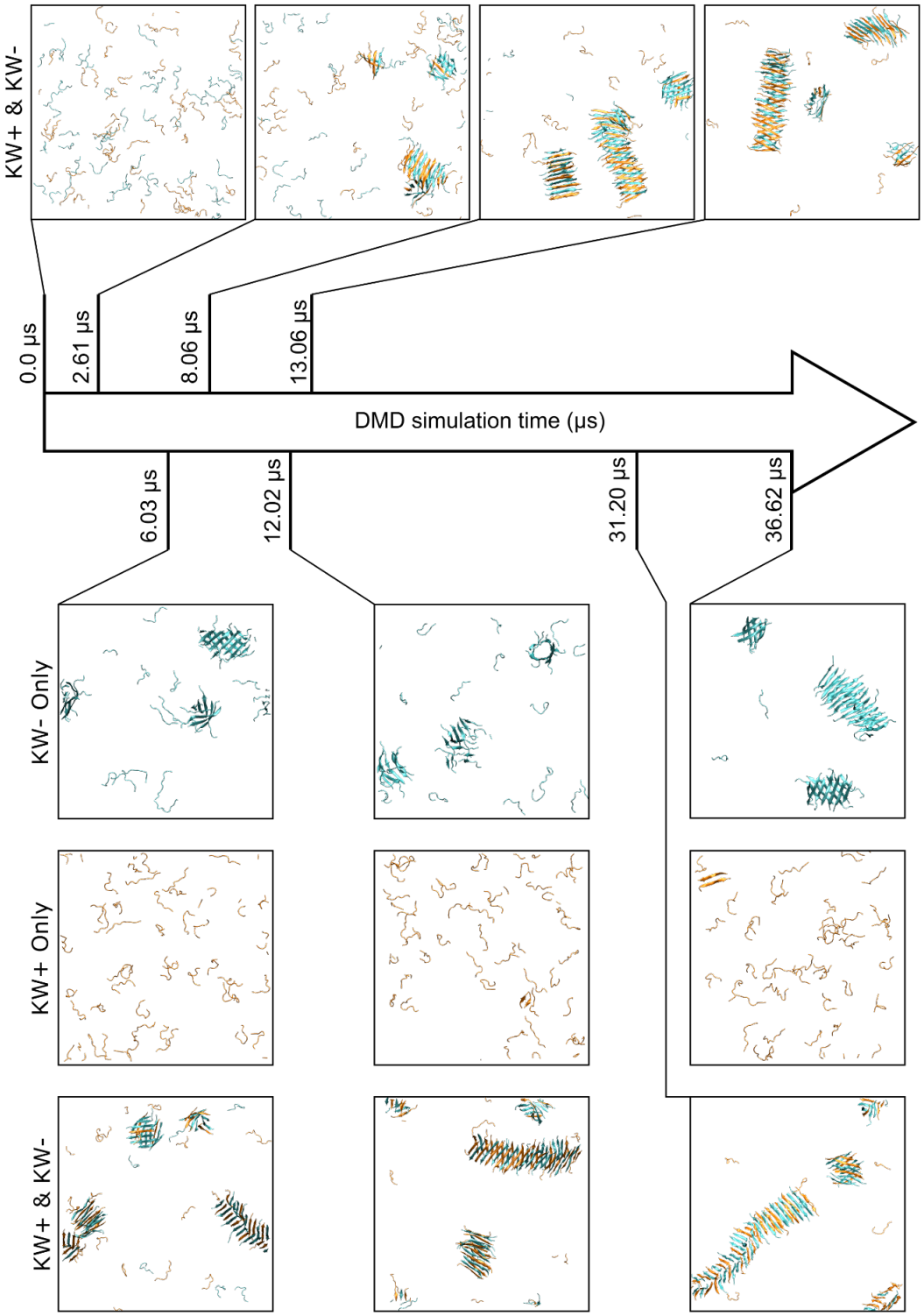

Figure 5 Snapshots of coarse-grained discontinuous molecular dynamics (DMD) simulations of King-Webb peptides at specified times.

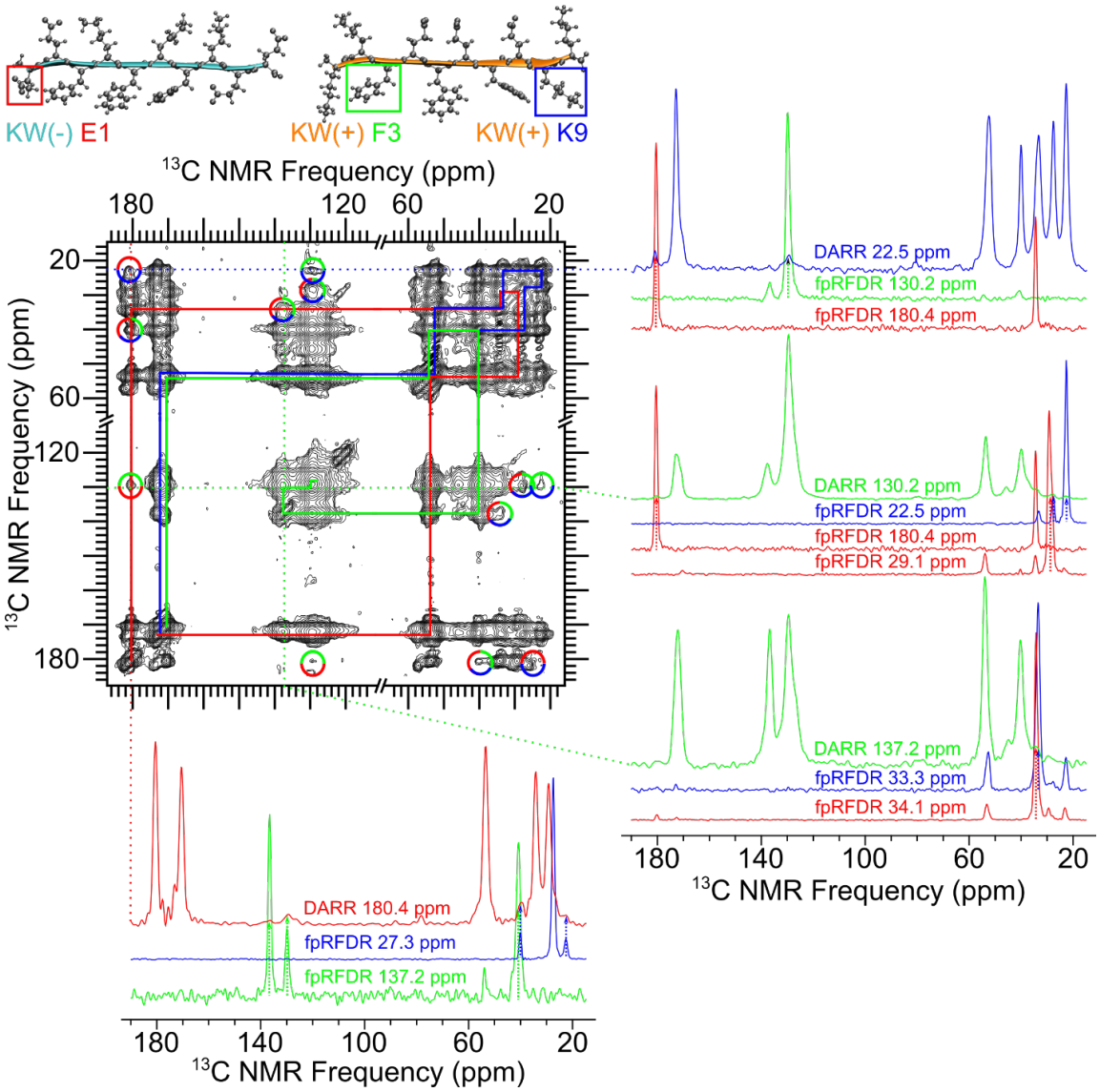

Figure 6 2D ^{13}C-^{13}C 500ms dipolar assisted rotational resonance (DARR) spectrum of an isotopically labeled KW peptide nanofiber sample (Sample A). Colored lines indicate spectral assignments for isotopically labeled residues determined by 2D fpRFDR. Bi-colored circles highlight off-diagonal crosspeaks resulting from interresidue ^{13}C-^{13}C couplings. Tri-colored circles indicate overlapping crosspeaks with signal contributions from 3 residues. 1D slices are shown to illustrate analysis of interresidue ^{13}C-^{13}C couplings at indicated frequencies.

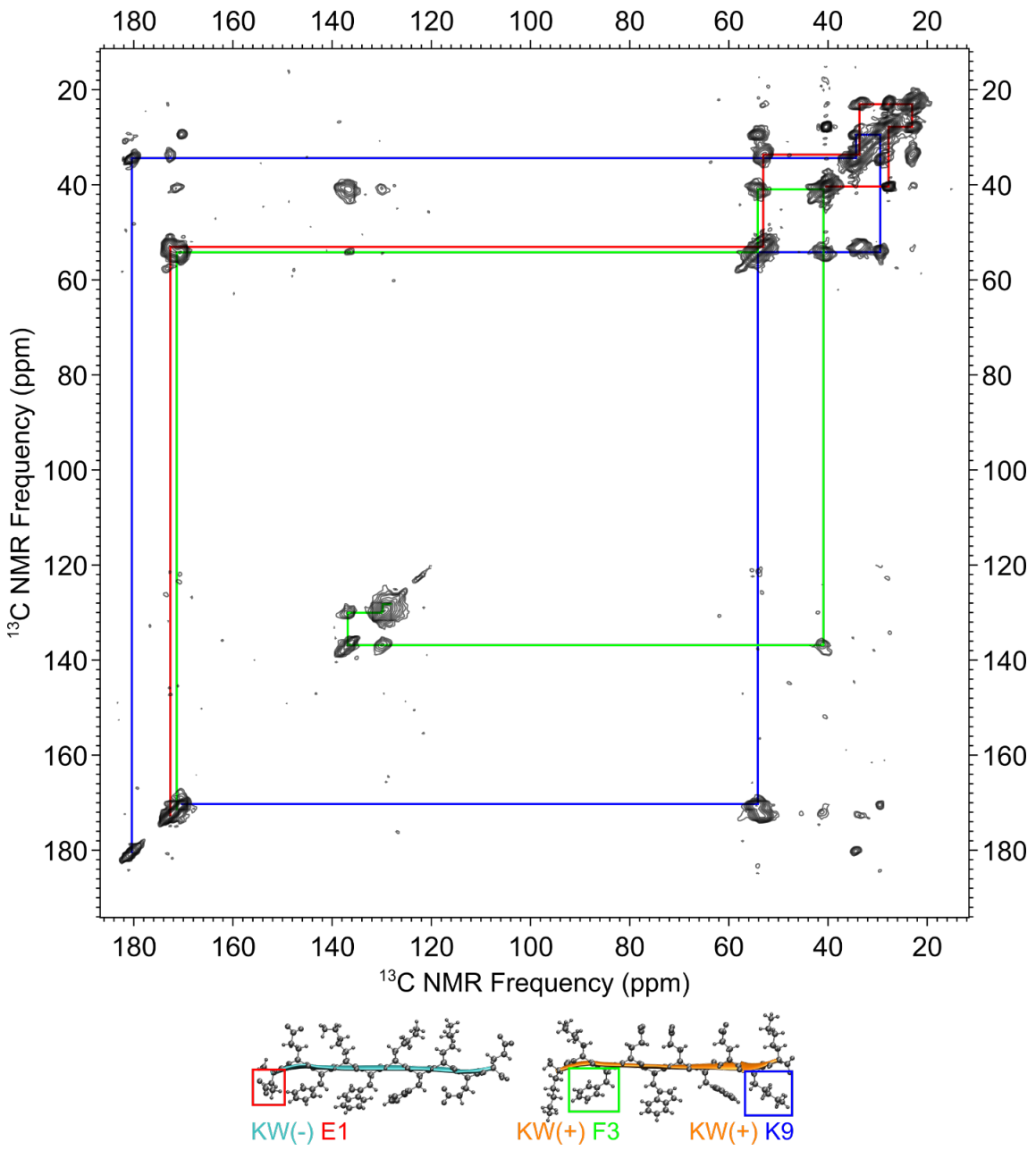

Figure 7 2D ^{13}C-^{13}C finite-pulse radio-frequency driven recoupling (fpRFDR) NMR spectrum of Sample A. Solid lines indicate spectral assignments determined by analysis of peak positions with random coil values from the BMRB.

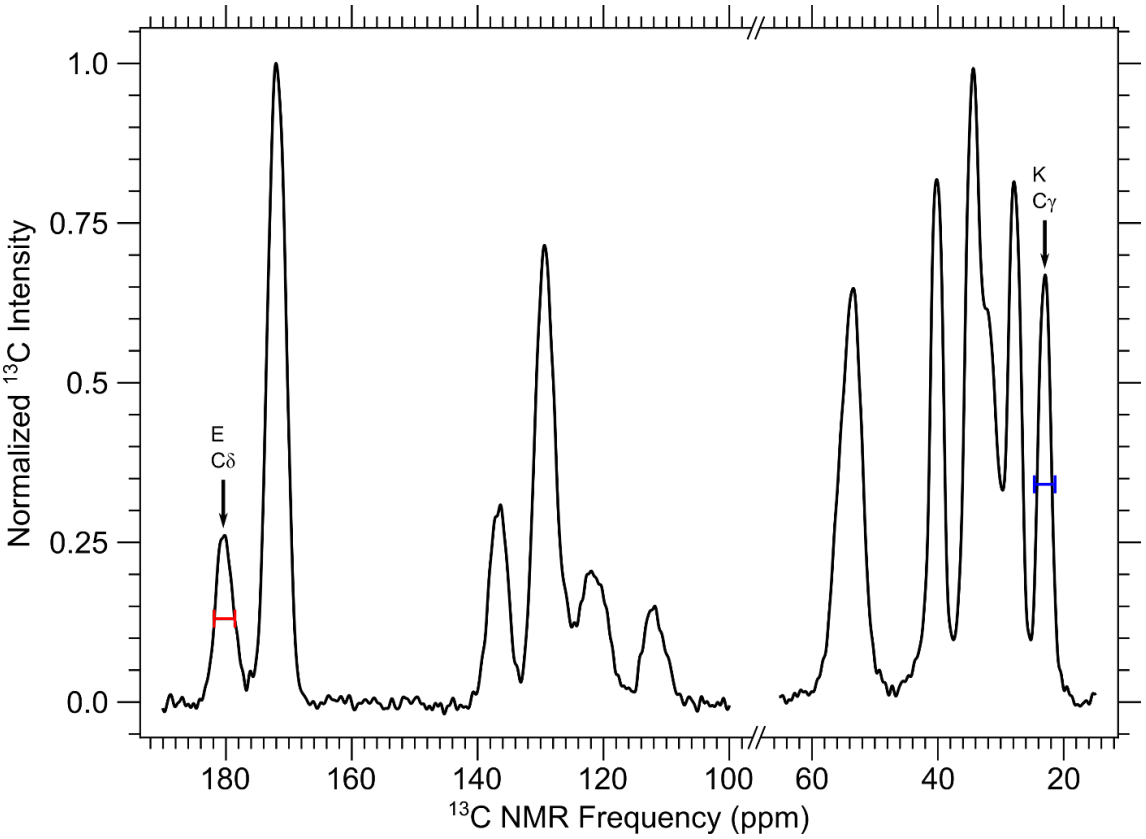

Figure 8 1D ^{13}C NMR spectrum of Sample D where signal intensity represents naturally abundant ^{13}C. NMR linewidths of glutamic acid δ-carbon and lysine γ-carbon are highlighted for reference.

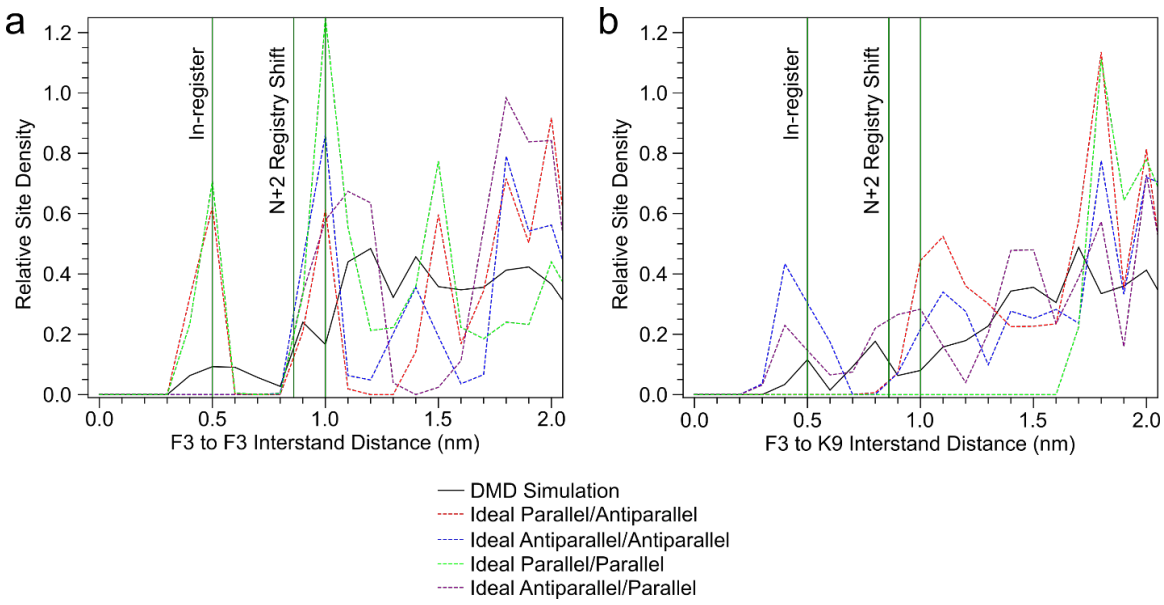

Figure 9 Analysis of parallel and antiparallel β-sheet content averaged over 6 coarse-grained DMD simulations. a) Distance distribution between F3 carbonyl sites as analyzed from the coarse-grained DMD simulation. b) Distance distribution between F3 carbonyl and K9 backbone nitrogen sites evaluated from the cg DMD simulations.

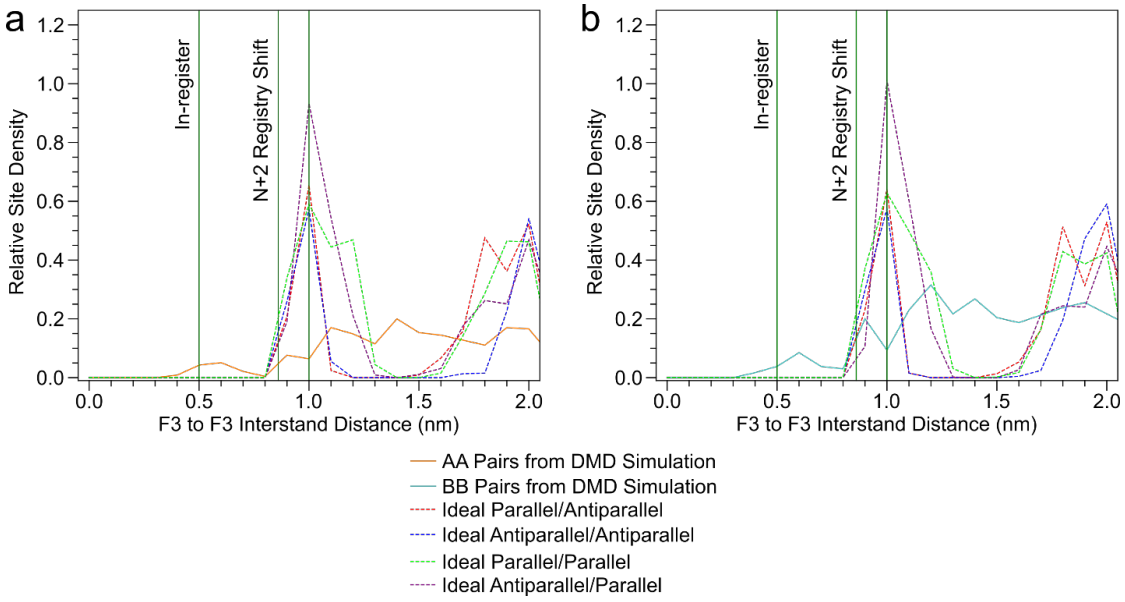

Figure 10 Analysis of self-association of King-Webb peptides averaged over 6 coarse-grained DMD simulations. a) Distance distribution of KW+ to KW+ (orange) peptides

and b) distance distribution of KW- to KW- (cyan) peptides. Calculations are based on F3 carbonyl sites on KW+ and KW- peptides.

APPENDIX B. SUPPLEMENTARY INFORMATION FOR CHAPTER 4

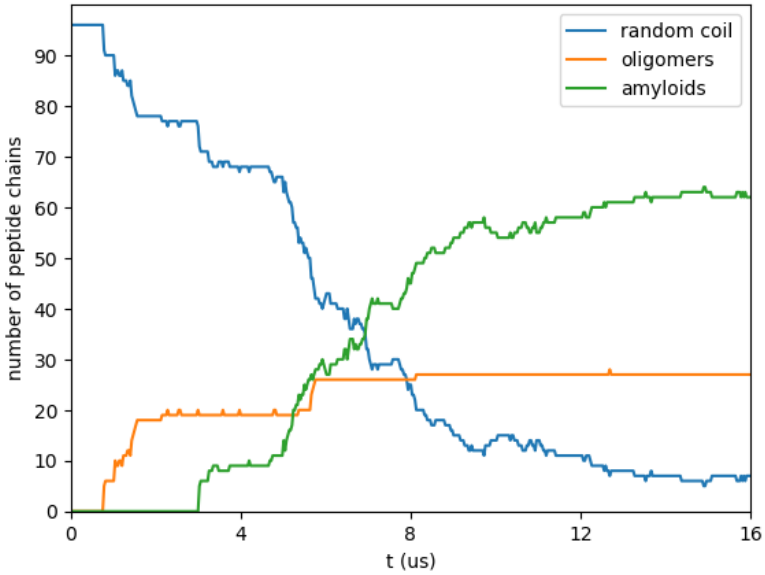

Figure 11 The numbers of peptide chains in random coil, β-barrel oligomers and amyloid as a function of simulation time. The number of random-coil peptides decreases monotonically as the simulation progresses. The number of peptides in β-barrel oligomers, which first appear at ~1 μs, increases until ~6 μs and remains constant thereafter. The number of peptides in amyloid structures, which first appear at ~3 μs, surpasses that in β-barrel oligomers at around 5 μs, increases rapidly thereafter, and eventually plateaus because the number of peptide chains are fixed in the simulation.

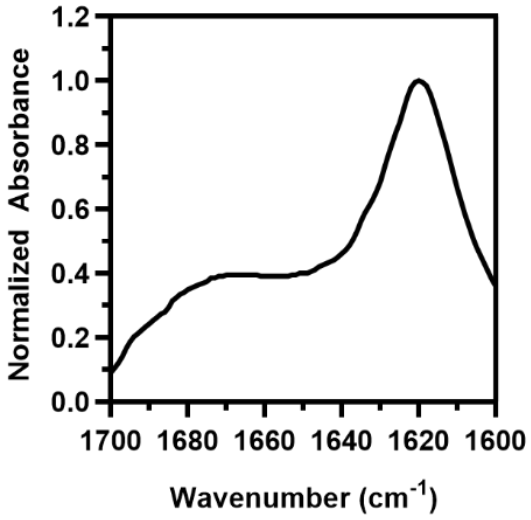

Figure 12 FTIR spectra of aqueous 10 mM CATCH(+/-) in 1x PBS demonstrating a β-sheet maximum at 1620 cm^{-1}.

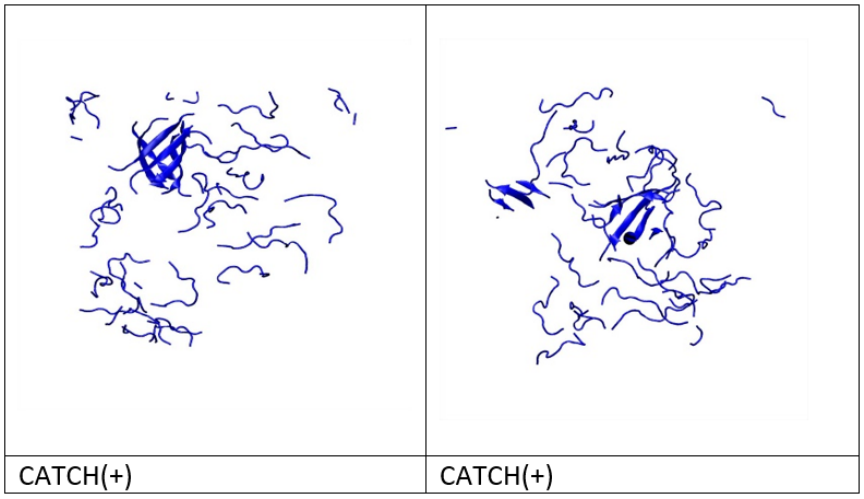

Figure 13 Two snapshots that demonstrate transient self-assembly of CATCH(+) peptides during DMD simulations.

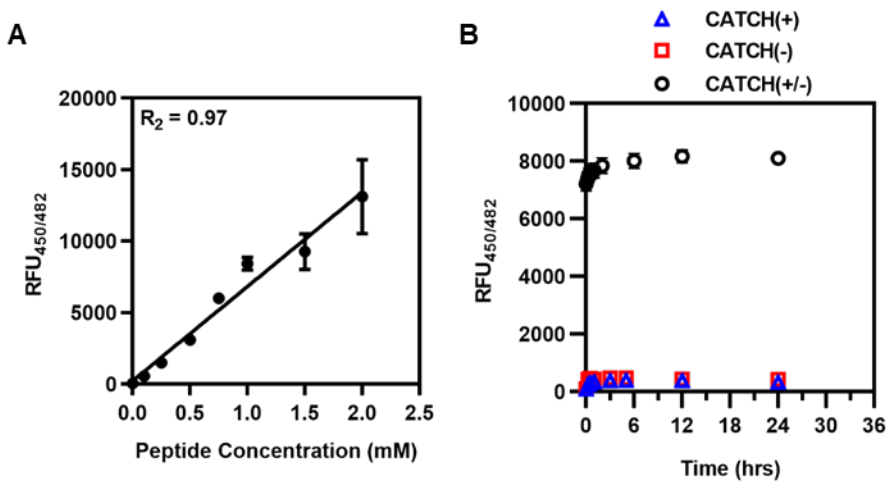

Figure 14 (A) Standard curve relating equimolar CATCH(+/-) peptide concentration to Thioflavin T fluorescence demonstrating linearity of RFU signal with peptide concentration. (B) ThT kinetics of 1 mM peptide alone or mixed. Key: (CATCH(+), blue triangle; CATCH(-), red square; CATCH(+/-), black circle).

B.1 Simulating effects of AA and BB nearest neighbors on PITHIRDS-CT measurements

The PITHIRDS-CT measurements on "isotopically diluted" CATCH(+/-) nanofibers in the presence of varying probabilities of CATCH(+):CATCH(+) and CATCH(-):CATCH(-) nearest neighbors was modeled using a combination of Monte Carlo simulations of co-assembled β-sheet arrangements with nuclear spin simulations. Figure B.5 illustrates the workflow used to generate predictions of PITHIRDS-CT decay curves for a given self-association probability. In this model, we assume an ideal antiparallel β-sheet structure. As shown in Figure B.6, an ideal antiparallel β-sheet fits the "isotopically pure" CATCH(+/-) nanofiber sample better than an ideal parallel β-sheet. Simulations of PITHIRDS-CT measurements do not vary significantly up to 30 ms of ^{13}C-^{13}C recoupling

time (Figure B.6 A-B). Therefore, we determine the probability of AA or BB pairs by evaluating the earlier ^{13}C signal decays using a linear fit of the two extreme cases, p =1 (self-sorting) and p=0 (ideal co-assembled).

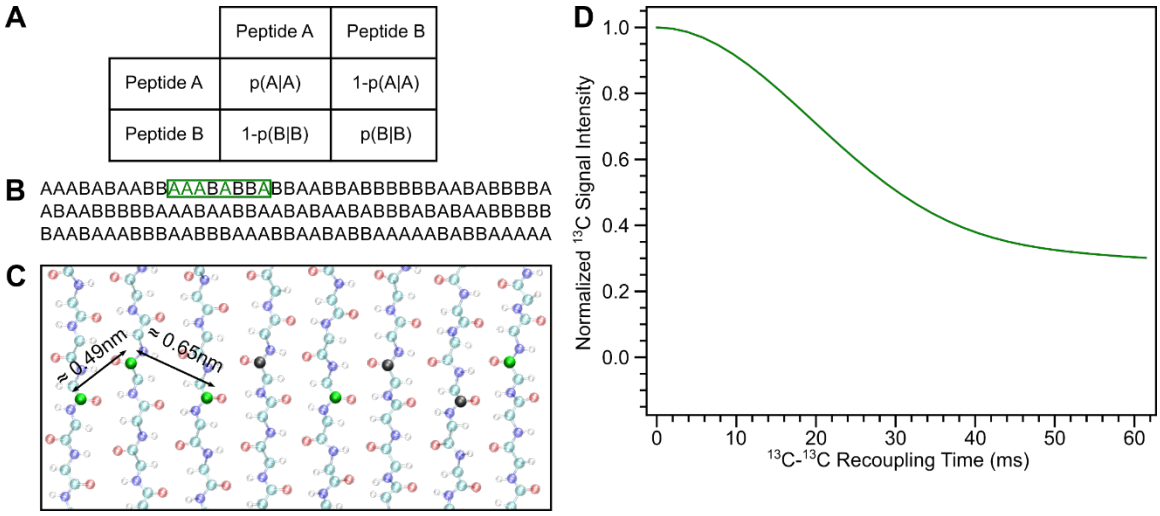

Figure 15 Calculation of a PITHIRDS-CT decay curve from a Monte Carlo simulation. A) Probability matrix for the Monte Carlo simulations of coassembled β-sheets, where p(A|A) indicates the probability of adding peptide A to the β-sheet end given A. B) An example sequence produced from a Monte Carlo simulation at a self-association probability of 50%. The green box indicates an 8-molecule sampled segment where isotopically labeled ^{13}C sites (peptide A) are highlighted by green letters. C) Space-filling model of the peptide backbones for an ideal 8-molecule antiparallel β-sheet. Green spheres indicate ^{13}C sites (peptide A) while gray spheres represent unlabeled ^{12}C sites (peptide B) according to the pattern highlighted in panel A. D) Simulated PITHIRDS-CT decay curve of the ^{13}C-spin arrangement depicted in panel B.

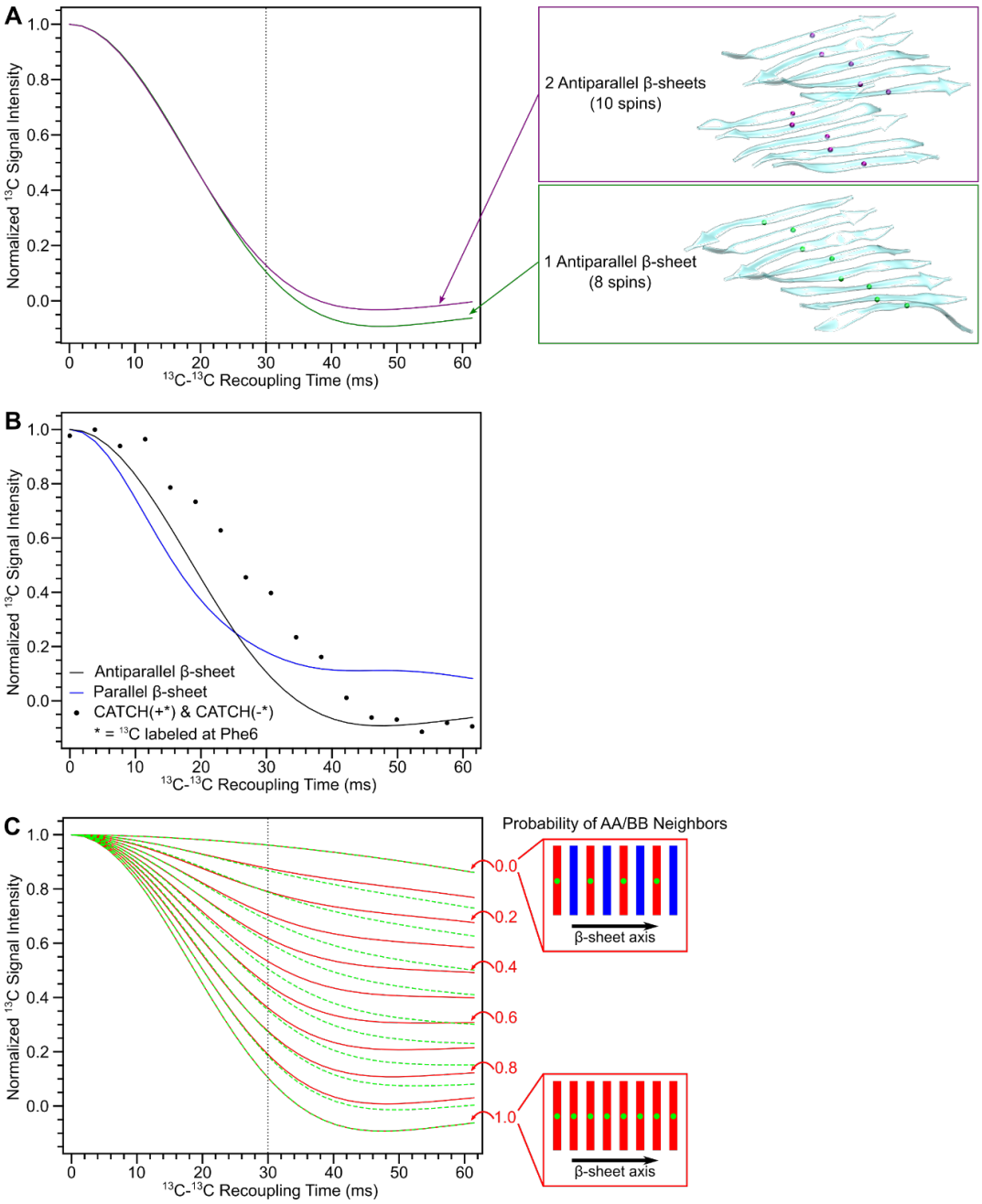

Figure 16 Effects of different β-sheet models on simulated PITHIRDS-CT decay curves. A) Comparison of simulated PITHIRDS-CT decay curves for a single antiparallel β-sheet (solid green) and two stacked antiparallel β-sheets (solid purple). B) Comparison of experimental PITHIRDS-CT measurement on an "isotopically pure" sample (black dots) against simulated PITHIRDS-CT decay curves for an ideal parallel β-sheet (solid blue) and an ideal antiparallel β-sheet (solid black). C) Comparison of simulated PITHIRDS-CT decay curves determined by Monte Carlo simulations (dashed green) or a linear combination (solid red) of the curves at probabilities of 1.0 and 0.0 assuming an ideal antiparallel β-sheet.

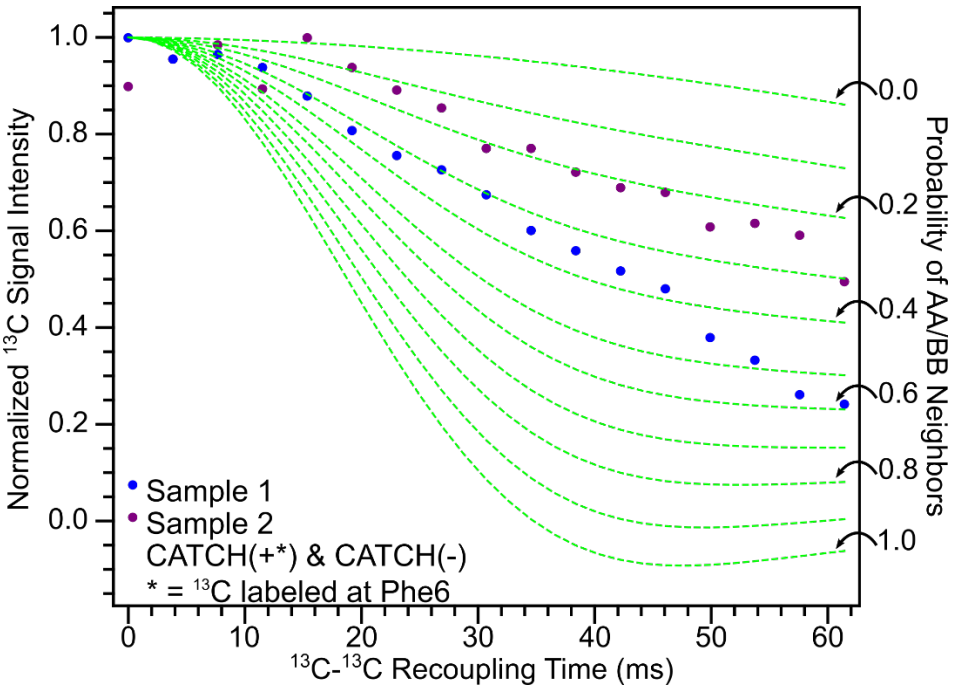

Figure 17 Comparison of PITHIRDS-CT decays for two different nanofiber samples in which CATCH(+) is isotopically labeled while CATCH(-) remains unlabeled.

B.2 Sampling effects on Monte Carlo predictions of β-sheet arrangements

To understand how the number of peptide strands and number of simulations affect the calculated probability of AA or BB nearest neighbors, we ran multiple Monte Carlo simulations of co-assembled β-sheet arrangements at two different self-association probabilities, 0.1 and 0.3. As can be seen in Figure B.8, the calculated self-association probability for a given Monte Carlo simulation run approaches the steady-state probability, depicted as a dashed line, only after thousands of β-strands are added. The Monte Carlo simulations show significant variability at 96 β-strands (the system size of the DMD simulations). Sufficient sampling by running multiple simulations and averaging over a series of simulations can reduce variability in the calculation of self-association propensities as shown in Figure B.9. Hundreds of simulations are needed to reduce sampling variability and approach the true steady-state probability. The size of simulation and number of simulation runs necessary to accurately predict self-association probabilities from DMD simulations would be too computationally costly.

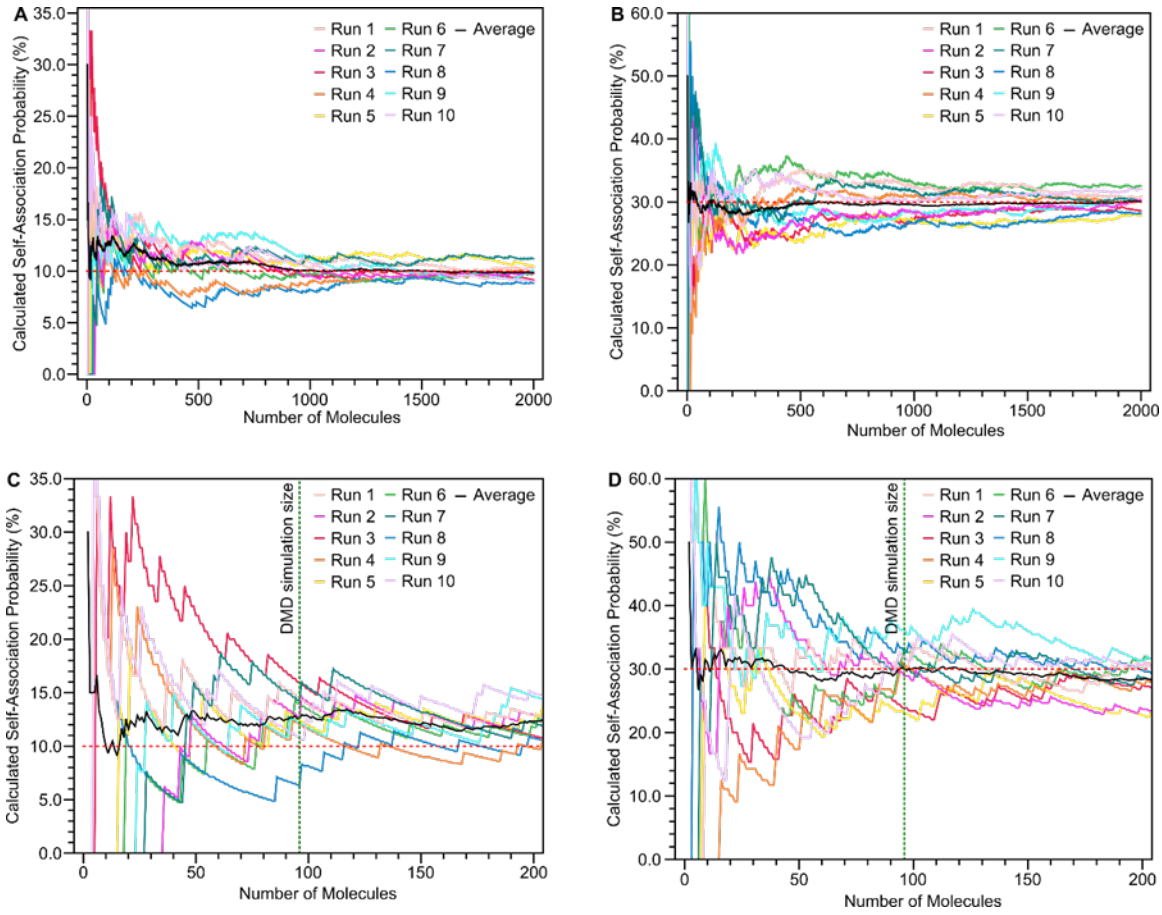

Figure 18 System size effects on calculated self-association probability from Monte Carlo simulations of coassembled β-sheets. A) Self-association probability set to 10%. B) Self-association probability set to 30%. C) Close-up of panel A. D) Close-up of panel B.

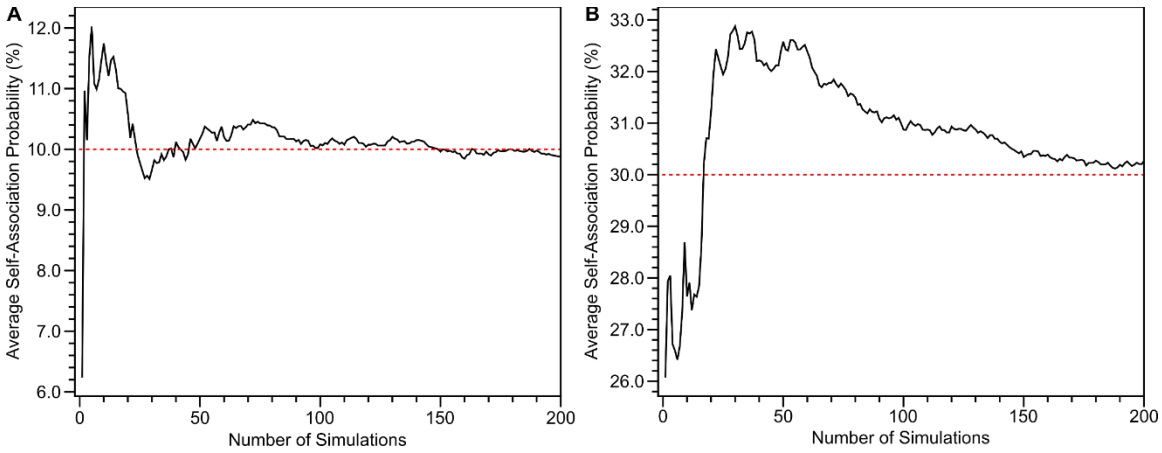

Figure 19 Effect of simulation runs on the calculated average self-association probability for Monte Carlo simulations of coassembled β-sheets consisting of 96 β-strands. A) Self-association probability set to 10%. B) Self-association probability set to 30%.

B.3 Dehydrated conditions promote CATCH peptide self-assembly

We observed that CATCH(+) and CATCH(-) self-associate into β-sheet structures when dehydrated, which contrasts with their resistance to aggregation in aqueous conditions. FTIR spectra of CATCH(+) and of CATCH(-) peptides individually lyophilized from water have strong maxima near 1620 cm^{-1} (Fig. S16A, B), indicating that the peptides are in a β-sheet conformation when dehydrated. Likewise, PITHIRDS-CT spectra of either lyophilized ^{13}C-labeled CATCH(+) or lyophilized ^{13}C-labeled CATCH(-) have strong signal decays (Figure B.10), indicating strong dipolar coupling between ^{13}C labeled sites. Such decays would only occur if ^{13}C labeled sites were within ~0.5 nm of each other, consistent with peptides assembled in a β-sheet structure. Collectively, these observations demonstrate that CATCH peptides can self-associate when water is depleted from the system, which may help to explain the formation of AA and BB neighbors in CATCH β-sheet co-assemblies.

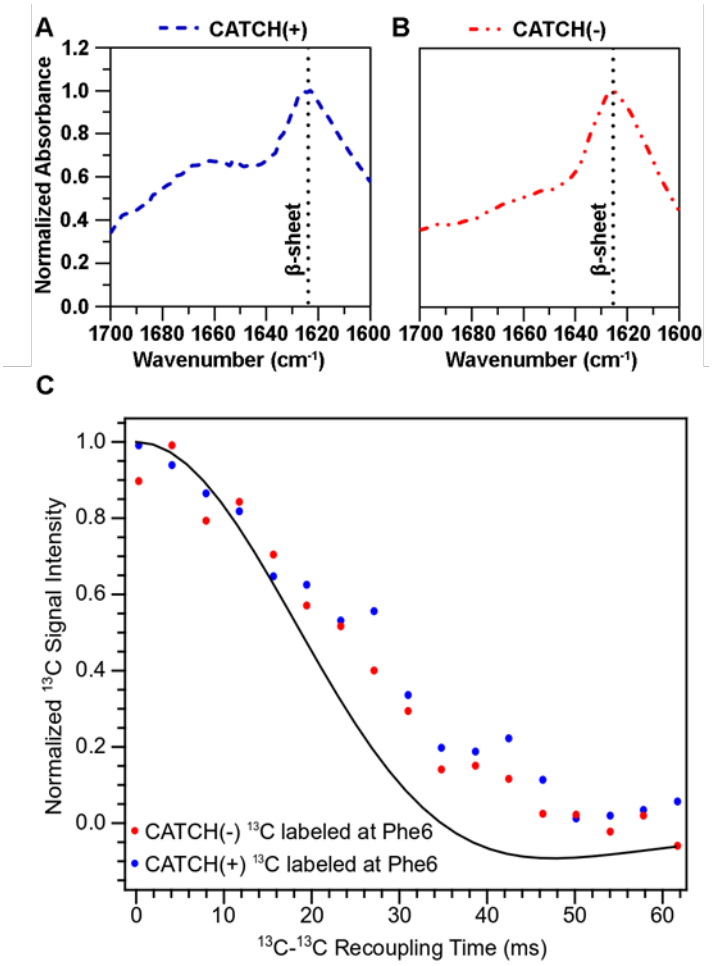

Figure 20 (A,B) FTIR spectra of CATCH(+) and CATCH(-) lyophilized (C) PITHIRDS-CT measurements of unassembled CATCH(+) and CATCH(-) peptides lyophilized. The solid black curve corresponds to the predicted signal decay in the PITHIRDS-CT experiment from a nuclear spin simulation of eight ^{13}C atoms along an ideal self-assembled antiparallel β-sheet.